

Review

# Progress in Icephobic Coatings for Wind Turbine Protection: Merging Chemical Innovation with Practical Implementation

Ghazal Minoofar <sup>1</sup>, Amirhossein Jalali Kandeloo <sup>2</sup>, Mohammad Sadegh Koochaki <sup>1</sup> and Gelareh Momen <sup>1,\*</sup>

<sup>1</sup> Department of Applied Sciences, University of Quebec in Chicoutimi (UQAC), 555, boul. de l'Université, Chicoutimi, QC G7H 4E5, Canada

<sup>2</sup> Department of Functional Materials and Catalysis, University of Vienna, Währinger Str. 42, 1090 Vienna, Austria

\* Correspondence: gelareh\_momen@uqac.com

**Abstract:** Ice accumulation on wind turbine blades poses a significant challenge to turbine performance and safety, and these issues have led to extensive research on developing effective anti-icing methods. Polymer-based icephobic coatings have emerged as promising solutions, given their passive nature and low energy requirements. However, developing effective icephobic coatings is a complex task. In addition to anti-icing properties, factors such as mechanical strength, durability, and resistance to UV, weathering, and rain erosion must be carefully considered to ensure these coatings withstand the harsh conditions faced by wind turbines. The main challenge in coating engineering is mastering the chemistry behind these coatings, as it determines their performance. This review provides a comprehensive analysis of the suitability of current icephobic coatings for wind turbine applications, emphasizing their alignment with present industrial standards and the underlying coating chemistry. Unlike previous works, which primarily focus on the mechanical aspects of icephobicity, this review highlights the critical yet underexplored role of chemical composition and explores recent advancements in polymer-based icephobic coatings. Additionally, earlier studies largely neglect the specific standards required for industrial applications on wind turbines. By demonstrating that no existing coating fully meets all necessary criteria, this work underscores both the urgency of developing icephobic coatings with improved durability and the pressing need to establish robust, application-specific standards for wind turbines. The review also combines insights from cutting-edge research on icephobic coatings that are coupled with active de-icing methods, known as the hybrid approach. By organizing and summarizing these innovations, the review aims to accelerate the development of reliable and efficient wind energy systems to pave the way for a cleaner and more sustainable future.

**Keywords:** ice protection requirements; wind turbine; passive methods; icephobic coatings; hybrid methods



Academic Editor: George D. Verros

Received: 29 December 2024

Revised: 18 January 2025

Accepted: 23 January 2025

Published: 27 January 2025

**Citation:** Minoofar, G.; Kandeloo, A.J.; Koochaki, M.S.; Momen, G. Progress in Icephobic Coatings for Wind Turbine Protection: Merging Chemical Innovation with Practical Implementation. *Crystals* **2025**, *15*, 139. <https://doi.org/10.3390/cryst15020139>

**Copyright:** © 2025 by the authors. Licensee MDPI, Basel, Switzerland. This article is an open access article distributed under the terms and conditions of the Creative Commons Attribution (CC BY) license (<https://creativecommons.org/licenses/by/4.0/>).

## 1. Introduction

Atmospheric icing occurs when ice or snow builds up on surfaces exposed to the surrounding air; this accumulation causes problems for the structure and function of objects and infrastructure. Broadly, atmospheric icing is typically classified into two primary types: “in-cloud icing”, which includes rime ice and glaze (Figure 1), and “precipitation icing”. Rime ice is primarily solidified supercooled droplets of water that typically can be formed at cold temperatures. Glazed ice consists of incompletely frozen supercooled droplets of water and is created at temperatures slightly below water’s freezing point; it is denser than

rime ice and exhibits a polished appearance. Mixed ice develops within the middle range of freezing temperatures, usually between 0 and  $-20\text{ }^{\circ}\text{C}$  and even as low as  $-40\text{ }^{\circ}\text{C}$  under extreme conditions [1–3]. Additionally, icing creates significant obstacles that hinder the optimal utilization of renewable energy sources, like wind power [4].



**Figure 1.** Icing forms of rime, glaze, and mixed ice [5].

Wind turbines are one of the most promising solutions for converting renewable wind energy into electricity. However, they face operational challenges in cold climates because of ice formation on their surfaces (Figure 2) [6–8]. Mild icing can create sufficient surface roughness to significantly impair aerodynamic performance, leading to marked power losses through increased drag from ice accretion. This reduction can produce up to a 30% loss in instantaneous power production, which translates into a potential annual reduction of up to 20% in wind turbine farm output. These losses significantly reduce profitability and compromise wind project viability [6,9,10]. During severe icing events, torque can drop completely, causing the turbine to stop and resulting in a complete loss of production [11,12]. Under uneven ice coverage [13], wind turbines may need to be forcefully stopped from rotating because of major vibrations that can damage the structure and cause large pieces of ice to detach. In certain cases, when great segments of ice are expelled, the wind turbine has to be halted to protect other devices in the field and ensure the safety of surrounding communities [14–16].



**Figure 2.** A blade of wind turbine in icy conditions [provided by Nergica-June 2020].

In icing conditions, wet ice growth typically poses a greater threat to wind turbine operations than dry rime ice growth. This is primarily due to the more pronounced degradation of aerodynamic characteristics associated with glaze icing conditions [17].

Therefore, all the impacts of ice accretion on wind turbines make ice protection systems essential [18,19]. Ice accumulation on turbine blades and the adhesion between the surface of a substrate and ice can be limited or mitigated using blade ice protection technologies

and applying a range of innovative approaches. The icephobicity of a surface refers to its ability to prevent ice accretion by delaying icing or reducing the temperature of ice nucleation, as well as inhibiting ice accumulation by decreasing the strength of ice adhesion. Indeed, measuring “ice adhesion strength ( $\tau_{ice}$ )” is a means of assessing the icephobicity of a surface [20].

Different approaches have been investigated to achieve effective ice protection on the surface of wind turbines. These strategies consist of two primary approaches: “active de-icing” and “passive anti-icing” methods. “Active methods” involve the use of external energy sources, such as thermal, electrical and mechanical energy, to prevent ice formation or remove accumulated ice from the surface. Various active de-icing methods have been developed, particularly in industrial settings, e.g., wind energy projects. These active approaches include electrothermal heating using heating elements, e.g., mats, laminates and coatings, placed on the outer surface of the blade, hot air injection at different blade areas, “low-frequency vibrations” using “high-power ultrasonic guided waves”, “microwave heating”, and “mechanical removal techniques”, including the manual de-icing and helicopter/drone de-icing through the dispersal of hot liquids [16,21,22]. A summary of the benefits and drawbacks of various “active de-icing systems” is outlined in Table 1 [22].

**Table 1.** Overview of the benefits and drawbacks of various ice protection systems [22].

Method	Advantages	Disadvantages
Hot air	Proven reliability, simple design, and a long track record of use Modification possibilities for specific blade types	Low efficiency: Heat must travel a long distance from the source to the blade tip, passing through the blade material before reaching the surface.
Electrothermal	Optimized power consumption: close to blade surface and can have spanwise heat control Established reliability with a long history of use	Requires extra effort to integrate into the blade production process Costly maintenance
Ultrasonic	Non-thermal and consumes much less power than other systems	This technique remains in the laboratory research stage
Microwaves	Optimized power consumption Wireless, repair-friendly Minor radio/radar interference	Not yet tested on a large scale Challenging to integrate into the blade design
Mechanical removal	No upfront investment in de-icing systems is necessary On-demand service providers are available, allowing for purchase as needed	Case examples only Potentially expensive Potential damage to the blade Health and safety issues for workers

However, despite the impressive performance of active methods, numerous disadvantages associated with these approaches affect their widespread use. For example, “de-icing electrical heating” systems consume approximately 10% to 25% of the entire energy generated by wind turbine blades. Hence, the use of passive methods is preferred, as they significantly reduce operational costs and energy consumption relative to active methods, as no external energy input is required [22]. The majority of these passive trajectories involve using coatings with icephobic properties that change or modify the physical and chemical characteristics of the surface of a blade.

Passive methods that use icephobic coatings do not require energy input and mechanisms such as (1) preventing water droplets from sticking to the surface, (2) inhibiting the formation of ice, and (3) decreasing the adhesion strength between ice and the surface [23]. Researchers have created various passive icephobic coatings, such as surfaces designed with multiscale crack initiators [24], superhydrophobic surfaces (SHS) [25], gels and elas-

tomers with low elastic modulus [26–28], slippery liquid-infused surfaces and aqueous lubricating layers [29–31].

Combining de-icing systems with icephobic coatings to create a hybrid approach appears to alleviate some of the technical challenges associated with implementing a de-icing system. For example, icing wind tunnel tests have shown a reduced energy consumption of over 50% for a heating system combined with icephobic coatings [32,33]. As a result, there has been increased research interest in this area, given the growing popularity of engineered surfaces produced with these coatings [20].

While most reported studies have primarily focused on enhancing and maintaining the icephobicity of developed icephobic coatings, other critical aspects, such as their mechanical properties, require more attention, as these are essential for coating performance in wind turbine applications. Because these surfaces can experience extreme conditions, various experiments have been conducted to study their performance under harsh environments. These tests fall into three main categories: assessing the mechanical strength of the coatings, examining the chemical resilience of the coatings, and evaluating the coating performance in different environments [34]. Anti-icing coatings for wind turbine blades must meet specific criteria, including excellent icephobicity (ISO/TS 19392-6:2023 [35]) and adequate mechanical strength (ISO 527-1 [36], ASTM D2240 [37], and ASTM D4060 [38]), such as a minimum elongation value of approximately 5–10% (especially when subjected to mechanical stresses caused by wind). Other important criteria include desirable UV and weathering resistance (ISO/TS 19392-5 [39], ISO 16-674-3 [40]), strong adhesion to the blade surface, resistance to delamination or peeling over time (ISO 4624 [41]), good rain erosion resistance (ISO/TS 19392-3 [42]) given the impinging water droplets striking at up to around 90 m/s near the blade tips of the wind turbines [43], abrasion durability in harsh environmental conditions. These attributes are typically determined by the choice of polymer used as the main resin. The various types of icephobic coatings, such as silicone, polyurethane and epoxy, exhibit distinct characteristics from one another [44]. Furthermore, the icephobicity of a coating depends not only on its intrinsic features but also on the additives in the formulation that are manipulated to achieve icephobic characteristics. In simpler terms, it is essential to modify the composition of these coatings, either through physical methods, e.g., incorporating various fillers, or chemical methods, e.g., adjusting the crosslink density and elastic modulus, surface modification and copolymerization or grafting with other functional groups, to obtain suitable coating properties for wind turbine applications.

Although several previous review articles have addressed anti-icing methods in the wind power industry [21,45–47], none have placed significant emphasis on the role of the chemistry of these anti-icing coatings. Therefore, this review examines the icephobic characteristics of various anti-icing coatings by exploring recent research and highlighting the crucial role of chemistry in determining the effectiveness of icephobic coatings for wind turbines. To categorize potential solutions for ice-repellent coatings and assess their suitability for wind turbine applications, the solutions are organized based on the primary polymer binder used in their formulations. Furthermore, a concise overview of hybrid systems is presented as a promising direction for future advancements in developing anti-icing surfaces.

## 2. Silicone-Based Coatings

Silicone elastomers have gained significant attention as icephobic coatings primarily because of their chemical inertness, tunable mechanical properties, low surface energy, and flexibility, especially at low temperatures [11–14,48–50]. Their low surface energy allows them to repel incoming water droplets and, as a result, prevent ice formation on

surfaces. The crucial factor in their low  $\tau_{ice}$  is the high deformation incompatibility (DI) with ice [51,52]. The mismatch between the low elastic modulus of silicone-based surfaces and the higher elastic modulus of ice can lead to the formation of “stress concentration points” at the ice–surface interface, which can result in ice detachment from the surface. In 1946, Loughborough and Haas [53] first used silicone-based materials to evaluate ice adhesion on surfaces known as de-icer surfaces. Polydimethylsiloxane (PDMS) is one of the most commonly used silicone-based polymers and offers numerous advantages, such as electrical insulation, resistance in either high or low temperatures, weather resistance, and so forth. Additionally, PDMS can be cured at room temperature with a highly controllable chemistry in the polymer curing reaction, enabling its use in various applications [54–64].

However, silicone-based coatings suffer from poor mechanical properties (modulus, strength) with low abrasion resistance and low adhesion to the substrate, which limits their use in certain industrial applications, such as on wind turbines. Furthermore, the  $\tau_{ice}$  of pure silicone coatings is rarely below 100 kPa, which is the critical adhesion strength beyond which ice cannot be naturally removed through forces such as wind [11,65–67].

Modification strategies for silicone-based icephobic coatings can be classified into two primary categories. The first involves external materials, e.g., micro/nanofillers, or additives, e.g., lubricants, to enhance coating icephobicity and mechanical properties. The second grouping relies on chemical modification, focusing on creating novel chemical structures, incorporating functional groups, favoring copolymerization, and adjusting crosslink density. Surface modifications, such as micro/nanostructures and the grafting of functional groups, also fall under this category.

### 2.1. Physically Modified PDMS-Based Icephobic and Superhydrophobic Coatings

A series of methods have been employed to physically improve the icephobic characteristics of PDMS using oils, fillers, and similar agents [68]. The use of fillers/solid particles incorporated within PDMS stands out as a promising candidate for producing icephobic coatings, given the inherent low surface energy and anti-icing characteristics of the resulting coatings. In its pure form, PDMS is unlikely to achieve a water contact angle (WCA) exceeding  $120^\circ$ . However, incorporating fillers like silica nanoparticles has been shown to augment both the hydrophobicity and icephobicity of PDMS by effectively reducing surface energy and bolstering the surface’s water-repelling capabilities [69]. Yang et al. [70] produced a physically modified PDMS-based icephobic coating by adding ZnO nanoparticles—their surfaces first modified with odecylfluoroheptyl-propyl-trimethoxysilane—to a PDMS coating. ZnO was selected as filler to facilitate the easy handling and direct construction of low surface energy micro/nanostructures. The modified PDMS coating produced a contact angle (CA) of up to  $159.5^\circ$  and less ice accretion. Water droplets did not freeze on the surface of the ZnO/PDMS sample (horizontal and tilted) at  $-5^\circ\text{C}$ , even after 120 min. Both the horizontal and tilted surfaces experienced extended delays in icing at  $-5$  and  $-10^\circ\text{C}$ , with icing only occurring on the mentioned surface at  $-15^\circ\text{C}$  (Table 2).

**Table 2.** Icing delay time on the ZnO/PDMS composite surface at varying temperatures and tilting angles ( $0^\circ$  and  $10^\circ$ ) [70].

Temperature ( $^\circ\text{C}$ )	Duration of Icing Delay (s)	
	Horizontal Surface	Tilted Surface
$-5$	$>1800$	$>1800$
$-10$	$1380 \pm 30$	$>1800$
$-15$	$210 \pm 25$	$870 \pm 42$

Liu et al. [71] prepared nano-anti-icing coatings based on  $\text{MoS}_2/\text{ZnO}/\text{PDMS}$ . The prepared surface was porous and rough, allowing an air cushion to form in contact with the added liquids. This layer reduced the interaction between the liquids and the coating surface, which in turn diminished the  $\tau_{\text{ice}}$ . They applied their innovative coating to a “glass fiber-reinforced plastic blade (GFRP)”. Figure 3a displays the icing test results for three different GFRP blades: one uncoated, one coated with  $\text{MoS}_2/\text{PDMS}$  nanomaterials, and one coated with  $\text{MoS}_2/\text{ZnO}/\text{PDMS}$  nanomaterials. The tests were performed at  $-10\text{ }^\circ\text{C}$ ,  $5\text{ m/s}$  and  $-15\text{ }^\circ\text{C}$ ,  $10\text{ m/s}$ , for a duration of 3 min.

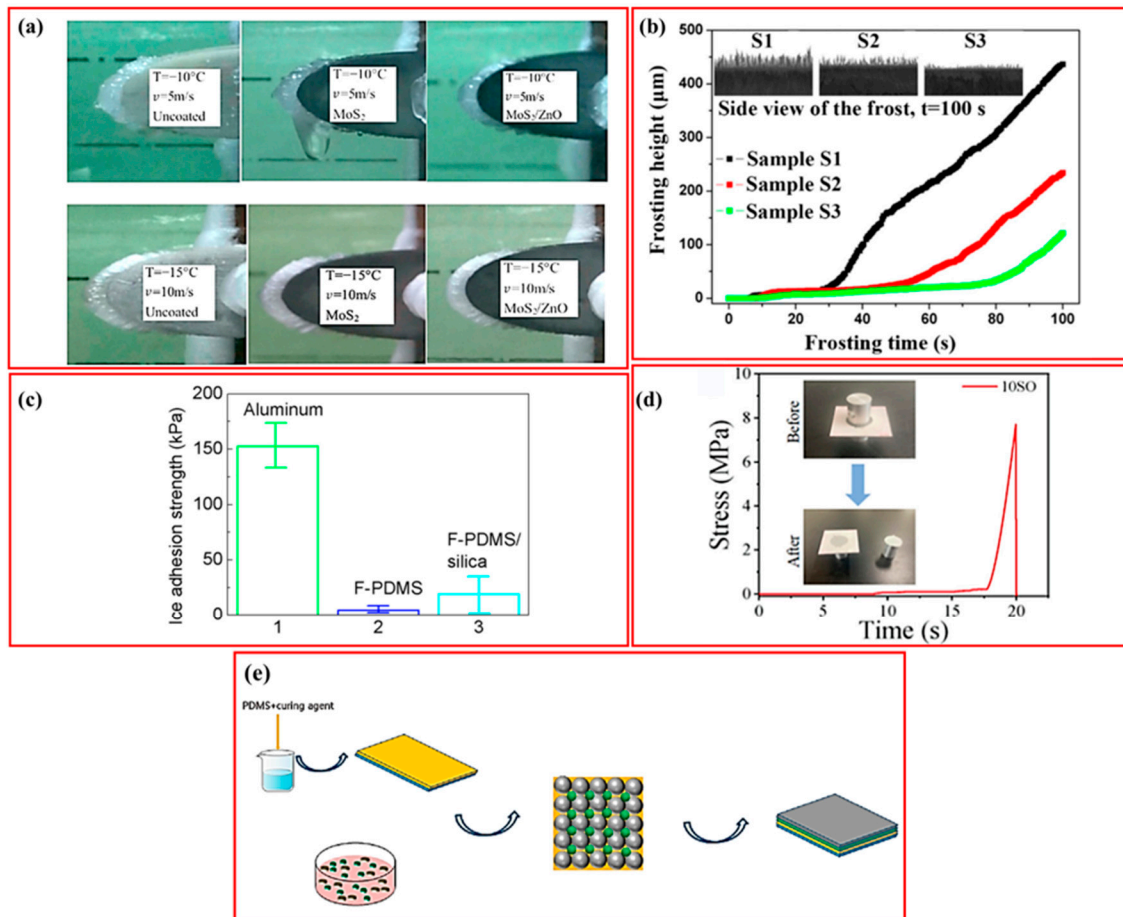


**Figure 3.** (a) The results of icing test for three different GFRP blades: one uncoated, one coated with  $\text{MoS}_2/\text{PDMS}$  nanomaterials, and one coated with  $\text{MoS}_2/\text{ZnO}/\text{PDMS}$  nanomaterials at  $-10\text{ }^\circ\text{C}$ ,  $5\text{ m/s}$  and  $-15\text{ }^\circ\text{C}$ ,  $10\text{ m/s}$  for 3 min [71]; (b) frosting morphology of hydrophilic (S1), hydrophobic (S2), and superhydrophobic (S3) surfaces at  $-12\text{ }^\circ\text{C}$  and  $100\text{ s}$  [72]; (c)  $\tau_{\text{ice}}$  of coated aluminium and untreated bare aluminium substrates [73]; (d) The electronic tensile testing machine showed the coating/substrate interfacial strength [74]; (e) Preparation process of ZnO/SiO<sub>2</sub> multi-scale superhydrophobic coating [75].

Lei et al. [72] developed a  $\text{SiO}_2/\text{silicone rubber}$  coating using a spray coating technique. This coating was superhydrophobic with a WCA of  $165.5^\circ \pm 2.7^\circ$  at room temperature and demonstrated anti-icing results at  $-8\text{ }^\circ\text{C}$ . The superhydrophobicity of the surface delayed icing accretion and reduced the volume of accumulated ice at  $-12\text{ }^\circ\text{C}$  (Figure 3b). The accumulated ice volume on the samples at  $100\text{ s}$  decreased as surface hydrophobicity increased.

Liu et al. [73] fabricated icephobic PDMS coatings modified with fluorosilane and incorporating silica nanoparticles. Hydrophobicity was improved by fluorinating PDMS and incorporating silica nanoparticles. However, they found low  $\tau_{\text{ice}}$  for fluorinated PDMS coatings with no added silica nanoparticles. The freezing of water droplets on the clean

aluminum substrate was 3.2 s, whereas it was 13.8 s for the F-PDMS/silica coating. The F-PDMS had a WCA of 125° before a 90-min erosion test and 127° after. In contrast, the WCA of the F-PDMS/silica coating lowered from 157° to 151° with the erosion. Both coatings showed a similar surface morphology after the erosion test. Moreover, a centrifugal ice adhesion test found shear stress between the ice and the F-PDMS or F-PDMS/silica coatings was well below the 100 kPa threshold of icephobicity and lower than that of the untreated aluminum substrate (Figure 3c).

Zhang et al. [74] recently produced spherical-shaped SiO<sub>2</sub> nanoparticles with a diameter of 90 nm through “RF (radio frequency) plasma spheroidization” and dispersed them effectively within an epoxy resin (E51), PDMS, and ethyl acetate. They subsequently sprayed this mixture on the surface of wind turbine blades that had previously been coated with a polyurethane primer (Figure 3d). This resulted in a superhydrophobic coating showing excellent anti-icing properties, durability against harsh environmental conditions, self-cleaning properties, and resistance to irradiation and abrasion. Coating adhesion is crucial for any coating applied to the surfaces of wind turbine blades. The maximum interfacial stress strength between the coating and substrate was 7.68 mPa, showing superior adhesive strength. Additionally, this coating was cost-effective in terms of raw material and processing.

Bao et al. [75] developed ZnO and SiO<sub>2</sub> multiscale superhydrophobic anti-icing PDMS-based coating for wind turbine blades. They used ZnO and SiO<sub>2</sub> to greatly enhance the mechanical flexibility and improve the coating resistance to heat, weather, and corrosion. Their product delayed freezing by 1511 s, 10.7 times longer than freezing on untreated blade surfaces. The icephobic properties of the coating were evaluated via a custom-made device. In an environment of −10 °C, the uncoated glass slide gradually started to freeze in approximately 6 min, whereas no ice formed on the surface of the ZnO/SiO<sub>2</sub> coating. The excellent mechanical durability of the coating was confirmed through 10 wear test cycles (using sandpaper), after which the CA of the coating remained relatively constant as it decreased only from 153° to 141°, and the sliding angle increased slightly from 3.3° to 6.8° but not by more than 10°. This indicates that even after repeated wearing, the coating retained excellent hydrophobic properties. Moreover, its good mechanical flexibility in outdoor settings and structures and anti-icing properties suggest a strong potential application of this coating in the wind turbine industry. The interfacial strength between the coated surface and the ice is demonstrated in Figure 3e.

A summary of the research conducted on physically modified icephobic silicone-based coatings is provided in Table 3.

**Table 3.** Summary of various studies carried out on silicone-based coatings.

Matrix	Ice Adhesion Measurement Approach	Ice Adhesion Strength	Icephobic Durability	Mechanical Properties	CA/CAH	Reference
ZnO/polydimethylsiloxane	N/A	N/A	Icing delay time: at −15° is 210 ± 25 s. After freezing and 20 thawing cycles (FTC), the CA remained >150°	N/A	CA: 159.5°	[70]
SiO <sub>2</sub> /silicone rubber coating	Accumulated ice of the samples with higher surface hydrophobicity reduced within 100 s	N/A	N/A	N/A	CA: 165.5° ± 2.7°	[72]

Table 3. Cont.

Matrix	Ice Adhesion Measurement Approach	Ice Adhesion Strength	Icephobic Durability	Mechanical Properties	CA/CAH	Reference
Fluorinated PDMS (F-PDMS)/silica	Centrifuge method	Below 100 kPa	After erosion, the WCA of F-PDMS/silica coatings decreased from 157° to 151°	N/A	CA: 157° CAH: 2 ± 0.6°	[73]
ZnO and SiO <sub>2</sub> nanoparticles in PDMS	Lab-made device	No ice was created on ZnO/SiO <sub>2</sub> coating	After 10 wear cycles, CA decreased from 153° to 141°	N/A	CA: 153°	[75]
Mixture of SiO <sub>2</sub> , E51, PDMS, and ethyl acetate	N/A	N/A	The coating exhibited a WCA of 148.82° and 150.02° after 100 icing/de-icing cycles	Interfacial strength of coating/substrate with a tensile machine: 7.68 MPa	CA: 158.1° CAH: 7.2°	[74]

### 2.1.1. Superhydrophobic Surfaces (SHS)

SHS has been presented as the first generation of icephobic materials to promote the rapid elimination of water droplets before they freeze and thereby delay ice nucleation. However, the air pockets that contribute to their hydrophobic properties are vulnerable to disruption in harsh environments, which can compromise the surface structure. As a result, this leads to increased adhesion between the surface and water, reducing the material's ability to repel fluids and diminishing its effectiveness as an icephobic coating. Furthermore, in wind turbine icing conditions, water droplets can impact the blade surface at high speeds, reaching up to approximately 90 m/s near the blade tips [43]. These water droplets that hit the surface can easily penetrate the texture, causing a shift from the “Cassie–Baxter” state to the “fully-wetted Wenzel” state (Figure 4) [76].

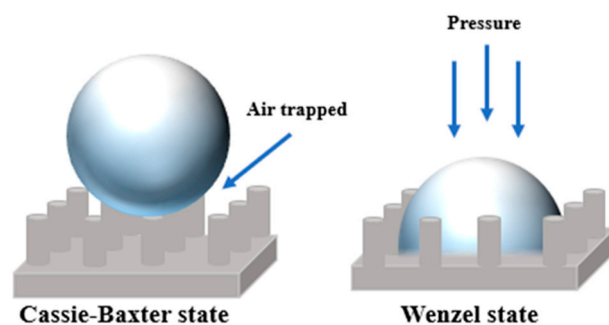


Figure 4. Superhydrophobic surface (SHS) with nano/microscale textures.

As a result, there is a need for the development of innovative, multifunctional surfaces that maintain stable hydrophobic characteristics.

### 2.1.2. Slippery Liquid-Infused Surfaces

Drawing on the functioning of pitcher plants, researchers have begun to investigate liquid-infused surfaces (LISs) [77]. The chemical properties of PDMS and silicone oil share significant similarities, which results in a strong affinity between them. This interaction helps prevent the lubricant in PDMS/silicone oil-based lubricant-infused surfaces (LISs) from being easily lost. This compatibility ensures that the lubricant remains more stable and effective in these systems, thereby enhancing their overall performance and longevity [78]. The preparation of silicon oil-infused polymers, such as dimethyl siloxane (PDMS), is one of the most cost-competitive techniques for creating icephobic coatings [79].

Zhu et al. [79] investigated the anti-icing features of “oil-infused siloxane coatings” with various silicon oil contents. With adding 20 to 40 wt % silicone oil,  $\tau_{ice}$  fell to less than 0.075 MPa, and the CA ranged from 70° to 120° under all testing conditions. However, no investigation was conducted into the durability of these coatings.

Taking inspiration from epidermal glands, Li et al. [80] devised a “slippery liquid-infused porous surface (SLIPS)” with an icephobic lubricant composed of hybrid surfactants, which were strategically placed within a PDMS matrix. After 20 icing/de-icing cycles, their coating exhibited strong mechanical durability. Additionally, its thermal stability was equally impressive, maintaining surfactant presence on the surface even after 60 h at 100 °C. This high thermal resilience is attributed to the encapsulation of the lubricant, which reduced its diffusion rate and effectively prolonged its stability at elevated temperatures. These kinds of coatings, when combined with superhydrophobic coating layers, produce an effective anti-icing method for wind turbines in icy weather conditions. In the study of Coady et al. [81], the durability and icephobic characteristics of “UV-cured silicone resins” mixed with silicone oil were explored. Their coating’s  $\tau_{ice}$  was under 10 kPa at −15 °C and maintained values below 50 kPa across seven icing/de-icing cycles. These properties indicate its significant suitability for turbine blade applications [73,82].

He et al. [83] manufactured a crosslinked solid lubricant SLIPS for wind turbine blades. In their study, a solid lubricant was integrated into industrial fluorinated silicone rubber, known for its hydrophobic nature and low sliding angle. This process created a durable bond with the substrate, producing a surface with excellent hydrophobic properties. The  $\tau_{ice}$  stayed consistently low at 44.1 kPa, even following 15 cycles of icing and de-icing. Cao et al. [84] studied and compared the wetting properties of “lotus leaf-based superhydrophobic” and “pitcher plant-based lubricant-infiltrated slippery surfaces”. The superhydrophobic silicone-based coating (WCA  $\sim 150^\circ \pm 2^\circ$ , SA  $\sim 4.3^\circ \pm 0.4^\circ$ , optical transparency  $< 10\%$ ) was developed on a glass substrate through dip coating, using a homogenous mixture of hydrophobic fumed silica nanoparticles and poly(dimethylsiloxane). Meanwhile, the slippery liquid-infused surface (WCA  $\sim 96^\circ \pm 1^\circ$ , SA  $\sim 7.8^\circ \pm 1.2^\circ$ , optical transparency  $\sim 90\%$ ) was achieved by infusing silicone oil into the superhydrophobic coating.

Lubricant infusion was achieved by using a syringe to inject the lubricants into the SHS, causing the fluid to spread spontaneously [85]. The applied lubricants were a per-fluorinated fluid (Fluorinert™ FC-70), kerosene, and silicone oil, collectively referred to as “SLIPS 1–3”. The surface demonstrated a CA of 162°, self-cleaning properties, and mechanical durability—the CA was 155° after 1100 cm of abrasion. Water droplets effortlessly slid off the SLIPS at −20 °C, while on the superhydrophobic surface, they stayed fixed at all temperatures. They claimed that the “slippery properties of SLIPS demonstrated outstanding mechanical durability, with resistance to abrasion, corrosion, tape peeling, and impact from drops”. Although SLIPS showed superior anti-icing properties compared to SHS, their wettability was also impacted by the condensation of air humidity. In “wet” and low-temperature conditions, the traveling speed was reduced [85]. Barthwal et al. [86] A slippery anti-icing coating was created by embedding non-toxic, affordable silicone oil into aluminum surfaces with superhydrophobic dual-scale micro/nanostructures (MNS). A process involving chemical etching and anodization, followed by surface modification with PDMS, was used to manufacture the superhydrophobic surfaces. They measured ice adhesion with a home-built cooling stage at −10 °C at a relative humidity of  $52\% \pm 6\%$ . The ice adhesion of the (silicone oil-infused polydimethylsiloxane) SOIP was the lowest compared to PDMS and Si oil ( $22 \pm 5$  kPa). The MNS surfaces, modified with low surface energy materials such as Superhydrophobicity, were achieved with PDMS and PFOTS, resulting in WCAs of 159° and 161°, respectively. Furthermore, after the infusion with Si

oil, the WCA of the resulting SOIP surface decreased to  $104^\circ$ . Following 15 icing/de-icing cycles, the MNS surface modified with the SOIP coating retained a low  $\tau_{ice}$  of 81 kPa.

Nonetheless, SLIPS may experience reduced durability due to the depletion of lubricant with each icing/de-icing cycle [81,87,88]. In contrast, self-crosslinking coatings could be more durable and show interfacial slippage [26]. For instance, Yuan et al. [66] prepared fluorinated polysiloxanes via varying grafting densities of fluorinated groups using a hydrosilylation reaction of PMHS and tridecafluorooctyl methacrylate (13FMA). After adding vinyltriethoxysilane (VTES), the prepared polymers underwent self-crosslinking to produce icephobic coatings. When the fluorinated polysiloxanes were grafted with an appropriate content of 13FMA and VTES, supercooled water droplets could easily slide off the tilted surface at  $-15^\circ\text{C}$ , attributed to its high receding CA and low ( $\tau_{ice}$ ) of  $83 \pm 2$  kPa. Table 4 provides an overview of these discussed studies.

**Table 4.** Summary selected research conducted on slippery liquid-infused surfaces.

Coating	WCA/CAH	Temperature ( $^\circ\text{C}$ )	Ice Adhesion (kPa)	Icing/De-Icing Cycles	Reference
PDMS coatings infused with Si oil in the presence of a Pt catalyst	CA: $118^\circ$	$-10$	50	N/A	[79]
SLIPS coating with gland-like storage	AA/RA <sup>1</sup> : $75.1^\circ/15.0^\circ$ to $80.2^\circ/12.0^\circ$	$-18$	46.2 to 18.0	40.8 kPa after 20 cycles	[80]
Silicone resins cured with UV light, combined with silicone oil	CA $100^\circ$	$-15$	<10	<50 kPa after 7 cycles	[81]
Introducing a solid lubricant in an inherently hydrophobic fluorinated silicone rubber	CA: $98^\circ$	$-20$	38.5	44.1 kPa after 15 cycles	[83]
SLIPS-coated aluminum surface	CAH: $2 \pm 1$	$-10, -20$	$15.6 \pm 3.6$	N/A	[84]
Perfluorotripropylamine, kerosene, and silicon oil within the superhydrophobic surface	CA: $162^\circ$	$-15, -20$	N/A	N/A	[85]
Superhydrophobic MN-surface modified with PDMS	CA: $104^\circ$	$-10$	$22 \pm 5$	81 kPa after 15 cycles	[86]

<sup>1</sup> AA: Advancing angle RA: Receding angle.

## 2.2. Chemically Modified PDMS-Based Icephobic Coatings

PDMS has been extensively used for anti-icing purposes. Because of the flexibility of PDMS at low temperatures ( $T_g = -123^\circ\text{C}$ ) and its low surface energy, these materials are fitting candidates for icephobic coatings. The difference in the mechanical properties of PDMS-based polymers and ice can minimize mechanical interlocking and thus decrease  $\tau_{ice}$  [11,49]. However, PDMS-based materials suffer from poor mechanical properties. Chemical modification strategies can be a good approach for improving the characteristics of silicone-based polymers. These modifications include tailoring the crosslink density and, thus, elastic modulus, surface modification, and copolymerization or grafting with other functional groups.

### 2.2.1. Tailoring the Crosslink Density/Elastic Modulus of Silicone

SYLGARD™ 184, a commercial two-part, platinum-cured silicone elastomer product, is characterized by good physical and chemical stability; it is used in a wide range of research [11,89,90]. The final modulus of the SYLGARD 184 is influenced by the mixing proportion of the resin and the curing agent—higher proportions of resin relative to the curing agent result in reduced stiffness [90]. Meuler et al. [89] showed an average  $\tau_{ice}$  of  $291 \pm 44$  kPa for a spin-coated SYLGARD 184 coating, and Wynne et al. [11] showed the inverse relationship between  $\tau_{ice}$  and the thickness of SYLGARD 184 film (Figure 5a). In a recent review, Zhang et al. [52] identified a reference coating thickness value ( $t_{10\%} = 500$   $\mu\text{m}$ ) that can be used for optimizing the design of icephobic polysiloxane coatings (Figure 5b).

Several works have concentrated on reducing the elastic modulus to decrease  $\tau_{ice}$  [24,26,91–93]. Varying the resin-to-curing agent ratio of the PDMS is a common strategy for altering the elastic modulus of PDMS [24]. Tuteja et al. [26] tailored the crosslink density ( $\rho^{CL}$ ) of PDMS to optimize the surface elastic modulus and enable interfacial slippage to achieve ultra-low ice adhesion ( $\tau_{ice} < 0.2$  kPa), regardless of material chemistry (Figure 5(c1–c4)). These coatings consistently retained  $\tau_{ice}$  values below 10 kPa, even after enduring harsh conditions, including high abrasion, “acidic/alkaline” treatment, 100 cycles of icing and de-icing, thermal fluctuations, corrosive environment, and prolonged exposure to winter weather. However, when the elastic modulus is reduced, the number of unattached PDMS chains increases, which negatively affects the robustness of PDMS for industrial applications, including wind turbines, which require a physically and chemically robust coating.

Organogels, which can release fluids from their inner gel frameworks to their external surfaces in response to an alteration in environmental conditions such as temperature, have a lower elastic modulus than elastomers. By relying on this feature, called syneresis, new coatings are developed that have exceptional surface functionalities. Hozumi et al. [92] developed self-lubricating organogels (SLUGs) through crosslinking PDMS in various organic liquids (Figure 5(d1)), demonstrating repellence to a variety of liquids, regeneratable superhydrophobicity and thermoresponsive anti-icing characteristics (Figure 5(d2,d3)).

Kota et al. [91] fabricated eco-friendly, inexpensive PDMS gels that provide super-low ice adhesion and improved mechanical endurance. Gels were prepared through the hydrosilylation reaction between vinyl-terminated PDMS (v-PDMS) and hydride-terminated PDMS (h-PDMS). To reduce the crosslink density, the authors also tuned the modulus by incorporating non-reactive trimethyl-terminated PDMS (t-PDMS) oil in the blend (Figure 5(e1)). Separation pulses separated the ice from the PDMS gels (Figure 5(e2)). Exposure to 1000 abrasion cycles using 400-grit sandpaper did not alter their super-low  $\tau_{ice}$  (Figure 5(e3)). These coatings’ low elastic modulus contributed to lowering the  $\tau_{ice}$  to lower than that of any commercially available icephobic coating (NuSil R2180,  $\tau_{ice} = 37$  kPa) [94].

Zhang et al. [95] simultaneously combined three mechanisms for lowering  $\tau_{ice}$ : decreasing surface energy, reducing elastic modulus, and raising possible crack length in the coating/ice interface. This approach yielded a super-low ice adhesion of around six times less than that reported in their earlier work [24]. They designed a series of 3D porous sandwich-like PDMS sponges (Figure 5(f1,f2)) by tuning the resin to curing agent proportion and achieved a minimal  $\tau_{ice}$  of 0.9 kPa for neat PDMS, which remained constant through 25 icing/de-icing cycles. A similar mechanism can be applied to fabricate icephobic coatings having ultra-low  $\tau_{ice}$ ; however, the significant thickness of the sandwich-like PDMS sponges (4.8 mm) remains an issue needing to be addressed for its practical application.

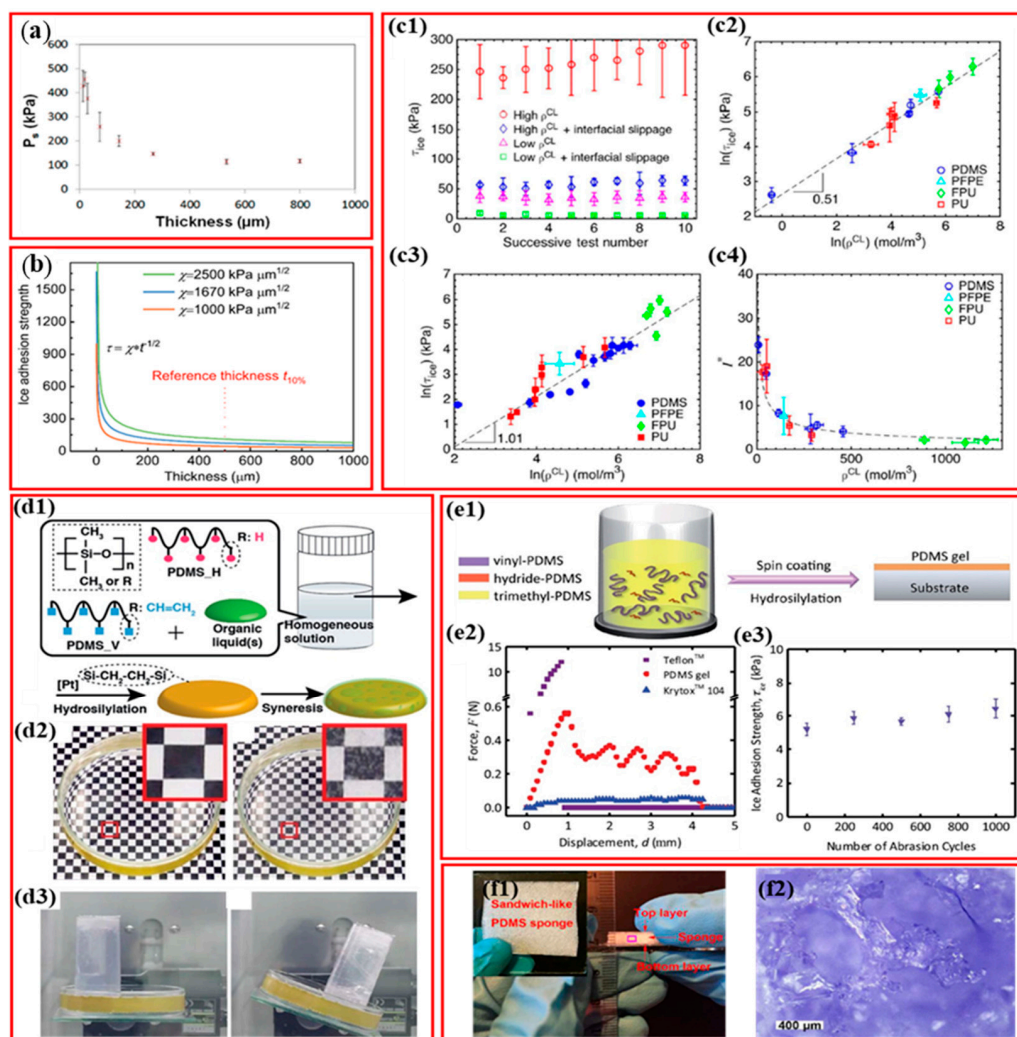


**Figure 5.** (a) Maximum shear removal force ( $P_s$ ) for ice release vs. thickness for Sylgard 184 on glass microscopic slide at a 0.05 mm/s shear velocity [11]. (b)  $\tau_{ice}$  vs. film thickness for polysiloxanes [52]. (c1–c4) Describing the mechanisms behind minimal ice adhesion by tailoring the cross-link density, (c1) PDMS films with low or high  $\rho^{CL}$ , with or without interfacial slippage, (c2) Correlation amid  $\rho^{CL}$  and  $\tau_{ice}$  for films without interfacial slippage, (c3) Change in  $\tau_{ice}$  with  $\rho^{CL}$  for films having interfacial slippage, (c4) Potential to decrease ice ( $I^*$ ) vs.  $\rho^{CL}$  [26]. (d1) schematic of creation of organized and syneresis induced by gelation, (d2) Thermoresponsive behavior of organogels ((left) initial and (right) after incubation for 6 h at  $-15\text{ }^\circ\text{C}$ ), (d3) Anti-icing properties of organogel [92]. (e1) Schematic illustration of the PDMS gels formation with tunable shear modulus, (e2) Force-displacement curves recorded through the  $\tau_{ice}$  measurement on Teflon<sup>TM</sup>, the PDMS gel, and Krytox<sup>TM</sup> 104 at  $0.8\text{ mm s}^{-1}$  probe velocity, (e3) The ultra-low  $\tau_{ice}$  of the PDMS gels remained nearly unaltered after 1000 abrasion cycles [91]. (f1) Photo of sandwich-like PDMS sponge (thickness = 4.8 mm), (f2) The microscopy images of the pink marked area in (f1) depicting the PDMS sponge structure [95].

Recently, linear nanometer-thick PDMS-based polymer brushes have gained significant interest for anti-icing applications [96–98]. The nearly negligible shear modulus of these PDMS coatings allows them to behave similarly to liquids. This property arises from the low rotational energy of PDMS ( $1.9\text{ kJ}\cdot\text{mol}^{-1}$ ), which is below the ambient thermal energy threshold ( $kT \approx 2.5\text{ kJ mol}^{-1}$ ) [99] and contributes to their exceptionally low glass transition temperature ( $T_g$ ), unattainable in carbon-based polymers [100]. These coatings enable ice to easily slide on their surface, resulting in ultra-low ice adhesion strength values that are even lower than 1 KPa [101].

The rebound properties of coating to rapidly shed impacting water/ice droplets also play a key role in reducing ice accumulation. Traditional strategies for reducing the contact time of impacting droplets focus on engineering superhydrophobic surfaces by introducing secondary textures at macroscopic or nanoscopic scales or creating specifically designed nanotextures. Recently, it has been shown that incorporating liquid-like polymer chains with surface micro-/nano-textures can significantly improve the rebound properties of coatings. This improvement is attributed to reduced adhesion of water droplets compared to coatings with low-surface-energy, solid-like polymer brushes [102]. Fan et al. [102] reported a 26% reduction in water contact time when transitioning from solid-like to liquid-like brushes on a textured surface.

On the other hand, while soft elastomers and gels can have ultra-low  $\tau_{ice}$ , as low as 10 kPa, their ultra-low modulus restricts their mechanical robustness, especially for high-performance applications, such as for wind turbines, that require durable coatings. These coatings cannot survive long-term exposure to high shear. Moreover, they show very low rain erosion resistance, which makes them unsuitable for wind turbines because they fail to meet the required standards. Enhancing the icephobicity of coatings solely by relying on ultrasoft elastomers is thus not realistic.

### 2.2.2. Surface Modification

The surface energy of silicon-based coatings can also be modified through various strategies [86–96]. For instance, Yan and coworkers [103] used a  $CF_4$  plasma modification to reduce the surface energy of PDMS samples. They found that short plasma durations ( $\leq 15$  min) adequately fluorinate PDMS surfaces and form a macromolecular fluorocarbon layer. This process increases the fluorine concentration, reduces surface energy, and decreases smoothness. For plasma durations of 15–30 min, a proper equilibrium amid fluorination and ablation ensures the stability of surface texture, fluorine levels, and the ratio of  $[F - Si]/[F - C]$ . Longer durations (45 min) remove the fluorinated layer, significantly increasing surface texture and the proportion of  $[F - Si]/[F - C]$  while decreasing the surface fluorine content.

Chen et al. [104] prepared sol-gel films with various surface energies and textures on glass substrates. These researchers utilized 3-glycidyloxypropyl trimethoxysilane (GLYMO), methyltriethoxysilane (MTEOS), and fluoroalkylsilane (FAS) to achieve a mechanically durable film. MTEOS served as the crosslinking agent, GLYMO as the coupling agent, and FAS as the agent to decrease the surface energy. They observed that reduced roughness in conjunction with decreased surface energy reduced the  $\tau_{ice}$ . Zhang et al. [105] reduced the surface energy of a silicon substrate with FAS (1H,1H,2H,2H-perfluorodecyltrichlorosilane; FAS-17) to investigate the ice nucleation kinetics on hydrophobic surfaces. The rate of ice formation on an unmodified hydrophilic silicon wafer surface was approximately ten times slower than that on a hydrophobic silicon surface modified with FAS-17. This difference was influenced by water viscosity at the interface and surface roughness. Higher water viscosity on hydrophilic surfaces increases the activation energy for ice nucleation, whereas the slightly rougher surface of hydrophobic surfaces may accelerate ice nucleation. Zhang et al. [24] decreased the PDMS surface energy via perfluorodecyltrichlorosilane silanization to enhance the nanoscale crack initiation at the ice-coating interface. Nevertheless, earlier studies have shown that the ice adhesion drop by mere surface modification is limited.

### 2.2.3. Copolymerization and the Grafting of Silicone

During the past few years, silicon-based copolymers have attracted significant interest due to their capacity to combine desirable qualities of organic polymers, e.g., low dielectric

constant, mechanical integrity and strength, with the exceptional bulk and surface characteristics of silicones. Chemically modified silicone copolymers are particularly attractive because they integrate the benefits of both silicones and the integrated components. Various strategies, such as living anionic polymerization, ring-opening polymerization (ROP), atom transfer radical polymerization (ATRP), and step-growth polymerization, are commonly used to prepare silicone-based copolymers [106,107]. A review by Yilgor et al. [106] delves into the synthesis methods and processes of silicone-based copolymers, which is beyond the scope of the present review.

Fluorinated polymers, which possess unique surface characteristics, including low surface energy and a small dielectric constant ( $\epsilon \approx 2.1$ ), are also considered excellent candidates for icephobic coatings [108,109]. Conversely, the water and fluorocarbon groups have an interaction energy that is 3 times greater than that of water and the siloxane group [110]. Consequently, water droplets do not easily slide on fluoropolymer surfaces because of the strong fluorocarbon–water interaction. Recently, a growing interest has emerged in creating fluorosilicone copolymers. By joining both fluorine and silicone on a heterogeneous polymer surface, the interaction energy of water and coating is reduced when a water molecule faces both groups [111]. Fluorosilicone coatings combine the merits of both silicone and fluorinated polymers, resulting in synergistic effects that decrease CAH and  $\tau_{ice}$  [110,112–114]. Furthermore, earlier research has shown that fluorosilicone coatings reduce ice adhesion relative to pure silicone coatings [110,114].

Yuan and coworkers have made significant advances in developing icephobic fluorosilicone copolymer coatings [49,66,111,115–120]. The incompatibility of block structures can cause microphase separation not only in bulk material but also on the surface of block copolymers. In this regard, Yuan et al. [111] developed icephobic coatings of polydimethylsiloxane-*b*-poly(fluorinated acrylate) (PDMS-*b*-PFA) block copolymers and spin-coated them onto a substrate. The synthesis process of the PDMS-*b*-PFA block copolymers, prepared via radical polymerization, is shown in Figure 6(a1). They found that as the PDMS concentration decreased from 50 to 15 wt % (PF1 to PF4), the size of domains was reduced from 90–200 nm to 40–65 nm (Figure 6(a2)), and they realized a decrease from  $46.1^\circ \pm 4.98^\circ$  to  $21.2^\circ \pm 3.05^\circ$  in CAH. In addition, the ice adhesion and shear strengths exhibited a declining trend from 28 kPa to 17 kPa and from 305 kPa to 187 kPa from PF1 to PF4, respectively (Figure 6(a3)). PF4, with 6.7% surface fluorine and 10.4% silicone (the highest studied F/Si ratio), displayed the best icephobic characteristics, primarily because of the surface “flexible–hard” microphase-separated morphologies and the collaborative impact of silicon and fluorine, which reduces the ice/coating interactions. In another study by this group [115], with the usage of a PMTFPS macroinitiator (PMTFPS-MAI), five block copolymers of polymethyltrifluoropropylsiloxane (PMTFPS) and polyacrylate (PMTFPS-*b*-polyacrylate) were prepared via free radical polymerization of methyl methacrylate, *n*-butylacrylate, and hydroxyethyl methacrylate (Figure 6(b1)). In this study, ice shear strength ( $\tau_{ice}$ ) was evaluated using a custom-built cooling stage (Figure 6(b2)). The surface and bulk characteristics of the coating were different due to the migration of PMTFPS segments to the air-surface interface as the film formed. The relative molar mass and composition of the PMTFPS-*b*-polyacrylate were linked with the microphase separation (Figure 6(b3,b4)). A PMTFPS-MAI content of 20 wt % produced the longest freezing delay (186 s at  $-15^\circ\text{C}$ ) and the lowest  $\tau_{ice}$  ( $301 \pm 10$  kPa) of the tested coatings.

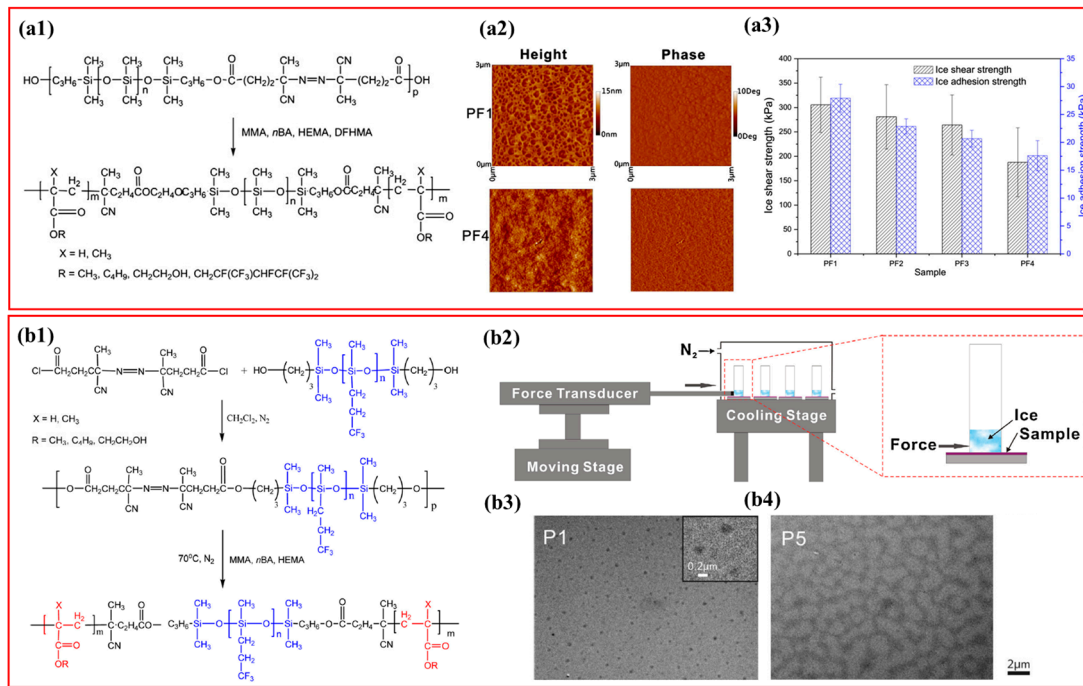


**Figure 6.** (a1) PDMS-b-PFA block copolymers preparation, (a2) AFM topography and phase photographs of the PDMS-b-PFA coatings (area of 3 μm × 3 μm), (a3) Ice adhesion and  $\tau_{ice}$  s of the PDMS-b-PFA coated on Al substrates [111]. (b1) PMTFPS-b-polyacrylate copolymers preparation, (b2)  $\tau_{ice}$  measurement setup, (b3,b4) TEM images of PMTFPS-b-polyacrylate on Al plates [115].

In icephobic systems, water droplets fail to slide off the copolymer surface and cannot rebound upon impact, leading to ice accumulation. Increasing the receding CA to over 100° or minimizing CAH can achieve rapid de-wetting and droplet rebound [115,116,121].

Surface morphology greatly affects the icephobic properties of materials. Surfaces with nanoscale roughness exhibit better icephobic behavior than those with microscale roughness [116,122–124]. Polyhedral oligomeric silsesquioxane (POSS) is a hybrid organic–inorganic framework with a cage-like inorganic silicon-oxygen cubic core surrounded by organic corner groups. It can enhance the mechanical properties, thermostability, hydrophobicity, and surface roughness of polymers [125–128]. POSS can be incorporated into polymers via free radical polymerization [49,129], living anionic polymerization [130,131], and ATRP [132–134]. Reversible addition–fragmentation chain transfer (RAFT) polymerization is another route for creating complicated polymer structures with controlled molecular weight [135–142] to improve the chemical stability and physical characteristics of the polymers. The adaptability of the RAFT technique makes it a favorable selection for incorporating sterically hindered POSS into polymers [138–140,143–145].

Yuan et al. [116] prepared POSS-containing fluorosilicone multi-block methacrylate copolymers (PDMS-b-(PMAPOSS-b-PFMA)<sub>2</sub>) using RAFT technique. They used methacryloisobutylPOSS (MAPOSS) with hexafluorobutyl methacrylate (HFBMA) or dodecafluoroheptyl methacrylate (DFHMA) and a dithiobenzoate-terminated PDMS as a macro-RAFT chain transfer agent. They observed that compared to PHFBMA, PDFHMA chains having longer fluorinated functionalities migrated more readily onto the surface. Adding PMAPOSS segments improved surface roughness and reduced the  $\tau_{ice}$  from 361 to 264 kPa. The multi-block PDMS-b-(PMAPOSS-b-PDFHMA)<sub>2</sub> coating had a fluorine-rich surface, a receding CA of 103.8 ± 0.5°, and a CAH of 8.7 ± 1.4°. Water droplets could effortlessly slide off the tilted coating (45°) at –20 °C. After the  $\tau_{ice}$  experiment, the absence of remaining ice on the S-POSS-12F (F/Si = 2.34) demonstrated a loose ice assembly at the ice–coating interface (Figure 7(a3)).

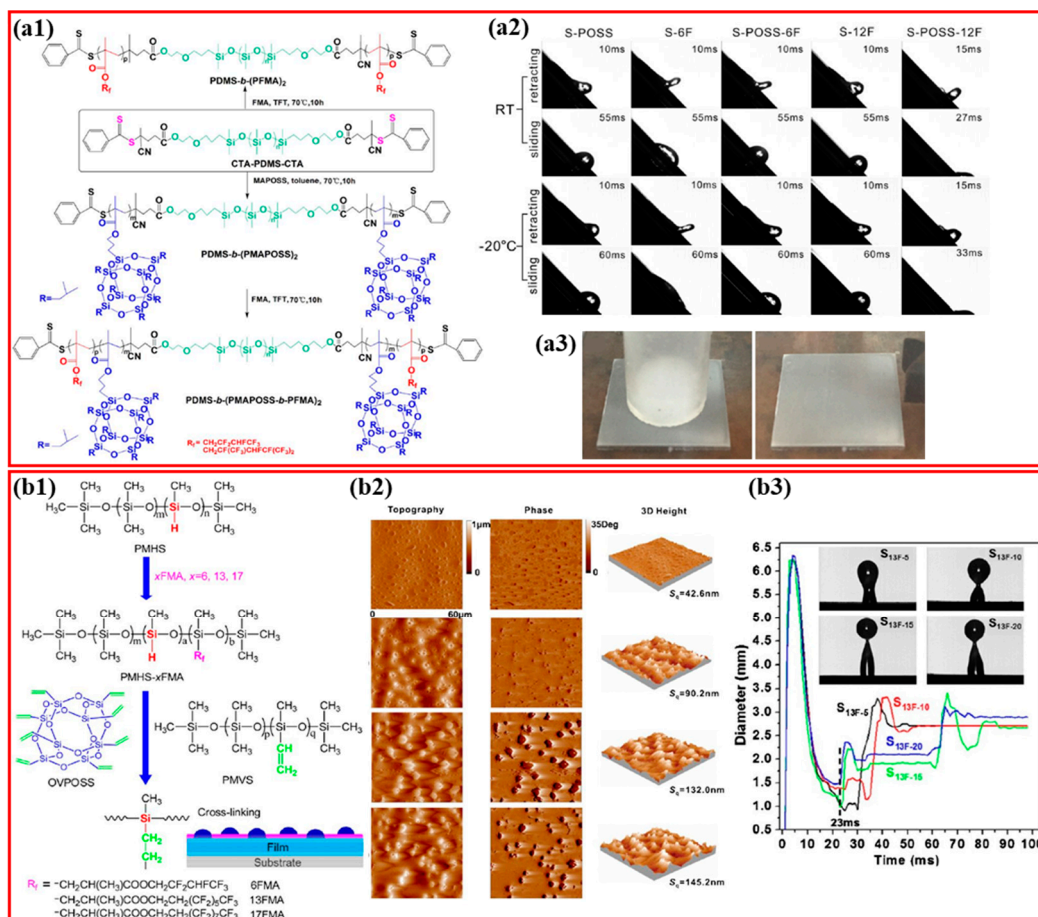


**Figure 7.** (a1) Preparation of “PDMS-b-(PMAPOSS)<sub>2</sub>, PDMS-b-(PFMA)<sub>2</sub> and PDMS-b-(PMAPOSS-b-PFMA)<sub>2</sub>” with RAFT technique, (a2) Photos of the dynamic behavior of 7 μL water droplets placed on the fluorosilicone multi-block copolymers coated on Al plates at a 45° tilting angle at RT or -20 °C, (a3) Photos of the S-POSS-12F film before (left) and after (right) ice shear strength test [116]. (b1) Preparation of fluorinated polymethylsiloxane (PMHS-xFMA) and the development of hybrid coatings by combining PMHS-xFMA with octavinyl-polyhedral oligomeric silsesquioxanes (OVPOSS), (b2) AFM topography images of S13F hybrid coatings with various mass ratio of OVPOSS (from top to bottom: S<sub>13F-5</sub>, S<sub>13F-10</sub>, S<sub>13F-15</sub>, S<sub>13F-20</sub>). (b3) During the droplet impact process on a horizontal S13F surface with different mass fractions of OVPOSS, the contact line diameter evolution was monitored. These copolymer coatings were applied to aluminum (Al) substrates [117].

In another study by Yuan and coworkers [117], they developed icephobic hybrid coatings consisting of fluorinated polymethylhydrosiloxane (PMHS-xFMA) that x can be 6, 13, or 17, in combination with octavinyl-POSS (OVPOSS). The preparation of fluorinated PMHS-xFMA and the creation of hybrid icephobic coatings is achieved through an additional reaction between the vinyl groups of PMHS-xFMA and the Si-H groups of OVPOSS, as shown in Figure 7(b1). By varying the OVPOSS content from 5 to 20 wt %, they could adjust the root-mean-square roughness (S<sub>q</sub>) from 42.6 nm to 145.2 nm (Figure 7(b2)). OVPOSS concentration above 10 wt % and S<sub>q</sub> values greater than 90 nm repelled water droplets (Figure 7(b3)). They also found that longer fluorinated side groups did not improve icephobicity despite enhancing hydrophobicity. Nevertheless, the τ<sub>ice</sub> of these fluorosilicone polymer films remained above 100 kPa, which is the critical τ<sub>ice</sub> beyond which ice cannot be detached naturally with wind and gravity [11,65–67].

Although the icephobicity of polysiloxane coatings has been greatly enhanced, there is still a need to strengthen their mechanical properties to meet practical requirements, such as use as wind turbine coatings.

To address this challenge, Yuan et al. [119] developed robust coatings with self-controlled surface texture using branched PDMS co-crosslinked with fluorinated POSS using a breath figure approach. The surface microtextured facilitated the formation of microcracks at the ice/coating interface with minimal external force, resulting in exceptional anti-icing characteristics. The prepared film with a self-controlled honeycomb texture showed a low  $\tau_{ice}$  of approximately  $19.7 \pm 2.5$  kPa. The coating exhibited a minor rise in  $\tau_{ice}$  after 30 icing/de-icing cycles and over 1600 abrasion cycles, but it remained icephobic ( $\tau_{ice} < 50$  kPa). Thus, the developed films possessed significantly improved anti-icing performance and mechanical robustness, making them suitable for real-world implications.

Photopolymerization has gained interest in recent years because of its fast-curing kinetics at ambient temperature, low energy consumption, and eco-friendly nature [146–149]. Thiol-ene reactions, in particular, have been extensively studied for developing crosslinked surfaces, as they are not affected by oxygen inhibition [150,151]. Inspired by efficient radiation curing technology, Yuan et al. [152] prepared icephobic coatings using thiol-terminated fluorosilicone methacrylate triblock copolymers (PDMS-b-(PFMA-SH)<sub>2</sub>), thiol-functionalized PDMS (PDMS-SH), and OVPOSS (Figure 8(a1)). The photopolymerization reaction of the triblock copolymer coating is shown in Figure 8(a2). However, these coatings achieved only an  $\tau_{ice}$  of approximately 210 kPa. In another study, Yuan et al. [120] synthesized POSS-containing fluorinated methacrylate block copolymers through the RAFT mechanism and altered them into etiolated copolymers via aminolysis to regulate self-assembly and adjust surface morphology (Figure 8(b1)). UV-curable thiol-end reactions were used to prepare icephobic coatings, incorporating varying quantities of thiol-functionalized POSS-fluorinated methacrylate diblock copolymers, vinyl-modified PDMS, and thiol-modified PDMS. These components were combined to create coatings with enhanced ice-repellent properties (Figure 8(b2)). By preventing the agglomeration of PMAPOSS and facilitating the migration of fluorine segments to the surface, the authors observed fluorinated polyacrylate segments in PMAPOSS-b-P13FMA-SH (S13F) and PMAPOSS-b-P17FMA-SH (S17F) (Figure 8(b3)). The prepared UV-cured coatings exhibited  $\tau_{ice}$  s of approximately 12.5% that of the aluminum surface, with the film having 5% S17F providing the minimal  $\tau_{ice}$  of  $105 \pm 12$  kPa. The icephobic action of these systems mainly arises from the combinatory impact between the POSS-fluorinated methacrylate copolymer and the PDMS segment.

The introduction of fluorinated POSS can lead to very low  $\tau_{ice}$  values. However, it is a difficult and costly preparation process that hinders its practical application, especially for large-scale industrial applications like wind turbines. Moreover, the degradation products of fluorosilicone polymers, which contain fluorine, can adversely affect the environment and potentially harm humans [153]. As a result, there has been a recent focus on limiting the use of fluorosilicone polymers. Researchers are now seeking more eco-friendly icephobic coatings to replace fluorosilicone-based coatings.

Epoxy-based coatings with excellent thermal properties, good abrasion resistance, superior chemical resistance, mechanical durability, and adhesion to metallic substrates [154,155] are another interesting candidate that improves the mechanical durability of silicone-based coatings for industrial anti-icing applications such as wind turbines. Epoxy-based coatings possess an outstanding Young modulus of about 3.8 GPa [156]. However, epoxy-based coatings have a brittle nature and poor hydrophobicity and icephobicity [157,158]. To address these issues, combining epoxy-based coatings with soft hydrophobic silicone-based components is an interesting approach that enhances their flexibility and icephobicity [159–161]. In silicone-epoxy hybrid coatings, the comparatively rigid epoxy polymer modifies the weak mechanical features of the silicone polymer and introduces firm siloxane linkages, which improves the UV resistance of the epoxy poly-

mer [162,163]. Furthermore, according to Kendall's theory, the small Young modulus of the silicone segment improves the icephobicity of the hybrid coating [159,164].

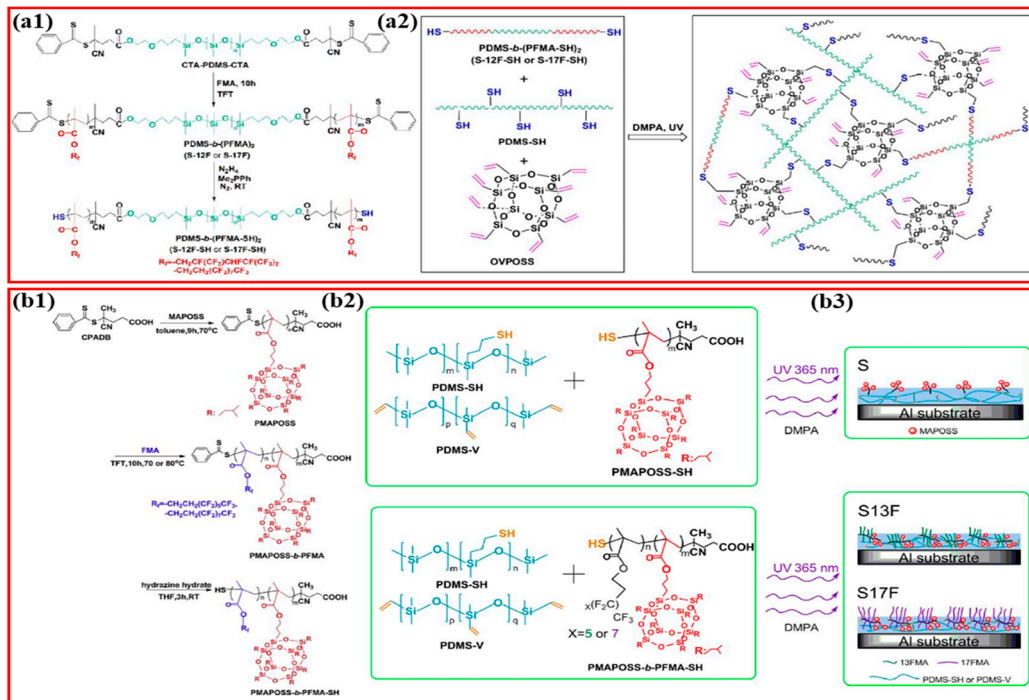


**Figure 8.** (a1) Preparation of PDMS-b-(PFMA)<sub>2</sub> and PDMS-b-(PFMA-SH)<sub>2</sub> copolymers, (a2) Synthesis of photocrosslinkable fluorosilicone triblock methacrylate copolymer coatings [152]. (b1) Preparation of thiol-modified PMAPOSS-b-PFMA-SH via RAFT approach, (b2) Schematic illustration of the development of the icephobic coating from photocrosslinkable POSS-fluorinated methacrylate diblock copolymers, (b3) PMAPOSS aggregates migrated to the surface throughout the spin coating process on Al and photocrosslinking in PMAPOSS-SH (S) comprising film [120].

Momen et al. [159] recently developed an icephobic coating for steel substrates on marine harbor infrastructures. The coating, based on silicone-epoxy hybrid resins (SILIKOPON<sup>®</sup> EF&ED, Evonik company) and amino-functional silane-curing agents, exhibited superior mechanical characteristics and weathering resistance for outdoor utilizations (Figure 9(a1–a4)). They also investigated the relationship between  $\tau_{ice}$  and various film properties and showed that ice adhesion behavior in silicon-epoxy hybrid coatings can be predicted by the Young modulus. Moreover, they modified the surface energy properties of the best-performing coating formulations using two fluorinated silicone additives, resulting in a decrease in  $\tau_{ice}$  from 362 to 94 kPa. Ziętkowska et al. [165] fabricated icephobic coatings for photovoltaic panel applications. They modified a silicone-epoxy hybrid resin (SILIKOPON<sup>®</sup> ED) using dually functionalized polysiloxanes and observed a significant improvement in icephobicity. The  $\tau_{ice}$  decreased by 69% (below 100 kPa), and the freezing delay time increased 17-fold relative to the unmodified coatings. The silicon-epoxy coatings exhibited a CAH of 7° to 11° and a roll-off angle of 32° to 55°.

Despite these promising findings, there remains a need for further research to develop mechanically robust icephobic silicone-epoxy hybrid coatings suitable for industrial applications.

Although acrylate-modified polysiloxanes, such as “poly(methylmethacrylate)-g-poly(dimethylsiloxane) (PMMA-g-PDMS)”, have been used in various applications, e.g., antifouling coatings [166,167], there are limited reports on the fabrication of icephobic silicone-polyacrylate coatings. In the work of Yuan et al. [49], two polyacrylate-PDMS copolymers were prepared: polyacrylate-b-PDMS and polyacrylate-g-PDMS. These copoly-

mers were designed to have PDMS blocks or side chains of various molecular weights (Figure 9(b1)). The copolymer solutions were then sprayed onto aluminum substrates. Microphase separation was evident in all samples, particularly the block copolymers (Figure 9(b2)). As a result, the aggregated PDMS chains on the copolymer surface reduced coating–water interactions, primarily hydrogen bonds, leading to a decrease in CAH ( $33.5^\circ$ – $44.7^\circ$ ). Incorporating PDMS into the copolymers resulted in significantly inferior  $\tau_{ice}$  values of 22–45 kPa in comparison with commercial polyacrylate-polyurethane coatings. Hence, these copolymers show promise for developing icephobic coatings for practical applications.

Several attempts have been made to modify silicone-based coatings with different polymers to develop icephobic coatings having improved properties over silicone. In their 1978 pioneering work, Jellinek et al. [168] prepared ice-releasing copolymer coatings using poly(PDMS-*b*-polycarbonate). They discovered that  $\tau_{ice}$  depends on several factors, including the copolymer's glass transition temperature, siloxane content, block length, and the hydrophobic nature of the coating surface. Kozera et al. [169] enhanced an unsaturated polyester polymer by incorporating double-organo-modified polysiloxanes, achieving a 30% reduction in ice adhesion and an enhancement in water contact angle (WCA) in comparison with the unmodified resin. In 2020, Xiao et al. [67] incorporated symmetric 4,4'-Methylenebis(phenyl isocyanate) (MPI) into the PDMS (Figure 9(c1)) and produced durable PDMS-based icephobic coatings with an  $\tau_{ice}$  of 52.2 kPa following 20 icing/de-icing cycles (Figure 9(c2)). The film also exhibited rapid self-healing capacity, with more than 80% self-healing within 45 min at RT because of the presence of abundant hydrogen bonds that ensure durability in harsh environments.

To achieve a future with effective anti-icing capabilities, it is crucial to investigate the synergistic effects of various icephobic strategies incorporated into coatings and discover new strategies to achieve super-low  $\tau_{ice}$ . Improving the durability of silicone-based coatings to obtain optimally low  $\tau_{ice}$  requires a delicate balance of low elastic modulus and mechanical robustness, which is a challenge that currently hinders the industrial application of silicone-based materials like wind turbines. Another major challenge is scaling up laboratory-prepared coatings for industry use, as it is uncertain what minimum value of ice adhesion is sufficient for industrial use. Considering that a variety of ice is present under various conditions, it is necessary to develop icephobic coatings tailored to specific applications, such as wind turbines. Strategies that accelerate self-healing may be greatly advantageous. Additionally, addressing the relatively low adhesion of soft silicone-based materials to solid substrates is another significant challenge that requires further research. Please refer to Table 5 for a summary of chemically modified silicone-based coatings.

Table 5. Summary of various studies performed on chemically modified Silicone-based coatings.

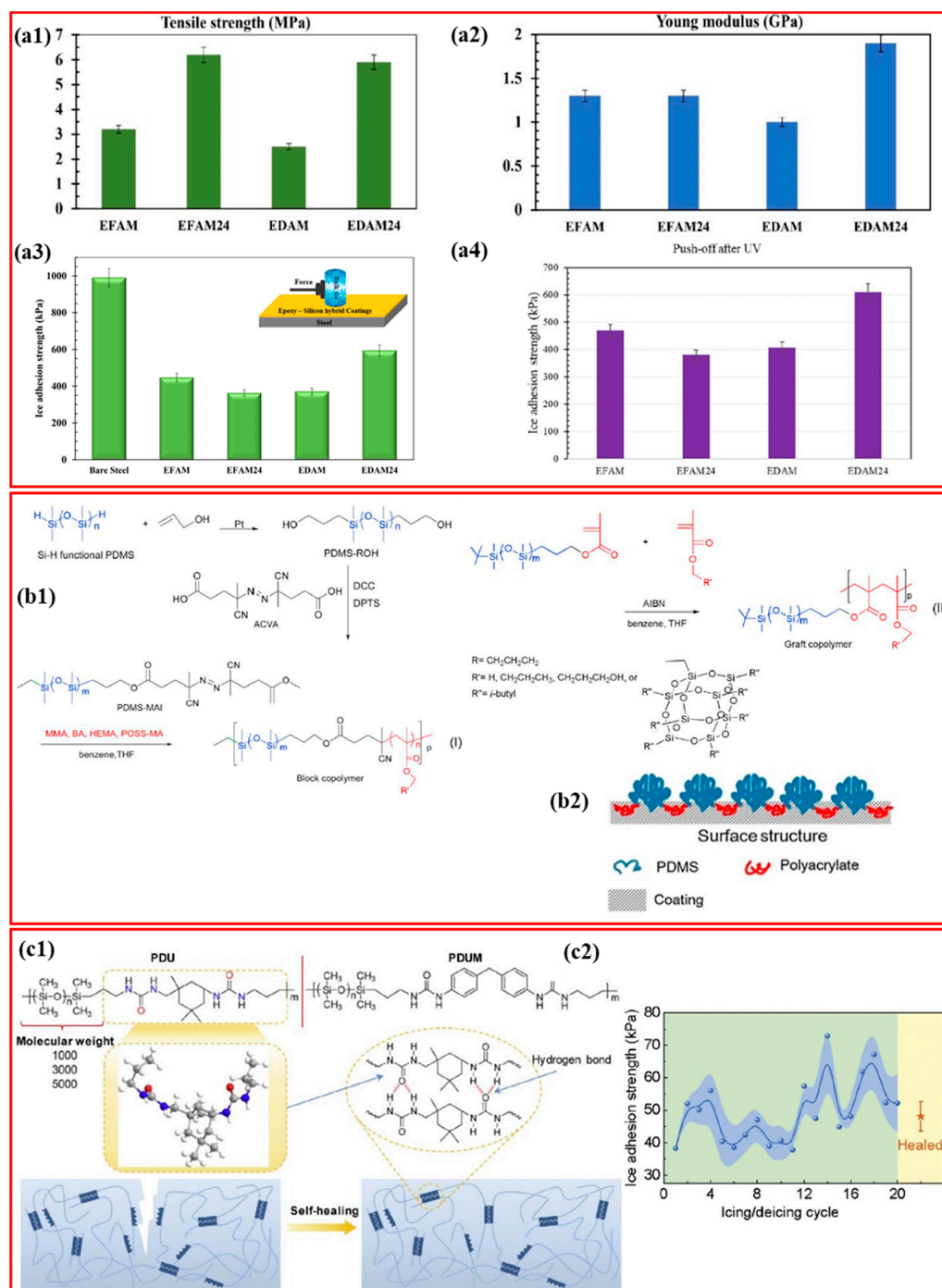
Coating	Ice Adhesion Measurement Approach	Ice Adhesion Strength ( $\tau_{ice}$ ) (kPa)	Icephobic Durability	Mechanical Properties	Weathering Resistance	Ref.
PDMS/interfacial slippage	A custom-built apparatus to test $\tau_{ice}$	<0.2	$\tau_{ice}$ after 5000 abrasion cycles (ASTM D4060), acid and base treatment, 100 cycles of icing/de-icing, thermal cycling, accelerated corrosion, and facing Michigan wintery climate more than 4 months: <10 kPa	Elongation at break: >1000%	N/A	[26]
V-PDMS-h-PDMS/t-PDMS gels	A custom-built apparatus to test $\tau_{ice}$	5.2	$\tau_{ice}$ following 1000 abrasion cycles using 400-grit sandpaper: <10 kPa	Shear modulus: 10–100 kPa	N/A	[91]
3D porous sandwich-like PDMS sponges	Vertical shear test using an Instron mechanical testing system equipped with a homemade cooling system	0.9	$\tau_{ice}$ after 25 icing/de-icing cycles: 1 kPa	Elastic modulus: 0.1–2.5 MPa	N/A	[95]
PDMS-b-PFA	A universal testing apparatus equipped with a 100 N load cell in a pull-off mode for $\tau_{ice}$	17	N/A	N/A	N/A	[111]
	A custom-built cooling stage in pull and push mode to test $\tau_{ice}$	187				
PMTFPS-b-polyacrylate	A custom-built cooling stage in pull and push mode to test $\tau_{ice}$	301	N/A	N/A	N/A	[115]
PDMS-b-(PMAPOSS-b-PFMA) <sub>2</sub>	A custom-built cooling stage in pull and push mode to test $\tau_{ice}$	264	N/A	N/A	N/A	[116]

Table 5. Cont.

Coating	Ice Adhesion Measurement Approach	Ice Adhesion Strength ( $\tau_{ice}$ ) (kPa)	Icepobic Durability	Mechanical Properties	Weathering Resistance	Ref.
PMHS-xFMA, x = 6, 13, 17	A custom-built cooling stage in pull and push mode to test $\tau_{ice}$	188	N/A	N/A	N/A	[117]
F-POSS-SiH	A custom-built cooling stage in pull and push mode to test $\tau_{ice}$	3.8	$\tau_{ice}$ following 15 icing/de-icing cycles: approx. 30 kPa	N/A	N/A	[118]
PMHS-13FMA-VTES	A custom-built cooling stage in pull and push mode to test $\tau_{ice}$	83	N/A	N/A	N/A	[66]
Branched PDMS co-crosslinked with F <sub>5</sub> -POSS-H <sub>3</sub>	A custom-built cooling stage in pull and push mode to test $\tau_{ice}$	19.7	$\tau_{ice}$ following 30 icing/de-icing cycles, and after 1600 abrasion cycles (400-grit sandpaper, 200 g weight, 4.9 kPa pressure at -15 °C): <50 kPa	N/A	N/A	[119]
PDMS-b-(PFMA-SH) <sub>2</sub>	A custom-built cooling stage in pull and push mode to test $\tau_{ice}$	210	N/A	N/A	N/A	[152]
PMAPOSS-b-P17FMA-SH	A custom-built cooling stage in pull and push mode to test $\tau_{ice}$	105	N/A	N/A	N/A	[120]
SILIKOPON <sup>®</sup> EF&ED-amino-functional silane-curing agent/flurosilicon additive	Push off test	94	N/A	Tensile strength: 2–7 MPa; Elastic modulus: 1–2 GPa; elongation at break: 3.3–3.6%	Gloss index before and after UV exposure: 80.3, 75.8 GU	[159]
SILIKOPON <sup>®</sup> ED-dually functionalized polysiloxanes	A universal testing apparatus to test $\tau_{ice}$	55	N/A	N/A	N/A	[165]

Table 5. Cont.

Coating	Ice Adhesion Measurement Approach	Ice Adhesion Strength ( $\tau_{ice}$ ) (kPa)	Icephobic Durability	Mechanical Properties	Weathering Resistance	Ref.
Polyacrylate-b-PDMS or polyacrylate-g-PDMS	A universal testing machine equipped with a 100 N load cell in a pull-off mode for $\tau_{ice}$	22–45	N/A	N/A	N/A	[49]
PDMS-MPI	Vertical shear test using an Instron mechanical testing system equipped with a homemade cooling system	37	$\tau_{ice}$ after 30 icing/de-icing cycles: approx. 52.2 kPa	Young's modulus: 0.28–20.71 MPa Elongation at break: over 200%; rapid self-healing capacity with more than 80% within 45 min at RT	N/A	[67]



**Figure 9.** (a1,a2) Mechanical properties of the silicone-epoxy matrices, (a3)  $\tau_{\text{ice}}$  of silicone-epoxy hybrid films applied on steel substrates (the inset shows the schematic of push-off testing), (a4)  $\tau_{\text{ice}}$  of films following 300 h UV exposure [159]. (b1) Preparation of polyacrylate-b-PDMS (I) and polyacrylate-g-PDMS (II), (b2) Schematic illustration depicting the surface structure of the copolymer coatings [49]. (c1) Chemical structures and self-healing behavior of PDMS-urea (PDU) and PDMS-modified PDU (PDUM), (c2)  $\tau_{\text{ice}}$  of the PDU3000 film through 20 icing/de-icing cycles (green zone), and following cut/healing test (yellow zone) (“R1 [170], R2 [171], R3 [172], R4 [173], R5 [174], R6 [175], and R7 [176]”) [67].

### 3. Fluoropolymer-Based Coatings

Polymers, exemplified by fluoropolymers, are frequently used in hydrophobic and icephobic coatings. For example, polytetrafluoroethylene (PTFE) is a flexible material

widely used for its water-repellent, non-adhesive and dense. It is particularly famous for its ability to resist sticking, and when tested using a centrifugal ice adhesion apparatus, PTFE exhibited almost no ice adhesion [1,177]. PTFE coating reduces ice adhesion on various infrastructures, such as wind turbine blades, thereby ensuring effective energy production. For instance, Belov et al. [178] developed a protective composite coating for wind turbine blades by applying polytetrafluoroethylene on commercially pure titanium VT1–0. Two types of fluoropolymer suspensions were used to create composite layers: a commercial suspension of F4-d and an isopropanol suspension of super-dispersed polytetrafluoroethylene (SPTFE). The latter produced a  $6\times$  decrease in  $\tau_{ice}$ .

Liu et al. [45] created an icephobic coating for wind turbine blades using fluorocarbon as the primary film-forming material and  $TiO_2$ ,  $SiO_2$ , and micro/nanocomposite particles as fillers. They found that fluorocarbon coupling agents enhance material hydrophobicity, resulting in a contact angle of over  $150^\circ$ . The freezing time of water droplets at  $10^\circ C$  was extended to 1601 s with an ice adhesion of only 76 kPa, demonstrating effective icephobic performance. The coating's resistance to erosion was tested with a sand-blasting machine designed to mimic wind-blown sand conditions. After 10 min of exposure, the coating maintained its hydrophobicity with a contact angle of  $152.5^\circ$ , demonstrating strong erosion resistance.

Adding ZnO to perfluoropolyether (PFPE) coatings can significantly modify their superhydrophobic properties by changing the microstructure of the coating surface [179]. The contact angle reached a peak value of  $158^\circ$  when the PFPE content was increased to 15%, after which it showed a slight decrease. (Figure 10a). The incorporation and elimination of ZnO powder created a micro-nano roughness on the coating and delayed the icing time to 107.1 s.

Lu et al. [180] used a perfluorosilane fluorinated ethanol solution to coat  $TiO_2$  nanoparticles and create a superhydrophobic coating by spraying or brushing it onto the substrate. The WCA remained within  $156^\circ$  to  $168^\circ$  after 40 abrasion cycles, indicating the maintenance of superhydrophobicity after mechanical abrasion. No other tests were performed to characterize its superhydrophobicity. Son et al. [181] developed a highly impact-resistant and recyclable “polyamide 6 (PA 6)-based carbon fiber-reinforced thermoplastic (CFRTP)” using a reactive liquid molding process. However, the mechanical properties degraded when external components were used in a humid environment. They resolved this issue by coating the PA 6-based CFRTP with fluorinated polydopamine (f-PDA) using the thermoplastic resin transfer molding process. The resulting coating exhibited improved water stability, reduced the surface energy by 49%, and demonstrated an anti-icing performance. This anti-icing ability remained effective for 30 min. Additionally, the f-PDA coating retained its integrity after being exposed to temperatures between  $-30$  and  $210^\circ C$ , as well as undergoing a sandpaper wear test for 200 cycles ( $CA > 85^\circ$ ).

Polyvinylidene fluoride (PVDF) is an excellent material for achieving a superhydrophobic surface with high physicochemical stability and self-cleaning ability [182,183]. However, pure PVDF cannot be utilized as an effective coating due to its weak adhesion [184]. For example, Peng et al. [185] developed a porous superhydrophobic PVDF coating for wind turbine blades that has excellent anti-icing properties. They investigated the weight gain due to icing in a climatic chamber maintained at  $-10^\circ C$  for 30 min. Ice accumulation was achieved by precipitation, approximately 1 mm in diameter, from sprinklers positioned 20 cm above the samples, as shown in Figure 10b. The weight of the uncoated hydrophilic wind turbine blade surface increased steadily throughout the experimental period, whereas the weight gain of the superhydrophobic PVDF coating was negligible.

Zhao et al. [186] fabricated the “PVDF-PDMS-PF@ $\mu/nSiO_2$  (PPPSS)” as a rough superhydrophobic coating. After 15 days of exposure, the WCA of the PPPSS coating remained

unchanged, changing by  $0.7^\circ$ , from  $162.6^\circ$  to  $161.9^\circ$ . However, no  $\tau_{ice}$  tests were conducted. According to Huang et al. [187], the alkali treatment of PVDF introduced hydroxyl groups improved the adhesion between the coating and substrate by enhancing the miscibility of PVDF and E51. This final coating exhibited superior anti-icing properties ( $WCA > 158^\circ$ ,  $SA < 1^\circ$ ). The WCA also remained elevated after 200 cycles of abrasion (approx.  $157^\circ$ ) (Figure 10(c-1)) and 72 h of UV-irradiation ( $WCA > 158^\circ$ ) (Figure 10(c-2)), although no  $\tau_{ice}$  estimates were provided.

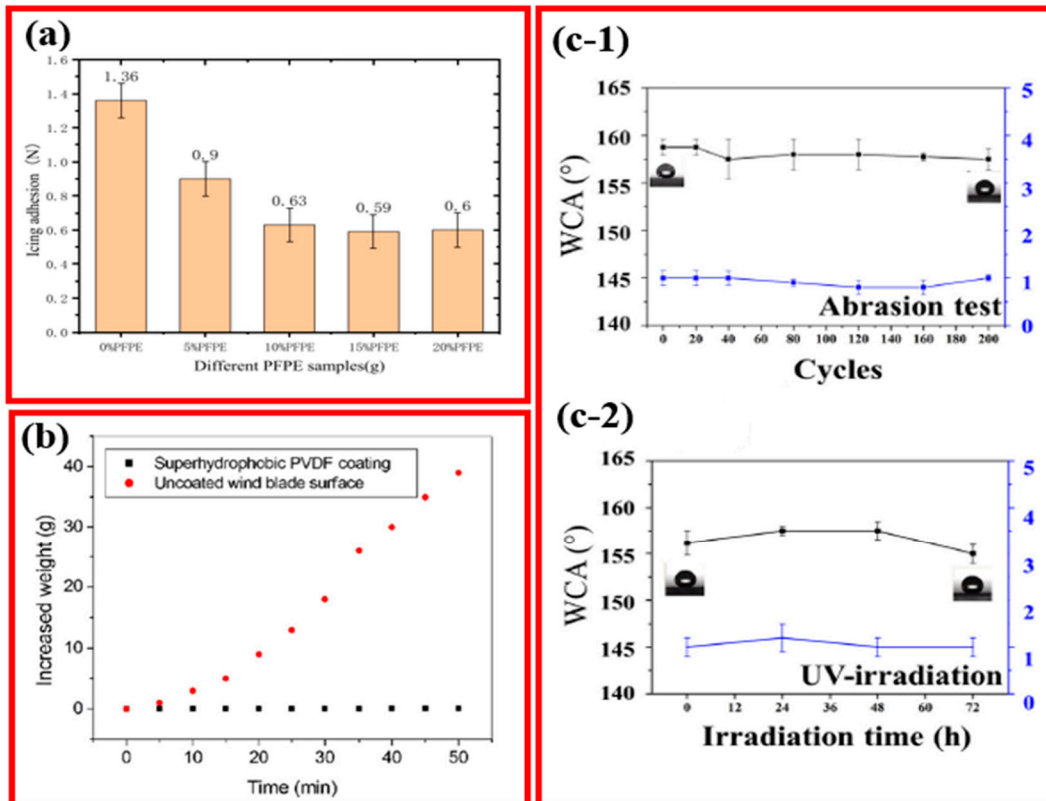


**Figure 10.** (a) Ice adhesion of different PFPE content [179].; (b) The connection between the weight gain from ice accumulation on the tested samples and the duration of supercooled water droplet exposure in a cold chamber set at a temperature of  $-10^\circ\text{C}$  [185]; (c-1) The WCA values exhibited only slight variation, staying above  $156^\circ$  after undergoing 50 tape peel tests or 200 abrasion cycles. (c-2) WCA of the coating surface was significantly unchanged under UV irradiation for 72 h [187].

In summary, fluorinated coatings are known for their ultra-low surface energy, high hydrophobicity, and icephobicity (Table 6). These properties make them highly effective at minimizing ice adhesion. Poor mechanical durability, especially under abrasive conditions, high cost, and environmental concerns associated with the use of fluorinated materials cannot be ignored. Thus, further research is needed to optimize formulation, application methods, and long-term performance under various environmental conditions.

**Table 6.** Summary of various research studies carried out on fluoropolymer-based coatings.

Coating	Ice Adhesion Measurement Approach	Ice Adhesion Strength	Hydrophobicity Durability	Mechanical Properties	CA/HCA	Reference
Fluorocarbon complemented by TiO <sub>2</sub> , SiO <sub>2</sub> , and micro/nanocomposite particles	76 kPa	107–157 kPa	Freezing delay of 1601.4 s	Erosion resistance	CA: > 150°	[180]

**Table 6.** *Cont.*

Coating	Ice Adhesion Measurement Approach	Ice Adhesion Strength	Hydrophobicity Durability	Mechanical Properties	CA/HCA	Reference
Perfluoropolyether/ZnO	Shear force de-icing test	0.6–1.36 N	delays icing time reached 107.1 s	N/A	CA: 158°	[179]
Fluorinated polydopamine ( <i>f</i> -PDA)	Anti-icing test	No ice accumulated on the surface	Remained intact after 200 cycles at −30 to 210 °C	Flexural strength: 823.1 MPa	CA: 93.2°	[181]
Porous superhydrophobic PVDF	Climatic chamber (spraying supercooled water droplets)	The water droplets rapidly slide off the surface	N/A	N/A	CA: 156 ± 1.9	[185]
PVDF-PDMS-SiO <sub>2</sub>	N/A	N/A	Air weathering for 15 days; WCA: 162.7–158.1°	N/A	CA: 162.7°	[186]
PVDF (MPVDF)/epoxy resin composites (SMECC)	N/A	N/A	Exposure to UV light for several days while maintaining superhydrophobicity: WCA > 158°	N/A	CA: approx. 158°	[187]

#### 4. Polyurethane-Based Coatings

Due to their mechanical strength, durability, elasticity, UV stability, chemical resistance, and low toxicity, polyurethane (PU) is widely utilized as “topcoats” [188]. The distinctive feature of PU coatings is their ability to form strong “interchain hydrogen bonding” between urethane linkages, resulting in superior mechanical features that surpass most other coating systems. However, creating durable superhydrophobic or hydrophobic PU-based coatings is particularly challenging in subfreezing temperatures. Hydrophobicity and icephobicity are major obstacles that limit the industrial use of PU coatings in harsh, cold climates. Despite attempts to address this limitation, further refinement of modification techniques is required to achieve stable superhydrophobic, anti-icing, or icephobic PU-based coatings [189]. Recent research has developed innovative technologies to enhance the hydrophobicity and icephobicity of PU coatings in various industries. For example, porous PU films incorporating polystyrene (PS) films have demonstrated superhydrophobic and superoleophilic properties [190]. Zheng et al. applied a thermal modification at 100 °C to enhance the adhesion of PS colloids in the porous PU structure. By utilizing the self-assembly of PS colloids, dual roughness was created on the porous PU films, which resulted in coatings exhibiting superhydrophobic behavior, e.g., WCA of 158°. Chauhan et al. [191] embedded PDMS into PU with a “transurethanation reaction”,

leading to phase separation between the soft and hard segments, which was influenced by the reaction temperature, the PDMS/PU blend ratio, and the molecular weight of the PDMS used. Roshan et al. [192] developed a polyurethane-based icephobic coating that contained fluoropolyol and isocyanate that was modified with hydroxyl-terminated silicone oil and fluoroalkyl polyhedral oligomeric silsesquioxane (F-POSS) particles. They claimed that the incorporation of silicone oil and F-POSS enhanced the water contact angle of their coating to  $127^\circ$  and  $\tau_{ice}$ , measured by push-off test after 15 icing/de-icing cycles, maintained at 9.3 kPa. Wong et al. [193] developed an ultra-durable superhydrophobic coating by depositing a colloidal suspension of PU-PMMA in a layer-by-layer fashion to form interpenetrated networks (IPNs), followed by applying a fluorinated-silica solution. The IPNs stably held the F-SiO<sub>2</sub> NPs, resulting in a coating with a hierarchical structure that exhibited high durability even after 200 cycles of abrasion, UV light, acid attack, and oil contamination. These coatings, which were not dependent on the substrate, exhibited high transparency with optical transmittance reaching up to 80%. They also demonstrated a WCA of  $165^\circ$  and an SA of less than  $10^\circ$ , attributed to the low surface energy of the fluorinated nanoparticles. Figure 11a presents SEM images and the schematic of the fabrication of PU-PMMA IPNs with and without F-SiO<sub>2</sub>, as well as after multiple abrasions. Zheng et al. [194] also introduced an in situ heating de-icing approach using CNT/WPU, which created a flexible and lightweight nanocomposite. The exceptional elongation of this nanocomposite was attributed to the even distribution of MWCNTs within the WPU matrix. This nanocomposite was designed for electrothermal de-icing applications on wind turbines. IR images and tensile stress–strain curves of the CNT/WPU films containing varying amounts of MWCNT are demonstrated in Figure 11(b-1,b-2).

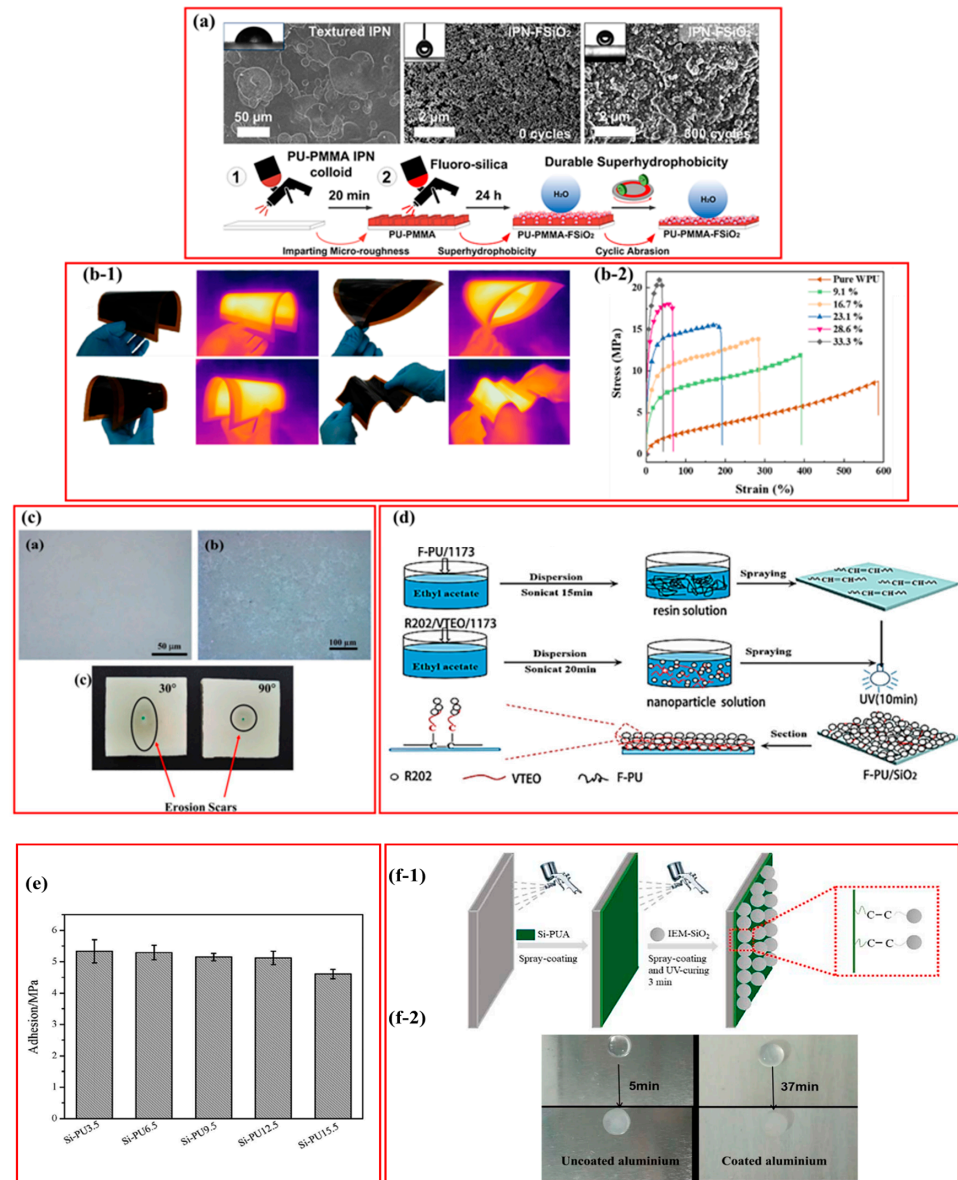


**Figure 11.** (a) fabrication of PU-PMMA interpenetrated polymer network (IPNs) with and without F-SiO<sub>2</sub> and after multiple abrasion cycles and SEM images [193]; (b-1) IR thermal images of the CNT/WPU electrothermal films, (b-2) tensile stress–strain curves of the CNT/WPU films containing varying amounts of MWCNT. The maximum strain of the CNT/WPU films [194]; (c) Optical microscopic

images of 5 wt % PUCMF coating: (a) as-synthesized (b) after solid particle erosion test, and (c) showing erosion scars at erodent angles of 30° and 90° [195], (d) Synthetic route of F-PU/SiO<sub>2</sub> coating [196]; (e) Adhesion strength of Si-PU<sub>x</sub> coatings [197]; (f-1) The fabrication of Si-PUA/IEM-SiO<sub>2</sub> superhydrophobic coating; (f-2) Photographs of delay in ice nucleation [198].

Pathak et al. [195] recently investigated the effects of different weight ratios (2, 5, and 10 wt %) of cellulose microparticles (CMP) and cellulose microfibrils (CMF) in water-based PU coatings for wind turbine blade protection. WPUCMP 5 wt % (Figure 11c) had the lowest average erosion rate. According to the authors, these cellulose-based composite coatings have significant promise for protecting wind turbine blades against particulate matter impact and rain erosion. Lv et al. [196] developed a “UV-curable high-strength, anti-icing, self-cleaning F-PU/SiO<sub>2</sub> superhydrophobic coating”. F-PU functioned as the primary binder, while vinyltriethoxysilane (VTEO) acted as a secondary binder to secure SiO<sub>2</sub>. The synthetic route for F-PU and the preparation process for F-PU-SiO<sub>2</sub> are shown in Figure 11d.

By controlling the nanosilica content, the researchers achieved a superhydrophobic coating with a SA of  $2^\circ$  and a WCA of  $165^\circ$ . The coating maintained its superhydrophobicity even after 750 friction cycles (WCA  $> 145^\circ$ ) and when exposed to  $-10^\circ\text{C}$  for 100 h (WCA  $> 145^\circ$ ), demonstrating good resistant anti-icing properties. The coating also exhibited excellent antifouling properties and acid/alkali resistance, making it suitable for various substrates.

Surface erosion of wind turbines occurs over their operational lifespan due to challenging environmental factors, such as UV radiation and precipitation impacts. Protecting them with PU coatings can be beneficial. Zhao et al. [199] engineered a “fluorine-free waterborne suspension containing hexadecyl polysiloxane-modified  $\text{SiO}_2$  ( $\text{SiO}_2\text{@HD-POS}$ )”, which they dispersed in a commercially waterborne polyurethane (WPU). The coatings exhibited exceptional abrasion resistance to a 4.5 kPa force over 200 cycles and were compatible with various substrates, all while maintaining superhydrophobicity with high WCAs of approximately  $164^\circ$  and low SAs of about  $3^\circ$ . Liu et al. [198] modified  $\text{SiO}_2$  nanoparticles using 2-isocyanatoethyl methacrylate (IEM) and OH-terminated PDMS, in combination with pentaerythritol triacrylate (PETA), to modify isophorone diisocyanate (IPDI). The modified components were applied using a spray coating technique with ethyl acetate solvent and then cured under UV light. By adjusting the IEM- $\text{SiO}_2$  concentration to 4%, impressive WCAs of about  $160^\circ$  and SAs close to  $2^\circ$  were attained. The final products showed excellent mechanical durability against sandpaper abrasion, enduring 400 cycles of 20 cm strokes while maintaining superhydrophobicity even in extremely acidic and basic environments. The “silicone-modified PU hybrid coating” also exhibited a sevenfold increase in freezing time at  $-10^\circ\text{C}$  compared to substrates without coating. The combination of PU and silica produces either anti-erosion or hydrophobic features. Incorporating crosslinking within PU, along with nano- $\text{SiO}_2$  particles, enhanced the coating’s hydrophobicity anti-aging properties and improved its chemical and mechanical characteristics, as concluded by several researchers [200]. Carreño et al. [201] produced a PU-paint based on OH-terminated-PDMS. They also sprayed a sol-gel solution consisting of tetraethylorthosilicate (TEOS) and (3-glycidylxypropyl) trimethoxysilane (GLYMO) onto the PU-paint before full curing. Coating the PU surfaces with a 5% PDMS sol-gel mixture before the final curing process resulted in an impressive 80% decrease in  $\tau_{\text{ice}}$ , with a value of approximately 90 kPa observed for the PU-paint. In the study of Golovin et al. [202] PDMS-silane and PU coatings with low crosslinking densities were fabricated and compared to commercial SLIPs and icephobic surfaces. They found that PU-based low crosslinking density coatings had good durability (after 100 icing/de-icing cycles), abrasion resistance (5000 cycles with Taber abrasion ASTM D4060), and lower  $\tau_{\text{ice}}$  (after 4 months in severe winter conditions) in comparison to PDMS-silanes, lubricant infused-PU coatings, and fluorinated PUs. Most notably, the PU coatings demonstrated 0.2 kPa  $\tau_{\text{ice}}$  and  $9 \pm 2$  kPa even after all the durability assessments. PU is inherently hydrophobic and, when combined with ceramic oxide nanoparticles (e.g.,  $\text{Al}_2\text{O}_3$ ,  $\text{ZrO}_2$ ,  $\text{CeO}_2$ ), it exhibits enhanced resistance to solid particle erosion, which is crucial for wind turbines. Furthermore, PU has significant advantages over epoxy resins, making it a convincing choice for important parts of wind turbine blades such as the main beam, web, and blade [203]. However, epoxy-based coatings also play a distinct and important role in wind towers.

Generally, creating durable superhydrophobic or hydrophobic PU-based coatings in subzero temperatures is currently a challenging task. The limited hydrophobicity and icephobicity of PU coatings in harsh, cold climates significantly hinder their industrial usage. Thus, further research is needed to enhance their properties for application in wind power industries. For example, incorporating advanced fillers like carbon nanotubes, graphene oxide, or nanoclays can improve both mechanical and icephobic properties. A

summary of the research that has been performed in PU-based coatings, as discussed in this section, is given in Table 7.

**Table 7.** Summary of various research projects on PU-based coatings.

Coating	Ice Adhesion Measurement Approach	Ice Adhesion Strength	Hydrophobicity Durability	Mechanical Properties	CA/HCA	Reference
PU-PMMA	N/A	N/A	It can be superhydrophobicity after 200 friction cycles	N/A	N/A	[193]
CNT/WPU	N/A	N/A	The electrothermal film can start working at $-35\text{ }^{\circ}\text{C}$ and heated to $35\text{ }^{\circ}\text{C}$ for 5 min	Endures 100,000 bending cycles (at $240^{\circ}$ ) with a resistance variation of 3.17% and withstands repeated stretching of 2.0% strain along the length direction.	N/A	[194]
Cellulose-reinforced Polyurethane	N/A	N/A	N/A	Erosion rate: $20 (\times 10^{-3} \text{ mm}^3 \cdot \text{g}^{-1})$	N/A	[195]
F-PU/SiO <sub>2</sub>	N/A	N/A	Can maintain superhydrophobicity after 750 friction cycles: WCA > $145^{\circ}$	N/A	CA: $165^{\circ}$	[196]
PDMS-silane and PU coatings featuring varying crosslinking densities	N/A	$\tau_{\text{ice}}$ as low as 0.2 kPa	after 5000 abrasion and 100 icing/ de-icing cycles, $\tau_{\text{ice}}$ was $9 \pm 2 \text{ kPa}$	N/A	N/A	[202]

## 5. Epoxy-Based Coatings

“Epoxy resins”, also known as “polyepoxides”, belong to a unique category of reactive polymers or prepolymers characterized by the presence of epoxide groups in their molecular structure. The designation “epoxy” is commonly used to describe both the uncured materials and the hardened end products formed from these resins [204]. Epoxy resins can be effectively tailored to meet the requirements of specific applications by properly selecting the resin, crosslinking agent, and modifiers [205,206]. ERs are commonly used as protective coating binders in such industries as aviation, power transmission, and wind power generation because of their excellent chemical resistance, thermal stability, and adhesion to various substrates [205–207]. In addition, neat epoxy coatings have polar groups on their surface that produce hydrophilicity. Modified epoxy coatings, however, have shown promising results in icephobic applications.

For instance, a modified epoxy-based resin with dopamine molecules improved hydrophilic properties by forming a lubricating aqueous layer on anti-icing coatings, which can reduce  $\tau_{\text{ice}}$  of them by a factor of 7.2 [208]. Another important modification approach in epoxy-based resins can be performed by utilizing nanoparticles. To give some examples, Zhou et al. [209] found that a composite coating of clustered ZnO/epoxy exhibited superior corrosion resistance and hydrophobicity, making it suitable for anti-rust and de-icing applications. The coating maintained its superhydrophobic nature even when damaged because of its high specific surface area. The coexistence of epoxy/ZnO seeds and cluster-like ZnO provided dual protection to the magnesium alloy substrate, resulting in increased corrosion resistance. After undergoing tape peeling 10 times, the coating maintained a contact angle of  $163^{\circ}$ , reflecting the excellent adhesion of cluster-like ZnO to the substrate and preservation of its superhydrophobic characteristics. However, no analysis of ice adhesion was conducted to validate the coating’s icephobicity.

Pan et al. [210] developed a novel carbon fiber/epoxy resin composite with anti-icing properties using the octadecylamine modification method and a sandblasted hard template. The surface had a static CA of  $155^\circ$  and a minimal SA of  $8^\circ$ . The adhesion strength of ice on the modified sample (50 kPa) was significantly lower than on the untreated sample (75 kPa) because of the irregular, rough surface texture that caused stress buildup in certain areas (Figure 12a).

Fan et al. [211] created a “two-layer epoxy-based nanocomposite coating” for hybrid anti-icing and de-icing purposes (Figure 12b). The bottom layer consisted of an electrothermal active de-icing layer composed of epoxy mixed with copper, which was coated with silver- (Ag-Cu) and epoxy with multi-walled carbon nanotubes (MWCNTs) nanocomposites. The epoxy/Ag-Cu coating exhibited good electrical conductivity and was capable of rapidly producing heat under electrical voltage. This layer was covered with a superhydrophobic coating made from an epoxy composite containing  $\text{SiO}_2$  and hexadecyltrimethoxysilane (HDTMS) [2,212]. Integrating electrothermal and superhydrophobic coatings reduced the energy consumption compared to using an electrothermal coating alone while also enhancing icephobic performance, making it an efficient hybrid anti-icing solution, especially for wind power generation.

Zhang et al. [213] coated the substrate surface with a superhydrophobic layer composed of micro-nanoscale ZnO and epoxy resin. They further roughened the coating's surface using stearic acid and acetic acid solutions, creating a micro/nanostructure and reducing surface energy to produce a mechanically stable and wear-resistant superhydrophobic coating. Zhao et al. [214] improved the icephobic characteristics of the coating by incorporating silane-modified graphene nanoplatelets. Nistal et al. [215] further modified the icephobic properties of their coating by adding silane-modified graphene nanoplatelets. These nanocomposite coatings were hydrophobic and possessed low surface energy, significantly reducing  $\tau_{\text{ice}}$  ( $9 \pm 3$  kPa) beneath the natural ice detachment. Moreover, even after being subjected to 1000 Taber abrasion cycles, the icephobic nanocomposite coating remained durable, with an average  $\tau_{\text{ice}}$  below 50 kPa (Figure 12c).

In other research, Atta et al. [216] evaluated the mechanical resilience of superhydrophobic iron oxide/HMT and Ag/HMT epoxy nanocomposites using an abrasion test. They analyzed WCAs post-abrasion testing to evaluate the effect of resistance and conducted impact tests, pull-off tests, and hardness measurements. The CA continued to increase after 5000 abrasion cycles, which showed improvements in the roughness of the prepared surface. Qin et al. [217] developed an epoxy-based anti-icing surface by applying a spray-coated layer of polytetrafluoroethylene (PTFE; Teflon) nanoparticles with a diameter of 300 nm diameter (Figure 12d). The static CA for deionized water was  $154^\circ$ , and the roll-off angle was below  $2^\circ$ . At  $-10^\circ\text{C}$ , the average ice detachment strength was around 30 kPa, roughly 2.5% of that for an aluminum substrate and approximately 20% of the value for a plain epoxy. They also observed that over 10 cycles, the strength required for ice shedding consistently remained around 27.5 kPa.

Kozera et al. [218] synthesized derivatives to modify epoxy resin composites using organosilicon compounds that incorporated multiple functional groups, such as octahydro-spherosilicate (OSS). The structure of the multifunctionalized silicone compounds (MFSC) is shown in Figure 12e. To measure the ice adhesion of this coating, they used a universal tensile testing machine. The control sample demonstrated an  $\tau_{\text{ice}}$  of  $264 \pm 14$  kPa, while the modified samples exhibited values ranging from 186 to 265 kPa. Chemical modification using spherosilicate compounds improved the surface's icephobicity. Low roughness samples showed a correlation between surface wettability and ice adhesion: as WCA increased, ice adhesion decreased. After 100 icing/de-icing cycles, the WCA values were lower relative to the initial values for all samples. The reference sample produced the largest decrease

in WCA, with a 10% reduction relative to its initial value. In contrast, the other modified samples experienced a WCA reduction ranging from 1% to 6%, with no notable change in hydrophobicity.

In conclusion, epoxy coatings are known for their excellent adhesion, hardness, and resistance to environmental degradation. They are often used in combination with nanoparticles to enhance icephobic properties and have advantages such as strong adhesion to substrates, high chemical resistance, and good structural integrity. However, they suffer from brittle nature and poor elongation that can limit their icephobic efficiency. Therefore, by developing flexible epoxy hybrid systems with other coatings like epoxy-silicone, brittleness and enhancement of icephobicity can be addressed.

Table 8 provides a brief summary of studies that have been carried out on Epoxy-based coatings.

**Table 8.** Summary of various research projects carried out on epoxy-based coatings.

Coating	Ice Adhesion Measurement Approach	Ice Adhesion Strength (kPa)	Hydrophobicity Durability	Mechanical Properties	CA/HCA	Reference
Epoxy/ZnO	N/A	N/A	Polish with 2000# sandpaper. By increasing friction distance, the contact angle is reduced to 132°	The friction coefficient of the EZZ surface is >the ZZ surface	CA: 163°	[209]
Carbon fiber/epoxy resin	Push off	52–75	Increasing abrasion length leads to an enhanced CA from 145° to 152°	N/A	CA: 155°	[210]
A hybrid of Epoxy/SiO <sub>2</sub> /HDTMS/kaolin nanocomposite and electro-thermal layer (epoxy/Ag-Cu/MWCNTs)	Pull-off	Adhesion strength < on glass (0.01 MPa for coatings with 0.2 mL HDTMS)	its superhydrophobicity for 240 wear test cycles (CA: 135.3°)	N/A	CA: 156.3°	[211]
Epoxy/ZnO	N/A	N/A	The 2400× abrasion removed the rough surface; minimum effect on the ZnO/ER coating	N/A	CA: 155 ± 2°	[213]
Fluorinated epoxy resin/carbon/PTFE particles	Dynamic anti-icing tests	2× higher than the neat sample	CA is still above 150° after 100 cycles of tape peeling and abrasion	N/A	CA: >155°	[214]

**Table 8.** Cont.

Coating	Ice Adhesion Measurement Approach	Ice Adhesion Strength (kPa)	Hydrophobicity Durability	Mechanical Properties	CA/HCA	Reference
Epoxy resin/GNP/3 different silane coupling agents	Pull-off	9 ± 3 kPa	1000 cycle abrasion times with 1 kg load, mass loss: 39 ± 5, mg and WCA would be increased	N/A	HCA: 25–32°	[215]
Modified epoxy resin using polytetrafluoroethylene (PTFE) nanoparticles	Custom-built goniometer	30 kPa	The ice detachment strength remained within a range of 27.5 kPa (mean value) and 11.4 kPa (deviation) over 10 cycles.	N/A	CA: 154°	[217]
Epoxy/OSS	Universal tensile testing machine Zwick/Roel Z050	186–265 kPa	100 icing/de-icing cycles, decrease 5–10% in WCA	N/A	CA: 89 ± 1 to 103 ± 0°	[218]

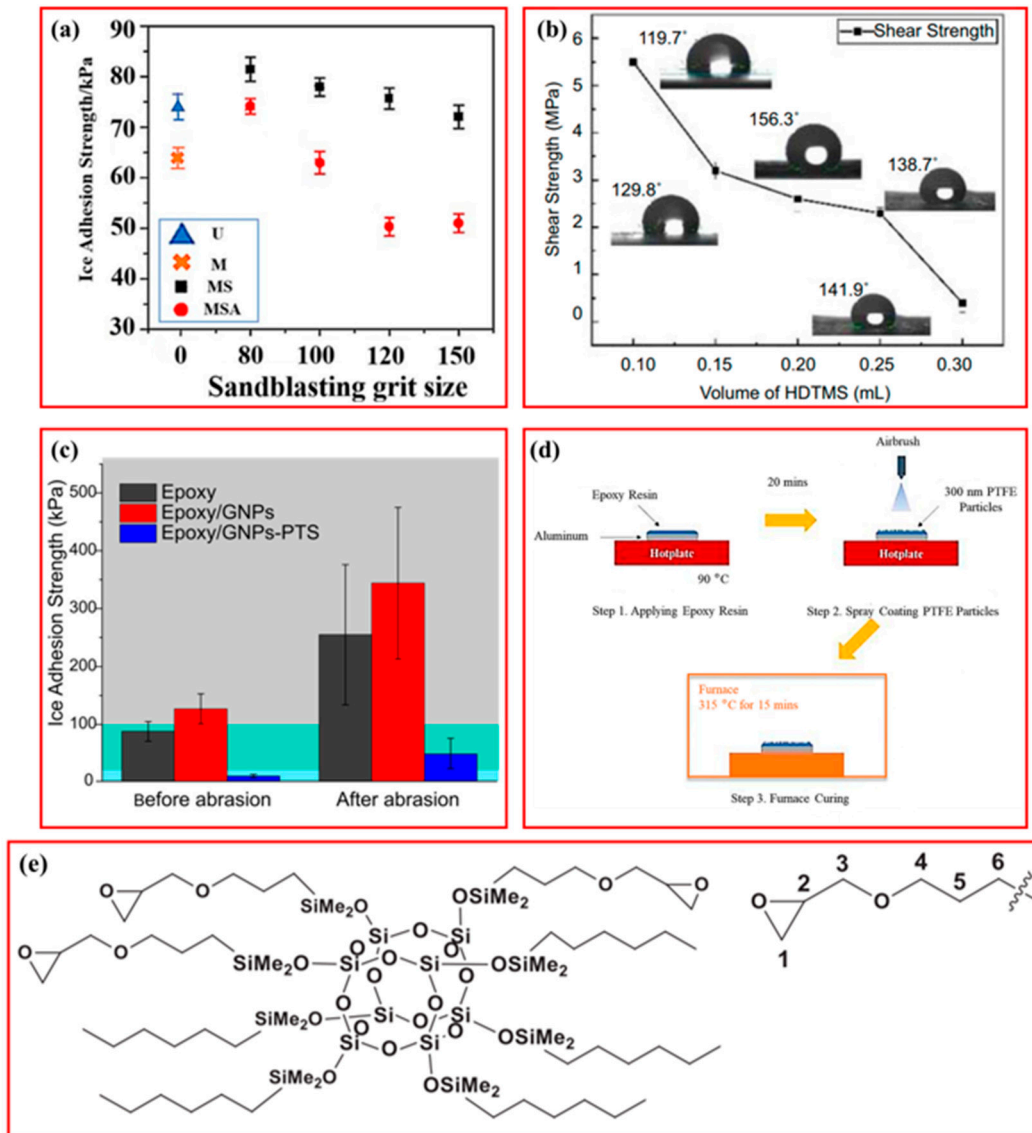


**Figure 12.** (a) The  $\tau_{ice}$  by using custom-built device [210]; (b) Hierarchical nano-microstructure observed at low HDTMS loadings, gradually disappearing with higher loadings [211]; (c) The  $\tau_{ice}$  before and after the abrasion test [215]; (d) Fabrication of epoxy-based anti-icing surface by applying a spray-coated layer of polytetrafluoroethylene (PTFE; Teflon) nanoparticles [217]; (e) Image of the structure of one the modifier MFSC [218].

## 6. Hybrid Approaches for Icephobic Surfaces

Despite advancements in minimizing ice buildup and reducing adhesion strength, passive anti-icing techniques still face challenges in terms of long-term durability and preserving low  $\tau_{ice}$  throughout multiple cycles of icing/de-icing [219]. Active de-icing methods often require significant energy inputs, such as electricity or heat, leading to increased operational costs and potential environmental implications. Additionally, anti-icing coatings may lose effectiveness over time because of factors like UV radiation, abrasion, and chemical degradation, especially in severe weather conditions or on complex surfaces. Both active and passive methods can also face reliability issues, compromising their effectiveness in preventing ice accumulation [31,33,205].

Therefore, to address the constraints of active and passive strategies, a hybrid approach offers the potential to create an effective, low-power, reliable, and resilient ice protection system. In the wind turbine industry, a hybrid approach involves integrating multiple anti-

icing methods, in particular, the combining of passive techniques (anti-icing coatings) with active technologies to improve overall performance [25,51]. The efficiency and energy usage of the hybrid anti-/de-icing approach have been evaluated and compared to traditional passive and active de-icing methods [220].

Active methods that use electrical heating to warm the blade surfaces can effectively mitigate wind turbine icing; however, they require high power consumption to maintain the blades at a high temperature. Another issue is the formation of dense ice from runback water, which poses safety risks when shed from the blades and can have aerodynamic implications [47,221,222]. Therefore, a potential solution to address ice buildup on wind turbines is a hybrid structure that complements thermal or mechanical ice protection methods with the usage of icephobic coatings, which reduce power inputs and the ecological footprint of current systems. Hybrid thermal de-icing strategies with icephobic coatings can be achieved through three approaches: electrosensitive coatings, photosensitive coatings, and magnetosensitive coatings.

### 6.1. Hybrid Electrothermal De-Icing Systems

The first report of an electrothermal anti-icing system was in 1939 [223]. Electrical energy dissipation in conductive objects may cause Joule or resistive heating, effectively removing ice from a substrate by melting a thin interfacial film and creating a water layer [224–229]. The water layer reduces ice adhesion and aids in its removal by natural forces [230]. An electrothermal de-icing system typically consists of multiple layers with varying material characteristics and thicknesses based on the design and application [1]. Good thermal/electrical conductivity is crucial for maximizing de-icing efficiency and minimizing energy consumption [227,231,232]. Heating systems such as hot air pumping [233], conductive polymer-based heaters [234,235], graphene-based heaters [226,236], and metallic systems [237–239] are used to melt interfacial ice. Nevertheless, every active de-icing technique requires the whole surface temperature to be higher than 0 °C, resulting in significant energy consumption for de-icing large surfaces like wind turbine blades. A hybrid system that utilizes both passive anti-icing and active de-icing technologies, therefore, offers an ideal solution to the icing issue.

Earlier research has indicated the need to further evaluate the performance of electrothermal de-icing systems with surface coatings. Selecting the appropriate surface coating is pivotal for enhancing anti-icing action, as it can reduce the energy needed to prevent ice formation and minimize the occurrence of runback ice [1,240]. Drawing upon results from icing wind tunnel experiments of  $\tau_{ice}$ , Bebaeu et al. [241] concluded that combining an electrothermal heating system and an icephobic coating is the best strategy for wind turbine blade icing safeguard. Perron et al. [242] at the Anti-icing Materials International Laboratory (AMIL) used two hydrophobic coatings and a superhydrophobic coating coupled with an electrothermal anti-icing assembly to simulate icing situations in an icing wind tunnel. Relative to the bare substrate, the hydrophobic coatings reduced the required power by 8% and 13% for rime and glaze ice; hydrophobic films lowered the required energy input up to 8% for rime and 13% for glaze ice. On the other hand, the superhydrophobic coating diminished the energy demand by up to 13% for rime and 33% for glaze ice. The hydrophobic coatings were unable to prevent runback water from freezing in unprotected regions; however, the superhydrophobic coating did prevent the freezing of runback water, resulting in a largely ice-free surface and suggesting that superhydrophobic coatings can meaningfully decrease the required power of anti-icing facilities.

Tour et al. [230] developed a conductive coating by incorporating stacks of graphene nanoribbons (GNR) into an epoxy matrix, with a conductivity of over 100 S/m at 5 wt % of GNR. Thermal energy was generated by enforcing a constant voltage through the

sample. They found that applying a  $0.5 \text{ W/cm}^2$  power density could remove 14 g of ice from a helicopter blade interface at  $-20 \text{ }^\circ\text{C}$ . This composite could be an ideal candidate for icephobic applications across a range of industries, including power-line networks, wind turbines, aerospace, and so forth. In another study [243], superhydrophobic films with anti-icing capabilities were created by spraying perfluorododecylated graphene nanoribbons (FDO-GNR) onto a surface. The films effectively prevented ice formation at temperatures as low as  $-14 \text{ }^\circ\text{C}$ . Additionally, by enforcing approximately 40 V to the interface, enough heat was generated to clear ice at colder temperatures. Remarkably, a minimal  $0.2 \text{ W/cm}^2$  power density was sufficient to keep the surface at RT even with a surrounding temperature of  $-32 \text{ }^\circ\text{C}$ . The researchers further enhanced the de-icing capacity by introducing a lubricant, which created slippery surfaces. The easy spray coating approach marks this material as a potential choice for large-scale utilizations such as wind turbines. Karim and coworkers [244] prepared a graphene-based de-icing composite via a microfluidic strategy. They used the ink to coat glass-fiber roving to achieve a minimal electrical resistance of approximately  $1.7 \ \Omega/\text{cm}$ . The researchers then used a vacuum resin infusion method to integrate the graphene-coated roving via an epoxy resin, forming glass-epoxy composite materials. They tested the de-icing action by immersing the sample in an ice-filled container and under 10 V. Over five minutes, the container temperature increased from  $-27.3 \text{ }^\circ\text{C}$  to  $-0.1 \text{ }^\circ\text{C}$ , resulting in ice melting.

Amirfazli et al. [240] studied the impact of superhydrophobic films on reducing power consumption in anti-icing systems. They used NACA0021 aluminum airfoil substrates with three inserts: untreated aluminum, aluminum covered with PMMA, and etched aluminum covered with Teflon. The researchers heated the leading-edge region using an electrical resistor and located a no-ice region on the insert to measure coating performance. They found that the surface coatings significantly reduced the energy input by up to 80% and decreased runback icing. The Teflon film protected the substrate from runback icing. In another study, Amirfazli and colleagues [245] investigated the presence of hydrophilic (untreated aluminum) and hydrophobic (etched aluminum superhydrophobic coating) interfaces on runback icing using the previous setup [240]. They found that ice buildup differed depending on the coating wettability. On the hydrophilic surface, droplets formed a liquid film that separated into ligaments while sliding downward. Outside the heating region, extensive ice buildup occurred. On the superhydrophobic surface, only isolated ice islands were observed, and some were removed via aerodynamic forces. These results highlight the significant role of superhydrophobic coatings in electrothermal icing protection systems. To minimize the power input, Hu et al. [47] used a combination of a superhydrophobic coating and an electro-thermal system only at the leading edge of the blade (5–10% of the blade). They coated the whole blade interface with a superhydrophobic coating (Hydrobead™ Standard with Hydrobead™ Enhancer) and wrapped an electric heating film strip (DuPont™ Kapton® RS, 50 mm thick) around the leading edge of the blade (Figure 13(a1)). A turbine blade model featuring a DU91-W2–250 airfoil in its cross-section was subjected to different icing conditions to assess performance under various ice-formation scenarios (Figure 13(a2)).

The hybrid strategy has demonstrated significant energy savings (up to approx. 90%) and similar anti-/de-icing performance compared to the traditional approach of warming up the whole surface to protect it from icing [47]. This makes it a capable technique for mitigating wind turbine freezing. Unlike the hydrophilic interface, the runback water did not re-freeze on the superhydrophobic interface. Earlier hybrid de-icing strategies demonstrated a serious problem. Hydrophobic films only resist liquid water; therefore, ice melting is necessary for the approach to be effective. Although the energy consumption in these earlier reports was lower than in merely active de-icing processes, the necessary

power is yet high and scales with the iced surface size. Given that the ice melting's latent heat (334 J/g) is around 160 times higher than the specific thermal capacity of ice (2.09 J/g °C), a dual de-icing strategy that avoids melting can offer significant power reduction advantages.

Films with low interfacial toughness (LIT) reduce the energy required to spread an interfacial crack at the ice/coating interface, facilitating more efficient mechanical de-icing. This is particularly suitable as a passive de-icing strategy for large, iced interfaces [246,247]. Golovin et al. [248] prepared smart hybrid de-icing coatings by integrating a LIT coating with printed circuit board heating elements and a microwave-based sensor for ice detection. This approach contrasts with previous hybrid de-icing systems, which relied heavily on energy-intensive methods to melt ice. With the usage of LIT films, the system allows mechanical de-icing, allowing ice to detach easily without requiring melting. The film's interfacial toughness and its  $\tau_{ice}$  changed with temperature and could be regulated by the incorporated heating elements (minimum at  $-5\text{ }^{\circ}\text{C}$ ) (Figure 13(b1,b2)). The inclusion of the incorporated microwave resonator sensors, which worked on the basis of the dissimilarity in dielectric properties of ice and water, enabled on-demand de-icing. Once the sensor detects an ice-free surface, the heating elements can be turned off immediately. The synergistic effect of the LIT film and periodic heating elements showed a higher de-icing efficiency than a fully covered heating system. The scalability of the smart coating was shown by utilizing iced surfaces as large as 1 m. This mechanical-de-icing approach is effective for ice removal from large surfaces such as wind turbine blades but not for the smaller parts. Moreover, the coatings' durability remains uncertain.

Electrothermal conversion efficiency under cold conditions is another key limitation of the practical use of hybrid electrothermal de-icing systems, particularly for large-scale applications like wind turbines. Moreover, there are no distinct standards regarding the utilization and impact of hybrid electrothermal de-icing systems. Additionally, data on the impact of speed on the physics of ice accretion on coatings is lacking. Therefore, despite coatings offering a promising direction for the enhancement of electrothermal systems, more research is needed to better comprehend the physics and optimize their application.

Lightning hazards are another issue in electro-thermal deicing systems [249], which use conductive materials to generate heat. When these materials are exposed to lightning, they can conduct electrical energy, leading to damage or failure of the system. Electro-thermal systems on wind turbine blades may attract lightning due to their height and conductive surfaces. If lightning strikes nearby, it can induce surges in the electrical system, potentially damaging sensitive electronic components due to overheating or short-circuiting within the system. Proper safety measures and regular maintenance checks should be implemented to reduce the risk of damage to the system.

## 6.2. Hybrid Photothermal De-Icing Systems

Solar radiation is an efficient energy source that can be used for non-contact de-icing systems through remote photothermal methods. Functional surfaces have been fabricated using this strategy [250–255]. Fan et al. [251] developed a superhydrophobic photothermogenic coating relying on a titanium nitride-polytetrafluoroethylene composite for de-icing applications. The fabricated film not only delayed ice formation by 400% relative to an uncoated steel surface but also melted the surface ice by converting absorbed light to heat. Zhang and coworkers [255] fabricated a photosensitive anti-icing/de-icing coating by introducing photothermogenic nanocarbon fibers (NFs) into an amphiphilic matrix composed of PDMS and hydrophilic polyvinylpyrrolidone (PVP) segments (to lower water freezing temperature) (Figure 13c). The developed coating delayed freezing time by 34 times relative to bare steel substrates and had an  $\tau_{ice}$  of 18 kPa, allowing for

easy ice detachment by natural wind action. NFs also reduced  $\tau_{ice}$  and provided rapid sunlight-responsive photothermal de-icing properties for the coating (up to 10 °C/min). The coatings remained icephobic ( $\tau_{ice} < 30$  kPa) after simulated acid rain (pH = 0) scouring, 200 abrasion cycle experiments, sand dropping, and 30 icing/de-icing cycles, making them promise for large-scale operations, e.g., outdoor, high-altitude equipment and vehicles.

Ferroferric oxide nanomaterials ( $Fe_3O_4$ ) have gained attention as photothermal agents due to their comparatively cost-efficiency and enhanced infrared-to-heat conversion yield [256–258]. Incorporating  $Fe_3O_4$  nanoparticles into superhydrophobic coatings combines passive anti-icing and active de-icing strategies, making them good candidates for icing problems in various conditions. Cui et al. [254] designed a multifunctional superhydrophobic coating using an inverse infiltration process with fluorinated epoxy resin containing  $Fe_3O_4$  nanoparticles (Figure 13d). The coating demonstrated excellent superhydrophobicity with a WCA of up to 161.0° and a SA down to 1.4°. The coatings maintained superhydrophobicity after 260 cycles of sandpaper abrasion, 400 cycles of tape peeling and 25 cycles of sand impact, suggesting good mechanical durability. The hydrophobic micro/nano hierarchical morphology, resulting from the aggregation of  $Fe_3O_4$  nanoparticles in the matrix, delayed water droplet freezing time by up to 35 min more than the bare substrate. The photothermal effect of the  $Fe_3O_4$  nanoparticles allowed the coating's surface temperature to quickly rise to 0 °C under infrared irradiation, melting ice on cold surfaces.

Hybrid de-icing strategies may include lubricant infusion. Dash et al. [252] also used the same strategy to create a laminate photothermal trap with three layers: a selective sunlight-radiation absorber (cermet), a heat spreader (aluminum layer), and insulation to minimize transverse heat loss (carbon foam) (Figure 13e). The system melted snow completely within 5 min of initial exposure to solar radiation with an intensity of 0.6 kW/m<sup>2</sup>. Zhang et al. [259] developed a slippery photothermal trap by adding a layer of silicone lubricant to a candle soot film, which acts as a natural light absorber using conductive  $Fe_3O_4$  nanoparticles as a heat spreader. With this approach, a completely frost-covered film was melted within 100 s at −20 °C under a sunlamp.

Wang et al. [260] designed a plasmonic photothermal superhydrophobic MXene@Au-waterborne polyurethane (MXene@Au-WPU) composite coating. The plasmonic MXene@Au facilitated a significant increase in temperature across the entire coating because of its high light energy absorption and fast heat transfer. To achieve superhydrophobicity, chemically modified silica nanoparticles were applied to the MXene@Au-WPU surface to produce a fSiO<sub>2</sub>/MXene@Au-WPU (fluoroalkyl silane-SiO<sub>2</sub>/MXene@Au-WPU) superhydrophobic photothermal coating, having a CA of 153°. This film demonstrated a prolonged icing delay time of 1053 s at −20 °C and 68% RH and a high photothermal de-icing efficiency of 73.1%. Furthermore, the coatings exhibited excellent resistance against corrosive liquids (pH: 1 to 13). These combined characteristics of the coating, including its anti-icing properties, corrosion resistance, and ease of implementation, demonstrated its potential application to various surfaces.

Integrating electro- and photothermal properties into a single coating presents a promising approach to mitigating ice accretion while reducing the complexity associated with multilayer designs. In a recent study, Guo et al. [261] developed an electro-photothermal SHS by incorporating hexadecyltrimethoxysilane-modified multiwalled carbon nanotubes (HDTMS-MWCNTs) into an epoxy matrix. The coating was applied via a simple spray technique and demonstrated delayed icing times of 264 s at −20 °C. It exhibited efficient photothermal deicing capabilities (1.5 sun, 175 s) and electrothermal deicing performance (25 V, 65 s). Additionally, the coating displayed excellent droplet rebound properties, with a 5 µL droplet bouncing 11 times after falling from a height of 2 cm. However, the rough surface of the coating limits its ability to achieve ice adhesion

strengths below 100 kPa due to increased mechanical interlocking between the ice and the surface. Moreover, the high concentration of HDTMS-MWCNT (20 wt.%) adversely affects the mechanical robustness of the coating.

However, considering ISO/TS 19392 standard [35], none of these developed coatings meet the minimum required visible light transmission of wind turbine coatings. Exploring coatings with selective absorption in the IR region or employing thin film technology can lead to the formation of transparent coatings.

### 6.3. Hybrid Magnetothermal De-Icing Systems

Using magnetic fields as a stimulus for magnetosensitive films is a hybrid de-icing technique with advantages including an eco-friendlier nature, convenience, and real-time action [262–264]. Magnetic nanoparticles in the coatings produce heat through magnetothermal properties, specifically Néel or Brownian relaxation [265,266]. The application of the Joule effect can effectively remove ice. The wettability and adhesion features of magnetosensitive coatings can be easily tailored to achieve the desired surface properties [267]. Ghasemi et al. [268] designed magnetic slippery surfaces (MAGSS) with low interfacial energy and icephobic properties. The physics of MAGSS's liquid–liquid interface formation is depicted in Figure 13f. MAGSS had an ice formation temperature down to  $-34\text{ }^{\circ}\text{C}$ , with an ultra-low  $\tau_{\text{ice}}$  of 2 Pa and high water and ice mobility on the surface. The prepared MAGSS showed self-healing properties and remained stable even at high-shear flows (Reynolds number  $\leq 105$ ).

Zhang and coworkers [269] prepared multifunctional superhydrophobic magnetic hybrid systems using a fluorinated copolymer-tethered epoxy matrix, a diethylenetriamine crosslinker, and amino-functionalized  $\text{Fe}_3\text{O}_4$  nanoparticles (Figure 13g). The coatings exhibited a magnetothermal capacity, with a temperature rise from 24 to 44  $^{\circ}\text{C}$  within 25 s exposure to external stimuli. The coatings significantly delayed icing time from 50 to 2878 s and showed excellent ice/water removal.

However, magnetothermal de-icing approaches have drawbacks, including high costs and increased energy input [20]. Nevertheless, the thermal capacity of magnetic nanoparticles exposed to magnetic fields makes them potential candidates for icephobic applications.

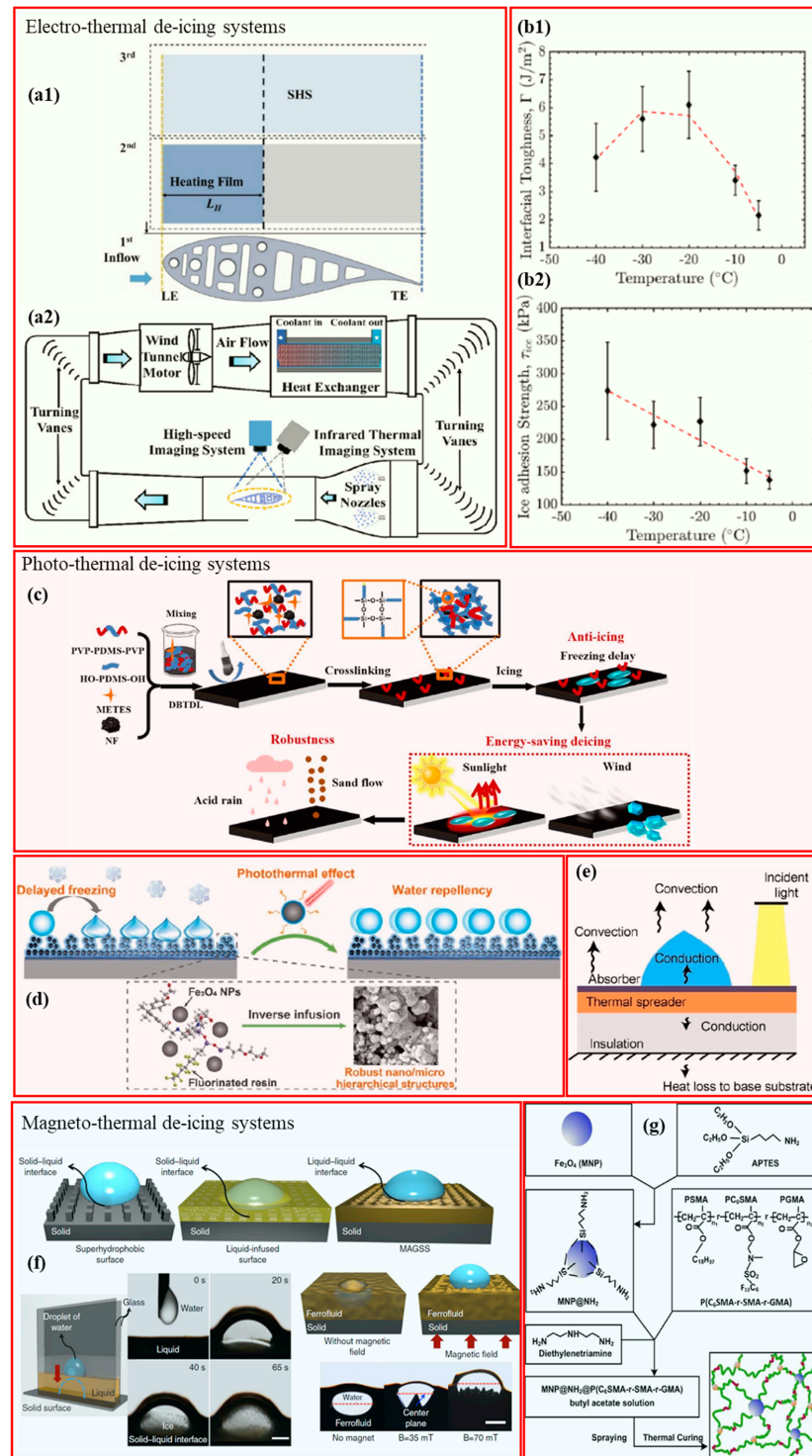


**Figure 13.** (a1) Schematic of the hybrid anti-/de-icing strategy, which utilizes a combination of active heating and passive superhydrophobic film to mitigate ice accumulation on wind turbines, (a2) Schematic of Icing Research Tunnel at Iowa State University (ISU-IRT) [47]. The effect of temperature on (b1) the toughness of the ice/coating interface and (b2)  $\tau_{ice}$  of ultra-high molecular polyethylene (UHMW-PE) [248]. (c) Schematic illustrates the fabrication of a durable sunlight-responsive anti-icing/de-icing coating [255]. (d) Schematic illustration of hierarchical coatings composed of fluorinated epoxy resin containing  $Fe_3O_4$  nanoparticles [254]. (e) The diagram illustrates the structure of a photothermal trap applied as a laminate, displaying the attributed heat transfer processes [252]. (f) Physics of the creation of a magnetic liquid-liquid interface in MAGSS [268]. (g) Synthesis path of  $MNP@NH_2@P(C_6SMA-r-SMA-r-GMA)$  film [269].

#### 6.4. Hybrid Electromechanical De-Icing Systems

“Electromechanical de-icing systems” operate by vibrational forces to remove ice. This de-icing method is applied in three main ways: ultrasonic [270], low-frequency systems, and those using piezoelectric materials. Ice buildup can be effectively dislodged from surfaces using “ultrasonic guided waves”, which overcome the “critical shear stresses” present at the interface [271]. “Ultrasonic de-icing” relies on the principle that the ice/substrate bond exhibits a relatively weak adhesive shear strength. It is worth noting that it is still in the experimental phase and has yet to be implemented for de-icing wind turbine blades [272]. However, Habibi et al. [18] highlighted the potential feasibility of applying ultrasonic de-icing to wind turbine blades through numerical simulation, though it has yet to undergo experimental validation.

Once the applied shear force exceeds the adhesive strength of the ice, the ice can be easily detached. A multi-transient actuation method showed a 70% increase in the de-iced area relative to continuously driven ultrasonic excitation. On the other hand, “low-frequency de-icing (LFDI) systems” use the resonant frequencies of the ice-covered structure to remove the ice by surpassing the critical shear and normal stresses [273,274]. For example, Marboeuf et al. [275] developed a low-energy solution to prevent ice buildup on aircraft. They employed a model derived from the “phase-field variational approach” to analyze the propagation of cracks and the detachment of ice, focusing on the impact of an electromechanical resonant de-icing strategy. In another study, Venna et al. [276] investigated the use of “piezoelectric activation patches” to induce low-frequency vibrational waves on an aluminum airfoil, aiming to match its resonance frequency for de-icing purposes. They observed ice to shed 130 s after the excitation, with measured 7.5 MPa for shear stress and 25 MPa for normal stress, respectively.

Ultrasonic waves produced by a piezoelectric transducer induce shear stress in the layered ice-material structure as they propagate. Applying a voltage to piezoelectric patch actuators positioned on the inner side of the leading edge causes these actuators to expand and contract, resulting in surface deformation. When resonant frequencies are reached, the structure undergoes considerable deformation with minimal power consumption as the actuator surpasses structural damping. This resonance-driven deformation results in significant bending and strain at the leading edge, promoting the removal of ice.

The piezoelectrics can convert electrical signals (from an electric field) to the displacement occurring in the expansion or contract of piezoelectric materials such as PZT ( $\text{Pb}[\text{Zr}_x\text{Ti}_{1-x}]\text{O}_3$ ), quartz, lithium tetraborate ( $\text{Li}_2\text{B}_4\text{O}_7$ ), and barium titanate ( $\text{BaTiO}_3$ ) [265,277]. Upon the application of an electric field, the piezoelectric material vibrates, generating shear stress on the surfaces, leading to ice removal [278]. For instance, Wang et al. [278] designed an ultrasonic de-icing technique using a lithium niobate transducer affixed to the inner surface of the aircraft wing. De-icing experiments found that a frequency of 140 kHz is optimal, with the method proving effective by using one transducer to generate a combination of shear and vibrational forces. This method can also be applied to wind generation industries because of the similarity between aircraft wings and wind turbine blades.

An electromechanical system can be achieved with a low Young’s modulus, as it generates minimal shear stresses at the interface, which requires more power for ice delamination. Haung et al. [1] recommended a coating with a Young’s modulus of at least 1 GPa. They also discovered that the elastic modulus of the coating significantly influences ice detachment within electromechanical de-icing systems. A lower Young’s modulus leads to minimal shear stresses present at the interface, which in turn requires more power for ice delamination.

The development and adoption of hybrid systems represent progress in effective ice management in challenging environmental conditions. However, the use of these systems is relatively new, and ongoing research and development efforts are actively underway.

One possible approach to implementing electromechanical de-icing systems in wind turbines may be to embed actuators within or near the structural spar of the blade to generate resonant vibrations at specific frequencies. These vibrations can cause high levels of stress and strain on the ice layer, initiating adhesive or cohesive ice fracture. Resistive heating elements can be integrated into the laminate of the blade's leading edge to soften ice before mechanical removal. This combination can reduce the power required by the piezoelectric actuators to dislodge ice, improving overall energy efficiency. Temperature and icing sensors can be embedded to detect ice formation and monitor the operating conditions to dynamically activate heating or actuation modes. Resonant modes can be selected based on finite element analysis of the blade structure, ensuring maximum vibratory efficiency for de-icing. Power may be routed from the nacelle to actuators and heaters via shielded cabling within the blade. A central control unit can ensure synchronized operation between heating and mechanical vibration for rapid ice removal.

Table 9 compares various hybrid approaches for wind turbine ice protection, followed by an explanation to provide a clearer understanding of their advantages, limitations, and effectiveness.

**Table 9.** Comparison of Hybrid de-icing Approaches for Wind Turbine Ice Protection.

Hybrid Approach	Advantages	Limitations	Performance Metrics
Electrothermal	<ul style="list-style-type: none"> <li>- Rapid</li> <li>- Reliable in various weather conditions</li> </ul>	<ul style="list-style-type: none"> <li>- High energy demand</li> <li>- Potential overheating of the surface</li> </ul>	<ul style="list-style-type: none"> <li>- High ice removal efficiency</li> <li>- High energy consumption</li> </ul>
Photothermal	<ul style="list-style-type: none"> <li>- Utilizes sunlight</li> <li>- Eco-friendly</li> <li>- Low operational cost</li> </ul>	<ul style="list-style-type: none"> <li>- Dependent on light availability</li> <li>- Requires efficient photothermal materials</li> </ul>	<ul style="list-style-type: none"> <li>- Moderate ice removal efficiency</li> <li>- Very low energy consumption</li> </ul>
Magnetothermal	<ul style="list-style-type: none"> <li>- Even heat distribution</li> <li>- Scalable for larger surfaces</li> </ul>	<ul style="list-style-type: none"> <li>- Requires advanced magnetic materials</li> <li>- High initial setup cost</li> </ul>	<ul style="list-style-type: none"> <li>- High ice removal efficiency</li> <li>- Moderate energy consumption</li> </ul>
Electromechanical	<ul style="list-style-type: none"> <li>- Low energy consumption</li> <li>- Minimal thermal damage to surfaces</li> </ul>	<ul style="list-style-type: none"> <li>- Requires precise mechanical alignment</li> <li>- It may cause wear on the turbine component</li> </ul>	<ul style="list-style-type: none"> <li>- Moderate-High ice removal efficiency</li> <li>- Low energy consumption</li> </ul>

The pivotal role of numerical simulation should also not be neglected in advancing the development and optimization of icephobic coatings for wind turbine applications. By modeling ice adhesion and detachment using tools like finite element analysis (FEA) and computational fluid dynamics (CFD), researchers can evaluate how coatings perform under mechanical and thermal stresses [272,273]. These simulations help optimize formulations by predicting ice removal efficiency, identifying failure points, and assessing durability against dynamic loadings, such as vibrations and rotational stresses typical of wind turbine operations.

Thermodynamic and heat transfer modeling further enhance coating development by simulating heat distribution during deicing processes, such as resistive heating or hot air application [274]. These models evaluate how polymer binder materials and additives influence thermal conductivity and energy efficiency. Additionally, aerodynamic simulations assess the effects of residual ice and coating wear on blade performance, ensuring that coatings minimize drag and maintain operational efficiency over time [275,276].

Future work should prioritize integrating multi-scale and multi-physics simulation approaches to capture the complex interactions between coating materials, ice formation,

and environmental variables. Standardized frameworks and machine learning-enhanced simulations can further accelerate the development of robust, high-performance icephobic coatings tailored for wind turbine applications, ensuring reliability and efficiency in harsh, icy conditions.

## 7. Conclusions

Addressing the challenges posed by ice formation on wind turbines is crucial, given the adverse effects on aerodynamic performance, mechanical stress, and energy production. Although significant research has been conducted to develop ice protection systems, mitigating ice accretion on turbine surfaces remains complex for wind turbine applications. Passive methods, such as surface modifications and icephobic coatings, show promise in enhancing icephobicity and improving turbine performance. However, selecting the appropriate approach or chemistry remains challenging. Coatings for these applications must consider factors beyond anti-icing properties, given the harsh conditions they may face. Standards, such as ISO/TS 19392, provide valuable guidance by considering mechanical properties, durability, UV, and weathering resistance, as well as rain erosion resistance. These considerations are essential for ensuring the effectiveness and longevity of ice protection systems in wind turbine applications. Continued research is necessary to address these challenges and optimize ice protection solutions for wind turbines.

This review delves into recent research on coatings, emphasizing the pivotal role of chemistry in enhancing the efficiency of icephobic coatings for wind turbines. Potential icephobic coating solutions are categorized and assessed for their suitability in wind turbine applications by classifying them based on the primary polymer binder used in their formulation. This classification aims to guide future researchers and industry professionals as to which polymers may be more appropriate for wind turbine applications. The categorized polymers include silicone, polyurethane, epoxy, and fluoropolymers, along with hybrid systems, which show promise for advancing wind turbine ice protection technology. Each coating category described in this paper exhibits different properties in terms of chemical, mechanical, thermal, and physical aspects, as well as UV resistance. Altering the structure of these coatings through physical methods, combinations of different fillers, or chemical methods, such as tailoring crosslink density, and surface modification through copolymerization or grafting with other functional groups, can yield different properties for applications where icephobicity is required.

In summary, silicone-based icephobic coatings, while promising in terms of flexibility, impact resistance, hydrophobicity, and weather resistance, suffer from poor mechanical properties. Efforts to improve them have mainly focused on incorporating fillers, creating SLIPS, and chemically modifying PDMS to enhance durability and icephobicity. However, challenges like rain erosion resistance, especially for wind turbines, persist. Incorporating self-healing mechanisms could offer avenues for further improvement. PU coatings offer strength, elasticity, UV stability, and chemical resistance, and recent improvements have enhanced their hydrophobicity, durability, and erosion resistance, but icephobicity and environmental concerns with isocyanates remain challenges. Epoxy coatings are valued for their mechanical properties, thermal stability, chemical resistance, erosion resistance, corrosion protection capabilities, and excellent adhesion. Innovative modification strategies of epoxy coating have led to promising icephobic properties. However, they are inherently hydrophilic. Approaches such as creating nanocomposites and silicone copolymerization have improved their hydrophobicity and weathering resistance, making them more suitable for mitigating ice accretion. Fluoropolymer coatings like PTFE and PVDF show promise for wind turbine applications due to low surface energy, hydrophobic properties, chemical inertness, and resistance to harsh environmental conditions. However, they still suffer from

low durability and have high production costs. More importantly, environmental concerns associated with using fluor-based materials remain a significant issue. Hybrid approaches combine passive and active methods, offering innovative ice protection through a more efficient, reliable approach, ensuring enhanced performance. However, these approaches are still in the early stages of development. Further research is required to adapt them to meet the specific guidelines for wind turbine applications, including minimum visible light transmission standards. Strategies such as wavelength selectivity and thin film technology can result in transparent coatings. Continued research and development efforts are crucial for optimizing these systems and realizing their full potential in practical applications, contributing to safer and more sustainable operations in icy environments. In addition to the previously discussed challenges with each coating chemistry and the current hybrid approach, several other issues must be addressed. Most of the developed coating systems are still unsuitable for large-scale production. Furthermore, for practical industrial applications, the coatings need to exhibit multifunctional properties, such as self-cleaning, anti-corrosion, wear resistance, and photothermal capabilities. However, most research on icephobic coatings has concentrated on reducing  $\tau_{ice}$  rather than on improving mechanical properties and wear resistance. The integration of theoretical simulations and experimental results is also essential to improve the understanding of the anti-icing mechanisms of each approach, a gap that is currently lacking in the literature. Future directions should aim to align with the standards for wind turbine coatings by emphasizing simple processes, accessible raw materials, cost-effectiveness, and eco-friendly methods in the formulation, fabrication and analysis of coatings.

The conclusion highlights a clear direction for future efforts in the development of icephobic coatings. Priority should be given to creating coatings with ultra-low ice adhesion that can also withstand the demanding conditions typical of wind turbine operations. Equally important is the establishment of comprehensive standards tailored to the application of icephobic coatings on wind turbines. These standards would provide a benchmark for performance and durability, guiding the formulation of coatings to ensure they meet both functional and industrial requirements. Additionally, interdisciplinary approaches that integrate advances in material science, engineering, and environmental testing could accelerate progress in this critical area. Employing numerical simulations is also crucial for optimizing the performance and durability of icephobic coatings on wind turbines by providing predictive insights into ice adhesion, thermal behavior, and aerodynamic impacts under real-world operating conditions. Future work should focus on developing standardized simulation frameworks to evaluate the performance of icephobic coatings under conditions representative of wind turbine operations.

**Author Contributions:** Conceptualization: G.M. (Ghazal Minoofar), A.J.K., M.S.K. and G.M. (Gelareh Momen); validation: G.M. (Ghazal Minoofar), A.J.K., M.S.K. and G.M. (Gelareh Momen); investigation: G.M. (Ghazal Minoofar), A.J.K., M.S.K. and G.M. (Gelareh Momen); resources: G.M. (Ghazal Minoofar), A.J.K.; data curation: G.M. (Ghazal Minoofar), A.J.K., M.S.K. and G.M. (Gelareh Momen); writing—original draft preparation: G.M. (Ghazal Minoofar), A.J.K., M.S.K. and G.M. (Gelareh Momen); writing—review and editing: G.M. (Ghazal Minoofar), A.J.K., M.S.K. and G.M. (Gelareh Momen); supervision: G.M. (Gelareh Momen); project administration: G.M. (Gelareh Momen); funding acquisition: G.M. (Gelareh Momen). All authors have read and agreed to the published version of the manuscript.

**Funding:** This work was supported by the Natural Sciences and Engineering Research Council of Canada (NSERC) with grant ID of ALLRP 580753-22.

**Acknowledgments:** The authors acknowledge all support from the Natural Sciences and Engineering Research Council of Canada (NSERC), the Institutional Research Chair in Innovative Anti-icing Materials (CiMAGI) and Université du Québec à Chicoutimi (UQAC).

**Conflicts of Interest:** The authors declare no conflict of interest.

## References

1. Huang, X.; Tepylo, N.; Pommier-Budinger, V.; Budinger, M.; Bonaccorso, E.; Villedieu, P.; Bennani, L. A survey of icephobic coatings and their potential use in a hybrid coating/active ice protection system for aerospace applications. *Prog. Aerosp. Sci.* **2019**, *105*, 74–97. [[CrossRef](#)]
2. Dierer, S.; Oechlin, R.; Cattin, R. Wind turbines in icing conditions: Performance and prediction. *Adv. Sci. Res.* **2011**, *6*, 245–250. [[CrossRef](#)]
3. Fortin, G.; Perron, J. Wind turbine icing and de-icing. In Proceedings of the 47th AIAA Aerospace Sciences Meeting including The New Horizons Forum and Aerospace Exposition, Orlando, FL, USA, 5–8 January 2009; p. 274.
4. Latthe, S.S.; Sutar, R.S.; Bhosale, A.K.; Nagappan, S.; Ha, C.-S.; Sadasivuni, K.K.; Liu, S.; Xing, R. Recent developments in air-trapped superhydrophobic and liquid-infused slippery surfaces for anti-icing application. *Prog. Org. Coat.* **2019**, *137*, 105373. [[CrossRef](#)]
5. Han, Y.; Palacios, J.; Schmitz, S. Scaled ice accretion experiments on a rotating wind turbine blade. *J. Wind Eng. Ind. Aerodyn.* **2012**, *109*, 55–67. [[CrossRef](#)]
6. Parent, O.; Ilinca, A. Anti-icing and de-icing techniques for wind turbines: Critical review. *Cold Reg. Sci. Technol.* **2011**, *65*, 88–96. [[CrossRef](#)]
7. Li, Y.; Sun, C.; Jiang, Y.; Feng, F. Scaling method of the rotating blade of a wind turbine for a rime ice wind tunnel test. *Energies* **2019**, *12*, 627. [[CrossRef](#)]
8. Madi, E.; Pope, K.; Huang, W.; Iqbal, T. A review of integrating ice detection and mitigation for wind turbine blades. *Renew. Sustain. Energy Rev.* **2019**, *103*, 269–281. [[CrossRef](#)]
9. Susoff, M.; Siegmann, K.; Pfaffenroth, C.; Hirayama, M. Evaluation of icephobic coatings—Screening of different coatings and influence of roughness. *Appl. Surf. Sci.* **2013**, *282*, 870–879. [[CrossRef](#)]
10. Laakso, T.; Peltola, E. Review on blade heating technology and future prospects. In Proceedings of the BOREAS VII: Impact of Icing on Wind Energy Production and Other Field of Activities, Saariselkä, Finland, 7–8 March 2005.
11. Wang, C.; Fuller, T.; Zhang, W.; Wynne, K.J. Thickness dependence of ice removal stress for a polydimethylsiloxane nanocomposite: Sylgard 184. *Langmuir* **2014**, *30*, 12819–12826. [[CrossRef](#)]
12. Johnston, I.D.; McCluskey, D.K.; Tan, C.K.; Tracey, M.C. Mechanical characterization of bulk Sylgard 184 for microfluidics and microengineering. *J. Micromechanics Microengineering* **2014**, *24*, 035017. [[CrossRef](#)]
13. Hong, S.; Wang, R.; Huang, X.; Liu, H. Facile one-step fabrication of PHC/PDMS anti-icing coatings with mechanical properties and good durability. *Prog. Org. Coat.* **2019**, *135*, 263–269. [[CrossRef](#)]
14. Liu, Y.; Ma, L.; Wang, W.; Kota, A.K.; Hu, H. An experimental study on soft PDMS materials for aircraft icing mitigation. *Appl. Surf. Sci.* **2018**, *447*, 599–609. [[CrossRef](#)]
15. Oelker, S.; Ait-Alla, A.; Lütjen, M.; Lewandowski, M.; Freitag, M.; Thoben, K.-D. A simulation study of feeder-based installation concepts for offshore wind farms. In Proceedings of the ISOPE International Ocean and Polar Engineering Conference, Sapporo, Japan, 10–15 June 2018; p. ISOPE-I-18-332.
16. Wang, Z. Recent progress on ultrasonic de-icing technique used for wind power generation, high-voltage transmission line and aircraft. *Energy Build.* **2017**, *140*, 42–49. [[CrossRef](#)]
17. Etemaddar, M.; Hansen, M.O.L.; Moan, T. Wind turbine aerodynamic response under atmospheric icing conditions. *Wind Energy* **2014**, *17*, 241–265. [[CrossRef](#)]
18. Habibi, H.; Cheng, L.; Zheng, H.; Kappatos, V.; Selcuk, C.; Gan, T.-H. A dual de-icing system for wind turbine blades combining high-power ultrasonic guided waves and low-frequency forced vibrations. *Renew. Energy* **2015**, *83*, 859–870. [[CrossRef](#)]
19. Kreutz, M.; Ait-Alla, A.; Varasteh, K.; Oelker, S.; Greulich, A.; Freitag, M.; Thoben, K.-D. Machine learning-based icing prediction on wind turbines. *Procedia Cirp* **2019**, *81*, 423–428. [[CrossRef](#)]
20. Shamshiri, M.; Jafari, R.; Momen, G. Potential use of smart coatings for icephobic applications: A review. *Surf. Coat. Technol.* **2021**, *424*, 127656. [[CrossRef](#)]
21. Fakorede, O.; Feger, Z.; Ibrahim, H.; Ilinca, A.; Perron, J.; Masson, C. Ice protection systems for wind turbines in cold climate: Characteristics, comparisons and analysis. *Renew. Sustain. Energy Rev.* **2016**, *65*, 662–675. [[CrossRef](#)]
22. Lehtomäki, V.; Krenn, A.; Jordaen, P.; Godreau, C.; Davis, N.; Khadiri-Yazami, Z.; Bredesen, R.E.; Ronsten, G.; Wickman, H.; Bourgeois, S. Available technologies for wind energy in cold climates. In Proceedings of the International Energy Agency Wind Technology Collaboration Programme (IEA Wind TCP), Denmark, Germany, 12 October 2018.
23. Hejazi, V.; Sobolev, K.; Nosonovsky, M. From superhydrophobicity to icephobicity: Forces and interaction analysis. *Sci. Rep.* **2013**, *3*, 2194. [[CrossRef](#)]
24. He, Z.; Xiao, S.; Gao, H.; He, J.; Zhang, Z. Multiscale crack initiator promoted super-low ice adhesion surfaces. *Soft Matter* **2017**, *13*, 6562–6568. [[CrossRef](#)] [[PubMed](#)]

25. Momen, G.; Jafari, R.; Farzaneh, M. Ice repellency behaviour of superhydrophobic surfaces: Effects of atmospheric icing conditions and surface roughness. *Appl. Surf. Sci.* **2015**, *349*, 211–218. [[CrossRef](#)]
26. Golovin, K.; Kobaku, S.P.; Lee, D.H.; DiLoreto, E.T.; Mabry, J.M.; Tuteja, A. Designing durable icephobic surfaces. *Sci. Adv.* **2016**, *2*, e1501496. [[CrossRef](#)]
27. Li, T.; Ibáñez-Ibáñez, P.F.; Håkonsen, V.; Wu, J.; Xu, K.; Zhuo, Y.; Luo, S.; He, J.; Zhang, Z. Self-deicing electrolyte hydrogel surfaces with Pa-level ice adhesion and durable antifreezing/antifrost performance. *ACS Appl. Mater. Interfaces* **2020**, *12*, 35572–35578. [[CrossRef](#)] [[PubMed](#)]
28. Zhuo, Y.; Xiao, S.; Håkonsen, V.; He, J.; Zhang, Z. Anti-icing ionogel surfaces: Inhibiting ice nucleation, growth, and adhesion. *ACS Mater. Lett.* **2020**, *2*, 616–623. [[CrossRef](#)]
29. Shamshiri, M.; Jafari, R.; Momen, G. Icephobic properties of aqueous self-lubricating coatings containing PEG-PDMS copolymers. *Prog. Org. Coat.* **2021**, *161*, 106466. [[CrossRef](#)]
30. Heydarian, S.; Maghsoudi, K.; Jafari, R.; Gauthier, H.; Momen, G. Fabrication of liquid-infused textured surfaces (LITS): The effect of surface textures on anti-icing properties and durability. *Mater. Today Commun.* **2022**, *32*, 103935. [[CrossRef](#)]
31. Alsabagh, A.S.Y.; Tiu, W.; Xu, Y.; Virk, M.S. A review of the effects of ice accretion on the structural behavior of wind turbines. *Wind Eng.* **2013**, *37*, 59–70. [[CrossRef](#)]
32. Rehfeld, N.; Berton, B.; Morita, K.; Kimura, S. A way forward to design efficient wing ice protection systems. In Proceedings of the Greener Aviation Conference, Brussels, Belgium, 11–13 October 2016.
33. Muthumani, A.; Fay, L.; Akin, M.; Wang, S.; Gong, J.; Shi, X. Correlating lab and field tests for evaluation of deicing and anti-icing chemicals: A review of potential approaches. *Cold Reg. Sci. Technol.* **2014**, *97*, 21–32. [[CrossRef](#)]
34. Nistal, A.; Sierra-Martín, B.; Fernández-Barbero, A. On the Durability of Icephobic Coatings: A Review. *Materials* **2023**, *17*, 235. [[CrossRef](#)]
35. *ISO/TS 19392-6:2023 (E); Paints and Varnishes—Coating Systems for Wind-Turbine Rotor Blades—Part 6: Determination and Evaluation of Ice Adhesion Using Centrifuge*. ISO: Geneva, Switzerland, 2023.
36. Wong, T.-S.; Kang, S.H.; Tang, S.K.; Smythe, E.J.; Hatton, B.D.; Grinthal, A.; Aizenberg, J. Bioinspired self-repairing slippery surfaces with pressure-stable omniphobicity. *Nature* **2011**, *477*, 443–447. [[CrossRef](#)]
37. *ASTM D2240; Standard Test Method for Rubber Property—Durometer Hardness*. ASTM International: West Conshohocken, PA, USA, 2021.
38. *ASTM D4060-19; Standard Test Method for Abrasion Resistance of Organic Coatings by the Taber Abraser*. ASTM International: West Conshohocken, PA, USA, 2019.
39. *ISO/TS19392-5:2023; Paints and Varnishes—Coating Systems for Wind-Turbine Rotor Blades—Part 5: Measurement of Transmittance Properties of UV Protective Coatings*. ISO: Geneva, Switzerland, 2023.
40. *ISO 16-674-3: 2013; Paints and Varnishes—Methods of Exposure to Laboratory Light Sources; Part 3: Fluorescent UV Lamps*. ISO: Geneva, Switzerland, 2013.
41. *ISO 4624:2023; Paints and Varnishes—Pull-Off Test for Adhesion*. ISO: Geneva, Switzerland, 2016.
42. *ISO/TS 19392-3; Paints and Varnishes—Coating Systems for Wind-Turbine Rotor Blades. Part 3: Determination and Evaluation of Resistance to Rain Erosion Using Water Jet*. ISO: Geneva, Switzerland, 2018.
43. Ma, L.; Zhang, Z.; Gao, L.; Liu, Y.; Hu, H. An exploratory study on using Slippery-Liquid-Infused-Porous-Surface (SLIPS) for wind turbine icing mitigation. *Renew. Energy* **2020**, *162*, 2344–2360. [[CrossRef](#)]
44. Piscitelli, F.; Chiariello, A.; Dabkowski, D.; Corrado, G.; Marra, F.; Di Palma, L. Superhydrophobic coatings as anti-icing systems for small aircraft. *Aerospace* **2020**, *7*, 2. [[CrossRef](#)]
45. Liu, Z.; Zhang, Y.; Li, Y. Superhydrophobic coating for blade surface ice-phobic properties of wind turbines: A review. *Prog. Org. Coat.* **2024**, *187*, 108145. [[CrossRef](#)]
46. Okulov, V.; Kabardin, I.; Mukhin, D.; Stepanov, K.; Okulova, N. Physical de-icing techniques for wind turbine blades. *Energies* **2021**, *14*, 6750. [[CrossRef](#)]
47. Gao, L.; Liu, Y.; Ma, L.; Hu, H. A hybrid strategy combining minimized leading-edge electric-heating and superhydro-/ice-phobic surface coating for wind turbine icing mitigation. *Renew. Energy* **2019**, *140*, 943–956. [[CrossRef](#)]
48. Colas, A. Silicones: Preparation, properties and performance. In *Dow Corning, Life Sciences*; Citeseer: University Park, PA, USA, 2005.
49. Yu, D.; Zhao, Y.; Li, H.; Qi, H.; Li, B.; Yuan, X. Preparation and evaluation of hydrophobic surfaces of polyacrylate-polydimethylsiloxane copolymers for anti-icing. *Prog. Org. Coat.* **2013**, *76*, 1435–1444. [[CrossRef](#)]
50. Owens, D.K.; Wendt, R. Estimation of the surface free energy of polymers. *J. Appl. Polym. Sci.* **1969**, *13*, 1741–1747. [[CrossRef](#)]
51. Golovin, K.; Tuteja, A. A predictive framework for the design and fabrication of icephobic polymers. *Sci. Adv.* **2017**, *3*, e1701617. [[CrossRef](#)]
52. Zhuo, Y.; Xiao, S.; Amirfazli, A.; He, J.; Zhang, Z. Polysiloxane as icephobic materials—The past, present and the future. *Chem. Eng. J.* **2021**, *405*, 127088. [[CrossRef](#)]

53. Loughborough, D.L.; Haas, E. Reduction of the adhesion of ice to de-icer surfaces. *J. Aeronaut. Sci.* **1946**, *13*, 126–134. [[CrossRef](#)]
54. Liu, M.; Sun, J.; Sun, Y.; Bock, C.; Chen, Q. Thickness-dependent mechanical properties of polydimethylsiloxane membranes. *J. Micromechanics Microengineering* **2009**, *19*, 035028. [[CrossRef](#)]
55. Lötters, J.C.; Olthuis, W.; Veltink, P.H.; Bergveld, P. The mechanical properties of the rubber elastic polymer polydimethylsiloxane for sensor applications. *J. Micromechanics Microengineering* **1997**, *7*, 145. [[CrossRef](#)]
56. Long, Y.; Yin, X.; Mu, P.; Wang, Q.; Hu, J.; Li, J. Slippery liquid-infused porous surface (SLIPS) with superior liquid repellency, anti-corrosion, anti-icing and intensified durability for protecting substrates. *Chem. Eng. J.* **2020**, *401*, 126137. [[CrossRef](#)]
57. Rogers, J.A.; Nuzzo, R.G. Recent progress in soft lithography. *Mater. Today* **2005**, *8*, 50–56. [[CrossRef](#)]
58. Wang, W.; Sun, S.; Hu, S.; Yang, B.; He, S.; Wang, R.; Zhang, L. Unprecedented strength polysiloxane-based polyurethane for 3D printing and shape memory. *ACS Appl. Mater. Interfaces* **2022**, *14*, 3324–3333. [[CrossRef](#)]
59. Cui, W.; Pakkanen, T.A. Fabrication of transparent icephobic surfaces with self-reparability: Effect of structuring and thickness of the lubricant-elastomer layer. *Appl. Surf. Sci.* **2020**, *504*, 144061. [[CrossRef](#)]
60. Zhu, G.; Tian, Y.; Wu, J.; Yang, G.; Hua, Z. Renewable plant oil-based polysiloxane coatings with efficient frost resistance and anti-icing properties. *ACS Appl. Polym. Mater.* **2022**, *4*, 7626–7633. [[CrossRef](#)]
61. Zhang, Z.; Xie, Q.; Zhang, G.; Ma, C.; Zhang, G. Surface-Enriched Amphiphilic Polysiloxane Coating with Superior Antifouling Ability and Strong Substrate Adhesion. *ACS Appl. Polym. Mater.* **2023**, *5*, 3524–3533. [[CrossRef](#)]
62. Jin, X.; Li, W.; Wang, S.; Li, Y.; Yang, C.; Lu, Z.; Dong, C. Developing flame-retardant, antibacterial cotton fabric by incorporating a linear polysiloxane-based coating. *Ind. Crops Prod.* **2023**, *191*, 115934. [[CrossRef](#)]
63. Shamshiri, M.; Jafari, R.; Momen, G. A novel hybrid anti-icing surface combining an aqueous self-lubricating coating and phase-change materials. *Prog. Org. Coat.* **2023**, *177*, 107414. [[CrossRef](#)]
64. Rashevskii, A.A.; Deriabin, K.V.; Parshina, E.K.; Islamova, R.M. Self-Healing Redox-Active Coatings Based on Ferrocenyl-Containing Polysiloxanes. *Coatings* **2023**, *13*, 1282. [[CrossRef](#)]
65. Sojoudi, H.; Wang, M.; Boscher, N.; McKinley, G.H.; Gleason, K.K. Durable and scalable icephobic surfaces: Similarities and distinctions from superhydrophobic surfaces. *Soft Matter* **2016**, *12*, 1938–1963. [[CrossRef](#)] [[PubMed](#)]
66. Li, X.; Li, Y.; Ren, L.; Zhu, K.; Zhao, Y.; Yuan, X. Self-crosslinking coatings of fluorinated polysiloxanes with enhanced icephobicity. *Thin Solid Film.* **2017**, *639*, 113–122. [[CrossRef](#)]
67. Zhuo, Y.; Xiao, S.; Håkonsen, V.; Li, T.; Wang, F.; He, J.; Zhang, Z. Ultrafast self-healing and highly transparent coating with mechanically durable icephobicity. *Appl. Mater. Today* **2020**, *19*, 100542. [[CrossRef](#)]
68. Owen, M. Elastomers: Siloxane. In *Encyclopedia of Materials: Science and Technology*; ADS: London, UK, 2001; pp. 2480–2482.
69. Paul, D.R.; Mark, J.E. Fillers for polysiloxane (“silicone”) elastomers. *Prog. Polym. Sci.* **2010**, *35*, 893–901. [[CrossRef](#)]
70. Yang, C.; Wang, F.; Li, W.; Ou, J.; Li, C.; Amirfazli, A. Anti-icing properties of superhydrophobic ZnO/PDMS composite coating. *Appl. Phys. A* **2016**, *122*, 1–10. [[CrossRef](#)]
71. Liu, B.; Liu, Z.; Li, Y.; Feng, F. A Wind Tunnel Test of the Anti-Icing Properties of MoS<sub>2</sub>/ZnO Hydrophobic Nano-Coatings for Wind Turbine Blades. *Coatings* **2023**, *13*, 686. [[CrossRef](#)]
72. Lei, S.; Wang, F.; Fang, X.; Ou, J.; Li, W. Icing behavior of water droplets impinging on cold superhydrophobic surface. *Surf. Coat. Technol.* **2019**, *363*, 362–368. [[CrossRef](#)]
73. Liu, J.; Wang, J.; Mazzola, L.; Memon, H.; Barman, T.; Turnbull, B.; Mingione, G.; Choi, K.-S.; Hou, X. Development and evaluation of poly (dimethylsiloxane) based composite coatings for icephobic applications. *Surf. Coat. Technol.* **2018**, *349*, 980–985. [[CrossRef](#)]
74. Zhang, L.-B.; Zhang, H.-X.; Liu, Z.-J.; Jiang, X.-Y.; Agathopoulos, S.; Deng, Z.; Gao, H.-Y.; Zhang, L.; Lu, H.-P.; Deng, L.-J. Nano-silica anti-icing coatings for protecting wind-power turbine fan blades. *J. Colloid Interface Sci.* **2023**, *630*, 1–10. [[PubMed](#)]
75. Bao, J.; He, J.; Chen, B.; Yang, H.; Jie, J.; Wang, R.; Zhang, S. Multi-scale superhydrophobic anti-icing coating for wind turbine blades. *Energy Eng* **2021**, *118*, 947–959. [[CrossRef](#)]
76. Lv, J.; Song, Y.; Jiang, L.; Wang, J. Bio-inspired strategies for anti-icing. *ACS Nano* **2014**, *8*, 3152–3169. [[CrossRef](#)] [[PubMed](#)]
77. Howell, C.; Vu, T.L.; Lin, J.J.; Kolle, S.; Juthani, N.; Watson, E.; Weaver, J.C.; Alvarenga, J.; Aizenberg, J. Self-replenishing vascularized fouling-release surfaces. *ACS Appl. Mater. Interfaces* **2014**, *6*, 13299–13307. [[CrossRef](#)]
78. Wang, P.; Zhang, D.; Lu, Z. Slippery liquid-infused porous surface bio-inspired by pitcher plant for marine anti-biofouling application. *Colloids Surf. B Biointerfaces* **2015**, *136*, 240–247. [[CrossRef](#)] [[PubMed](#)]
79. Zhu, L.; Xue, J.; Wang, Y.; Chen, Q.; Ding, J.; Wang, Q. Ice-phobic coatings based on silicon-oil-infused polydimethylsiloxane. *ACS Appl. Mater. Interfaces* **2013**, *5*, 4053–4062. [[CrossRef](#)] [[PubMed](#)]
80. Li, T.; Zhuo, Y.; Håkonsen, V.; Rønneberg, S.; He, J.; Zhang, Z. Epidermal gland inspired self-repairing slippery lubricant-infused porous coatings with durable low ice adhesion. *Coatings* **2019**, *9*, 602. [[CrossRef](#)]
81. Coady, M.J.; Wood, M.; Wallace, G.Q.; Nielsen, K.E.; Kietzig, A.-M.; Lagugné-Labarthe, F.o.; Ragogna, P.J. Icephobic behavior of UV-cured polymer networks incorporated into slippery lubricant-infused porous surfaces: Improving SLIPS durability. *ACS Appl. Mater. Interfaces* **2018**, *10*, 2890–2896. [[CrossRef](#)] [[PubMed](#)]

82. Raman, A.; Jayan, J.S.; Deeraj, B.; Saritha, A.; Joseph, K. Electrospun nanofibers as effective superhydrophobic surfaces: A brief review. *Surf. Interfaces* **2021**, *24*, 101140. [[CrossRef](#)]
83. He, J.; Wang, M.; Wang, R.; Chen, B.; Yang, K.; Jie, J.; Bao, J.; Luo, J. Durable solid lubricant wind turbine blade anti-icing coating based on saturated chain polyhydrocarbons. *J. Adhes. Sci. Technol.* **2023**, *37*, 3485–3500. [[CrossRef](#)]
84. Cao, M.; Guo, D.; Yu, C.; Li, K.; Liu, M.; Jiang, L. Water-repellent properties of superhydrophobic and lubricant-infused “slippery” surfaces: A brief study on the functions and applications. *ACS Appl. Mater. Interfaces* **2016**, *8*, 3615–3623. [[CrossRef](#)] [[PubMed](#)]
85. Wang, N.; Xiong, D.; Pan, S.; Wang, K.; Shi, Y.; Deng, Y. Robust superhydrophobic coating and the anti-icing properties of its lubricants-infused-composite surface under condensing condition. *New J. Chem.* **2017**, *41*, 1846–1853. [[CrossRef](#)]
86. Barthwal, S.; Lee, B.; Lim, S.-H. Fabrication of robust and durable slippery anti-icing coating on textured superhydrophobic aluminum surfaces with infused silicone oil. *Appl. Surf. Sci.* **2019**, *496*, 143677. [[CrossRef](#)]
87. Khammas, R.; Koivuluoto, H. Durable Icephobic Slippery Liquid-Infused Porous Surfaces (SLIPS) Using Flame-and Cold-Spraying. *Sustainability* **2022**, *14*, 8422. [[CrossRef](#)]
88. Mahmut, T.; Memon, H.; Xu, F.; Ahmed, I.; Hou, X. Electrospun nanofibre membrane based transparent slippery liquid-infused porous surfaces with icephobic properties. *Colloids Surf. A Physicochem. Eng. Asp.* **2020**, *585*, 124177.
89. Meuler, A.J.; Smith, J.D.; Varanasi, K.K.; Mabry, J.M.; McKinley, G.H.; Cohen, R.E. Relationships between water wettability and ice adhesion. *ACS Appl. Mater. Interfaces* **2010**, *2*, 3100–3110. [[CrossRef](#)] [[PubMed](#)]
90. Petit, J.; Bonaccorso, E. General frost growth mechanism on solid substrates with different stiffness. *Langmuir* **2014**, *30*, 1160–1168. [[CrossRef](#)]
91. Beemer, D.L.; Wang, W.; Kota, A.K. Durable gels with ultra-low adhesion to ice. *J. Mater. Chem. A* **2016**, *4*, 18253–18258. [[CrossRef](#)]
92. Urata, C.; Dunderdale, G.J.; England, M.W.; Hozumi, A. Self-lubricating organogels (SLUGs) with exceptional syneresis-induced anti-sticking properties against viscous emulsions and ices. *J. Mater. Chem. A* **2015**, *3*, 12626–12630. [[CrossRef](#)]
93. Wang, Y.; Yao, X.; Chen, J.; He, Z.; Liu, J.; Li, Q.; Wang, J.; Jiang, L. Organogel as durable anti-icing coatings. *Sci. China Mater.* **2015**, *58*, 559–565. [[CrossRef](#)]
94. Bharathidasan, T.; Kumar, S.V.; Bobji, M.; Chakradhar, R.; Basu, B.J. Effect of wettability and surface roughness on ice-adhesion strength of hydrophilic, hydrophobic and superhydrophobic surfaces. *Appl. Surf. Sci.* **2014**, *314*, 241–250. [[CrossRef](#)]
95. He, Z.; Zhuo, Y.; He, J.; Zhang, Z. Design and preparation of sandwich-like polydimethylsiloxane (PDMS) sponges with super-low ice adhesion. *Soft Matter* **2018**, *14*, 4846–4851. [[CrossRef](#)]
96. Jalali Kandeloo, A.; Eder, T.; Hetey, D.; Bismarck, A.; Reithofer, M.R.; Cordill, M.J.; Chin, J.M. Expanding Transparent Covalently Attached Liquid-Like Surfaces for Icephobic Coatings with Broad Substrate Compatibility. *Adv. Mater. Interfaces* **2025**, 2400808. [[CrossRef](#)]
97. Khatir, B.; Serles, P.; Wen, T.; Vuong, T.V.; Shayesteh, A.; Au, S.; Sinton, D.; Master, E.R.; Filleter, T.; Golovin, K. Autophobic polydimethylsiloxane nanodroplets enable abrasion-tolerant omniphobic surfaces. *Chem. Eng. J.* **2024**, *502*, 157718. [[CrossRef](#)]
98. Chen, L.; Huang, S.; Ras, R.H.; Tian, X. Omniphobic liquid-like surfaces. *Nat. Rev. Chem.* **2023**, *7*, 123–137. [[CrossRef](#)]
99. Agapov, A.; Sokolov, A.P. Size of the dynamic bead in polymers. *Macromolecules* **2010**, *43*, 9126–9130. [[CrossRef](#)]
100. Cheng, D.F.; Urata, C.; Yagihashi, M.; Hozumi, A. A statically oleophilic but dynamically oleophobic smooth nonperfluorinated surface. *Angew. Chem.-Ger. Ed.* **2012**, *124*, 3010. [[CrossRef](#)]
101. Zhao, X.; Khatir, B.; Mirshahidi, K.; Yu, K.; Kizhakkedathu, J.N.; Golovin, K. Macroscopic evidence of the liquidlike nature of nanoscale polydimethylsiloxane brushes. *ACS Nano* **2021**, *15*, 13559–13567. [[CrossRef](#)]
102. Fan, Y.; Wu, C.; Yang, J.; Wang, Y.; Zhou, Y.; Zhou, J.; Luo, J.; Zhang, J.; Huang, S.; Tian, X. Reducing the contact time of impacting water drops on superhydrophobic surfaces by liquid-like coatings. *Chem. Eng. J.* **2022**, *448*, 137638. [[CrossRef](#)]
103. Yan, Y.; Chan-Park, M.; Yue, C. CF<sub>4</sub> plasma treatment of poly (dimethylsiloxane): Effect of fillers and its application to high-aspect-ratio UV embossing. *Langmuir* **2005**, *21*, 8905–8912. [[CrossRef](#)] [[PubMed](#)]
104. Fu, Q.; Wu, X.; Kumar, D.; Ho, J.W.; Kanhere, P.D.; Srikanth, N.; Liu, E.; Wilson, P.; Chen, Z. Development of sol-gel icephobic coatings: Effect of surface roughness and surface energy. *ACS Appl. Mater. Interfaces* **2014**, *6*, 20685–20692. [[CrossRef](#)]
105. Li, K.; Xu, S.; Shi, W.; He, M.; Li, H.; Li, S.; Zhou, X.; Wang, J.; Song, Y. Investigating the effects of solid surfaces on ice nucleation. *Langmuir* **2012**, *28*, 10749–10754. [[CrossRef](#)] [[PubMed](#)]
106. Yilgör, E.; Yilgör, I. Silicone containing copolymers: Synthesis, properties and applications. *Prog. Polym. Sci.* **2014**, *39*, 1165–1195. [[CrossRef](#)]
107. Liu, J.; Yao, Y.; Li, X.; Zhang, Z. Fabrication of advanced polydimethylsiloxane-based functional materials: Bulk modifications and surface functionalizations. *Chem. Eng. J.* **2021**, *408*, 127262. [[CrossRef](#)]
108. Yang, S.; Xia, Q.; Zhu, L.; Xue, J.; Wang, Q.; Chen, Q.-m. Research on the icephobic properties of fluoropolymer-based materials. *Appl. Surf. Sci.* **2011**, *257*, 4956–4962. [[CrossRef](#)]
109. Menini, R.; Farzaneh, M. Advanced icephobic coatings. *J. Adhes. Sci. Technol.* **2011**, *25*, 971–992. [[CrossRef](#)]
110. Murase, H.; Nanishi, K.; Kogure, H.; Fujibayashi, T.; Tamura, K.; Haruta, N. Interactions between heterogeneous surfaces of polymers and water. *J. Appl. Polym. Sci.* **1994**, *54*, 2051–2062. [[CrossRef](#)]

111. Li, H.; Li, X.; Luo, C.; Zhao, Y.; Yuan, X. Icephobicity of polydimethylsiloxane-b-poly (fluorinated acrylate). *Thin Solid Film.* **2014**, *573*, 67–73. [[CrossRef](#)]
112. Niu, M.; He, L.; Liang, J.; Pan, A.; Zhao, X. Effect of side chains and solvents on the film surface of linear fluorosilicone pentablock copolymers. *Prog. Org. Coat.* **2014**, *77*, 1603–1612. [[CrossRef](#)]
113. Liang, J.; He, L.; Zhao, X.; Dong, X.; Luo, H.; Li, W. Novel linear fluoro-silicon-containing pentablock copolymers: Synthesis and their properties as coating materials. *J. Mater. Chem.* **2011**, *21*, 6934–6943. [[CrossRef](#)]
114. Murase, H.; Fujibayashi, T. Characterization of molecular interfaces in hydrophobic systems. *Prog. Org. Coat.* **1997**, *31*, 97–104. [[CrossRef](#)]
115. Li, X.; Zhao, Y.; Li, H.; Yuan, X. Preparation and icephobic properties of polymethyltrifluoropropylsiloxane–polyacrylate block copolymers. *Appl. Surf. Sci.* **2014**, *316*, 222–231. [[CrossRef](#)]
116. Li, X.; Zhang, K.; Zhao, Y.; Zhu, K.; Yuan, X. Formation of icephobic film from POSS-containing fluorosilicone multi-block methacrylate copolymers. *Prog. Org. Coat.* **2015**, *89*, 150–159. [[CrossRef](#)]
117. Li, Y.; Luo, C.; Li, X.; Zhang, K.; Zhao, Y.; Zhu, K.; Yuan, X. Submicron/nano-structured icephobic surfaces made from fluorinated polymethylsiloxane and octavinyl-POSS. *Appl. Surf. Sci.* **2016**, *360*, 113–120. [[CrossRef](#)]
118. Tao, C.; Li, X.; Liu, B.; Zhang, K.; Zhao, Y.; Zhu, K.; Yuan, X. Highly icephobic properties on slippery surfaces formed from polysiloxane and fluorinated POSS. *Prog. Org. Coat.* **2017**, *103*, 48–59. [[CrossRef](#)]
119. Peng, J.; Liu, B.; Gao, S.; Zhu, K.; Zhao, Y.; Li, X.; Yuan, X. Enhanced anti-icing properties of branched PDMS coatings with self-regulated surface patterns. *Sci. China Technol. Sci.* **2020**, *63*, 960–970. [[CrossRef](#)]
120. Zhang, K.; Li, X.; Zhao, Y.; Zhu, K.; Li, Y.; Tao, C.; Yuan, X. UV-curable POSS-fluorinated methacrylate diblock copolymers for icephobic coatings. *Prog. Org. Coat.* **2016**, *93*, 87–96. [[CrossRef](#)]
121. Kim, P.; Wong, T.-S.; Alvarenga, J.; Kreder, M.J.; Adorno-Martinez, W.E.; Aizenberg, J. Liquid-infused nanostructured surfaces with extreme anti-ice and anti-frost performance. *ACS Nano* **2012**, *6*, 6569–6577. [[CrossRef](#)]
122. Kulinich, S.; Farhadi, S.; Nose, K.; Du, X. Superhydrophobic surfaces: Are they really ice-repellent? *Langmuir* **2011**, *27*, 25–29. [[CrossRef](#)]
123. Jung, S.; Dorrestijn, M.; Raps, D.; Das, A.; Megaridis, C.M.; Poulikakos, D. Are superhydrophobic surfaces best for icephobicity? *Langmuir* **2011**, *27*, 3059–3066. [[CrossRef](#)]
124. Meuler, A.J.; McKinley, G.H.; Cohen, R.E. Exploiting topographical texture to impart icephobicity. *ACS Nano* **2010**, *4*, 7048–7052. [[CrossRef](#)] [[PubMed](#)]
125. Hussain, H.; Shah, S.M. Recent developments in nanostructured polyhedral oligomeric silsesquioxane-based materials via ‘controlled’ radical polymerization. *Polym. Int.* **2014**, *63*, 835–847. [[CrossRef](#)]
126. Zhang, W.; Müller, A.H. Architecture, self-assembly and properties of well-defined hybrid polymers based on polyhedral oligomeric silsesquioxane (POSS). *Prog. Polym. Sci.* **2013**, *38*, 1121–1162. [[CrossRef](#)]
127. Pan, A.; Yang, S.; He, L.; Zhao, X. Star-shaped POSS diblock copolymers and their self-assembled films. *RSC Adv.* **2014**, *4*, 27857–27866. [[CrossRef](#)]
128. Wu, J.; Mather, P.T. *POSS Polymers: Physical Properties and Biomaterials Applications*; Taylor & Francis: Abingdon, UK, 2009.
129. Amir, N.; Levina, A.; Silverstein, M.S. Nanocomposites through copolymerization of a polyhedral oligomeric silsesquioxane and methyl methacrylate. *J. Polym. Sci. Part A Polym. Chem.* **2007**, *45*, 4264–4275. [[CrossRef](#)]
130. Hirai, T.; Leolukman, M.; Jin, S.; Goseki, R.; Ishida, Y.; Kakimoto, M.-a.; Hayakawa, T.; Ree, M.; Gopalan, P. Hierarchical self-assembled structures from POSS-containing block copolymers synthesized by living anionic polymerization. *Macromolecules* **2009**, *42*, 8835–8843. [[CrossRef](#)]
131. Ahn, B.; Hirai, T.; Jin, S.; Rho, Y.; Kim, K.-W.; Kakimoto, M.-a.; Gopalan, P.; Hayakawa, T.; Ree, M. Hierarchical structure in nanoscale thin films of a poly (styrene-b-methacrylate grafted with POSS)(PS214-b-PMAPOSS27). *Macromolecules* **2010**, *43*, 10568–10581. [[CrossRef](#)]
132. Hussain, H.; Tan, B.; Mya, K.Y.; Liu, Y.; He, C.; Davis, T.P. Synthesis, micelle formation, and bulk properties of poly (ethylene glycol)-b-poly (pentafluorostyrene)-g-polyhedral oligomeric silsesquioxane amphiphilic hybrid copolymers. *J. Polym. Sci. Part A Polym. Chem.* **2010**, *48*, 152–163. [[CrossRef](#)]
133. Tan, B.; Hussain, H.; He, C. Tailoring micelle formation and gelation in (PEG– P (MA-POSS)) amphiphilic hybrid block copolymers. *Macromolecules* **2011**, *44*, 622–631. [[CrossRef](#)]
134. Pyun, J.; Matyjaszewski, K.; Wu, J.; Kim, G.-M.; Chun, S.B.; Mather, P.T. ABA triblock copolymers containing polyhedral oligomeric silsesquioxane pendant groups: Synthesis and unique properties. *Polymer* **2003**, *44*, 2739–2750. [[CrossRef](#)]
135. Pouget, E.; Tonnar, J.; Lucas, P.; Lacroix-Desmazes, P.; Ganachaud, F.; Boutevin, B. Well-architected poly (dimethylsiloxane)-containing copolymers obtained by radical chemistry. *Chem. Rev.* **2010**, *110*, 1233–1277. [[CrossRef](#)]
136. Shinoda, H.; Matyjaszewski, K. Improving the structural control of graft copolymers. Copolymerization of poly (dimethylsiloxane) macromonomer with methyl methacrylate using RAFT polymerization. *Macromol. Rapid Commun.* **2001**, *22*, 1176–1181. [[CrossRef](#)]

137. Kessler, D.; Theato, P. Reactive surface coatings based on polysilsesquioxanes: Defined adjustment of surface wettability. *Langmuir* **2009**, *25*, 14200–14206. [[CrossRef](#)] [[PubMed](#)]
138. Mya, K.Y.; Lin, E.M.; Gudipati, C.S.; Shen, L.; He, C. Time-dependent polymerization kinetic study and the properties of hybrid polymers with functional silsesquioxanes. *J. Phys. Chem. B* **2010**, *114*, 9119–9127. [[CrossRef](#)]
139. Zhang, W.; Fang, B.; Walther, A.; Müller, A.H. Synthesis via RAFT polymerization of tadpole-shaped organic/inorganic hybrid poly (acrylic acid) containing polyhedral oligomeric silsesquioxane (POSS) and their self-assembly in water. *Macromolecules* **2009**, *42*, 2563–2569. [[CrossRef](#)]
140. Ramirez, S.M.; Diaz, Y.J.; Sahagun, C.M.; Duff, M.W.; Lawal, O.B.; Iacono, S.T.; Mabry, J.M. Reversible addition–fragmentation chain transfer (RAFT) copolymerization of fluoroalkyl polyhedral oligomeric silsesquioxane (F-POSS) macromers. *Polym. Chem.* **2013**, *4*, 2230–2234. [[CrossRef](#)]
141. Liao, W.; Zou, L.; Zheng, S.; Zhao, L.; Huang, X.; Ye, L.; Zhong, G. Effects of colloidal silica on the properties of POSS-containing fluorinated poly (styrene–acrylate)/SiO<sub>2</sub> composite materials. *J. Coat. Technol. Res.* **2021**, *18*, 107–116. [[CrossRef](#)]
142. Moad, G.; Rizzardo, E.; Thang, S.H. Radical addition–fragmentation chemistry in polymer synthesis. *Polymer* **2008**, *49*, 1079–1131. [[CrossRef](#)]
143. Li, B.; Li, X.; Zhang, K.; Li, H.; Zhao, Y.; Ren, L.; Yuan, X. Synthesis of POSS-containing fluorosilicone block copolymers via RAFT polymerization for application as non-wetting coating materials. *Prog. Org. Coat.* **2015**, *78*, 188–199. [[CrossRef](#)]
144. Deng, Y.; Bernard, J.; Alcouffe, P.; Galy, J.; Dai, L.; Gérard, J.F. Nanostructured hybrid polymer networks from in situ self-assembly of RAFT-synthesized POSS-based block copolymers. *J. Polym. Sci. Part A Polym. Chem.* **2011**, *49*, 4343–4352. [[CrossRef](#)]
145. Yang, C.; Deng, Y.; Zeng, B.; Yuan, C.; Chen, M.; Luo, W.; Liu, J.; Xu, Y.; Dai, L. Hybrid amphiphilic block copolymers containing polyhedral oligomeric silsesquioxane: Synthesis, characterization, and self-assembly in solutions. *J. Polym. Sci. Part A Polym. Chem.* **2012**, *50*, 4300–4310. [[CrossRef](#)]
146. Jalali Kandeloo, A.; Bastani, S.; Mashayekhan, S. Architecting oxidized alginate methacrylate hydrogels with tunable characteristics by altering the sequence of the cross-linking steps, methacrylation reaction time, and polymer concentration. *J. Biomater. Appl.* **2023**, *38*, 25–38. [[CrossRef](#)]
147. Kandeloo, A.J.; Jalili, M.; Ghahari, M. Upconversion Particles’ Role in Composite Materials: From Light Absorption to Energy Conversion. *Res. Dev. Mater. Sci.* **2022**, *16*, 2576–8840.
148. Kandeloo, A.J.; Bastani, S.; Jalili, M.; Ghahari, M.; Ghahrizjani, R.T.; Mohajerani, E. Employing NaYF<sub>4</sub>: Yb, Tm upconversion particles (UCPs) in combination with rGO and PANI nanomaterials for the fabrication of radiation-curable anticorrosion composites/coatings. *Prog. Org. Coat.* **2023**, *180*, 107547. [[CrossRef](#)]
149. Bastani, S.; Jalali Kandeloo, A.; Jalili, M.; Ghahari, M. Nanocomposites Based on Upconversion Nanoparticles. In *Upconversion Nanoparticles (UCNPs) for Functional Applications*; Springer: Berlin/Heidelberg, Germany, 2023; pp. 127–163.
150. Xue, L.; Zhang, Y.; Zuo, Y.; Diao, S.; Zhang, J.; Feng, S. Preparation and characterization of novel UV-curing silicone rubber via thiol-ene reaction. *Mater. Lett.* **2013**, *106*, 425–427. [[CrossRef](#)]
151. Yang, Z.; Bai, Y.; Wei, B.; Cui, Y.; Huang, J.; Li, Y.; Meng, L.; Wang, Y. A facile preparation method of UV rapid curing fluorosilicone coatings with good hydrophobicity and excellent corrosion resistance based on thiol-ene click reaction. *Prog. Org. Coat.* **2023**, *174*, 107248. [[CrossRef](#)]
152. Li, X.; Zhang, K.; Zhao, Y.; Zhu, K.; Yuan, X. Enhancement of icephobic properties based on UV-curable fluorosilicone copolymer films. *RSC Adv.* **2015**, *5*, 90578–90587. [[CrossRef](#)]
153. Zhang, S.; Huang, J.; Cheng, Y.; Yang, H.; Chen, Z.; Lai, Y. Bioinspired surfaces with superwettability for anti-icing and ice-phobic application: Concept, mechanism, and design. *Small* **2017**, *13*, 1701867. [[CrossRef](#)]
154. Kandeloo, A.J.; Attar, M. The diffusion and adhesion relationship between free films and epoxy coated mild steel. *Prog. Org. Coat.* **2023**, *179*, 107561. [[CrossRef](#)]
155. Kausar, A. Role of thermosetting polymer in structural composite. *Am. J. Polym. Sci. Eng* **2017**, *5*, 1–12.
156. Tzetzis, D.; Tsongas, K.; Mansour, G. Determination of the mechanical properties of epoxy silica nanocomposites through FEA-supported evaluation of ball indentation test results. *Mater. Res.* **2017**, *20*, 1571–1578. [[CrossRef](#)]
157. Bellido-Aguilar, D.A.; Zheng, S.; Huang, Y.; Zeng, X.; Zhang, Q.; Chen, Z. Solvent-free synthesis and hydrophobization of biobased epoxy coatings for anti-icing and anticorrosion applications. *ACS Sustain. Chem. Eng.* **2019**, *7*, 19131–19141. [[CrossRef](#)]
158. Marczak, J.; Kargol, M.; Psarski, M.; Celichowski, G. Modification of epoxy resin, silicon and glass surfaces with alkyl- or fluoroalkylsilanes for hydrophobic properties. *Appl. Surf. Sci.* **2016**, *380*, 91–100. [[CrossRef](#)]
159. Adja, A.A.S.; Sobhani, S.; Momen, G.; Fofana, I.; Carrière, J. Step by step progress to achieve an icephobic silicone-epoxy hybrid coating: Tailoring matrix composition and additives. *J. Appl. Polym. Sci.* **2023**, *140*, e54262. [[CrossRef](#)]
160. Verma, S.; Das, S.; Mohanty, S.; Nayak, S.K. A facile preparation of epoxy-polydimethylsiloxane (EP-PDMS) polymer coatings for marine applications. *J. Mater. Res.* **2019**, *34*, 2881–2894. [[CrossRef](#)]
161. Sobhani, S.; Jannesari, A.; Bastani, S. Effect of molecular weight and content of PDMS on morphology and properties of silicone-modified epoxy resin. *J. Appl. Polym. Sci.* **2012**, *123*, 162–178. [[CrossRef](#)]

162. Bajpai, P.; Bajpai, M. Development of a high performance hybrid epoxy silicone resin for coatings. *Pigment Resin Technol.* **2010**, *39*, 96–100. [[CrossRef](#)]
163. Noè, C.; Hakkarainen, M.; Sangermano, M. Cationic UV-curing of epoxidized biobased resins. *Polymers* **2020**, *13*, 89. [[CrossRef](#)] [[PubMed](#)]
164. Xie, Q.; Hao, T.; Wang, C.; Kang, Z.; Shi, Z.; Zhang, J. The mechanical mechanism and influencing factors of ice adhesion strength on ice-phobic coating. *J. Mar. Sci. Eng.* **2021**, *9*, 315. [[CrossRef](#)]
165. Ziętkowska, K.; Przybyszewski, B.; Grzęda, D.; Kozera, R.; Boczkowska, A.; Liszewska, M.; Pakuła, D.; Przekop, R.E.; Sztorch, B. Transparent Silicone&ndash;Epoxy Coatings with Enhanced Icephobic Properties for Photovoltaic Applications. *Appl. Sci.* **2023**, *13*, 7730. [[CrossRef](#)]
166. Smith, S.; DeSimone, J.; Huang, H.; York, G.; Dwight, D.; Wilkes, G.; McGrath, J. Synthesis and characterization of poly (methyl methacrylate)-g-poly (dimethylsiloxane) copolymers. I. Bulk and surface characterization. *Macromolecules* **1992**, *25*, 2575–2581. [[CrossRef](#)]
167. Meraa, A.E.; Goodwin, M.; Pike, J.K.; Wynne, K.J. Synthesis, characterization and surface analysis using dynamic contact angle measurements of graft copolymers: Poly (methyl methacrylate)-g-poly (dimethylsiloxane) and poly (methyl methacrylate)-g-poly (trifluoropropylmethylsiloxane). *Polymer* **1999**, *40*, 419–427. [[CrossRef](#)]
168. Jellinek, H.H.G.; Kachi, H.; Kittaka, S.; Lee, M.; Yokota, R. Ice releasing block-copolymer coatings. *Colloid Polym. Sci.* **1978**, *256*, 544–551. [[CrossRef](#)]
169. Kozera, R.; Przybyszewski, B.; Żołyńska, K.; Boczkowska, A.; Sztorch, B.; Przekop, R.E. Hybrid modification of unsaturated polyester resins to obtain hydro-and icephobic properties. *Processes* **2020**, *8*, 1635. [[CrossRef](#)]
170. Chen, Y.; Kushner, A.M.; Williams, G.A.; Guan, Z. Multiphase design of autonomic self-healing thermoplastic elastomers. *Nat. Chem.* **2012**, *4*, 467–472. [[CrossRef](#)] [[PubMed](#)]
171. Li, C.-H.; Wang, C.; Keplinger, C.; Zuo, J.-L.; Jin, L.; Sun, Y.; Zheng, P.; Cao, Y.; Lissel, F.; Linder, C. A highly stretchable autonomous self-healing elastomer. *Nat. Chem.* **2016**, *8*, 618–624. [[CrossRef](#)]
172. Rekondo, A.; Martin, R.; de Luzuriaga, A.R.; Cabañero, G.; Grande, H.J.; Odriozola, I. Catalyst-free room-temperature self-healing elastomers based on aromatic disulfide metathesis. *Mater. Horiz.* **2014**, *1*, 237–240. [[CrossRef](#)]
173. Wu, J.; Cai, L.H.; Weitz, D.A. Tough self-healing elastomers by molecular enforced integration of covalent and reversible networks. *Adv. Mater.* **2017**, *29*, 1702616. [[CrossRef](#)] [[PubMed](#)]
174. Yan, X.; Liu, Z.; Zhang, Q.; Lopez, J.; Wang, H.; Wu, H.-C.; Niu, S.; Yan, H.; Wang, S.; Lei, T. Quadruple H-bonding cross-linked supramolecular polymeric materials as substrates for stretchable, antitearing, and self-healable thin film electrodes. *J. Am. Chem. Soc.* **2018**, *140*, 5280–5289. [[CrossRef](#)] [[PubMed](#)]
175. Zhang, Q.; Shi, C.-Y.; Qu, D.-H.; Long, Y.-T.; Feringa, B.L.; Tian, H. Exploring a naturally tailored small molecule for stretchable, self-healing, and adhesive supramolecular polymers. *Sci. Adv.* **2018**, *4*, eaat8192. [[CrossRef](#)] [[PubMed](#)]
176. Kim, S.M.; Jeon, H.; Shin, S.H.; Park, S.A.; Jegal, J.; Hwang, S.Y.; Oh, D.X.; Park, J. Superior toughness and fast self-healing at room temperature engineered by transparent elastomers. *Adv. Mater.* **2018**, *30*, 1705145. [[CrossRef](#)]
177. Karthikeyan, N.; Anand, R.; Suthakar, T.; Barhate, S. Materials, innovations and future research opportunities on wind turbine blades—Insight review. *Environ. Prog. Sustain. Energy* **2019**, *38*, e13046. [[CrossRef](#)]
178. Belov, E.; Nadaraia, K.; Mashtalar, D.; Sinebryukhov, S.; Gnedenkov, S. Anti-icing composite fluoropolymer coatings on titanium. *Научно-технические ведомости Санкт-Петербургского государственного политехнического университета. физико-математические науки* **2022**, *15*, 204–209.
179. Zeng, Z.; He, J.; Jie, J.; Zhou, C.; Chen, B.; Bao, J.; Yang, K.; Luo, J. Effect of perfluoropolyether and the micro nano structure of ZnO on anti icing performance of fluorinated organic superhydrophobicity coatings on wind turbine blade surface. *Mater. Res. Express* **2021**, *8*, 115008. [[CrossRef](#)]
180. Lu, Y.; Sathasivam, S.; Song, J.; Crick, C.R.; Carmalt, C.J.; Parkin, I.P. Robust self-cleaning surfaces that function when exposed to either air or oil. *Science* **2015**, *347*, 1132–1135. [[CrossRef](#)] [[PubMed](#)]
181. Son, S.M.; Kim, M.; Yoo, J.J.; Kim, M.S.; Kim, B.-S.; Seong, D.G. Fabrication of carbon fiber/polyamide 6 composites with water resistance and anti-icing performance using a superhydrophobic fluorinated-polydopamine coating. *Compos. Sci. Technol.* **2023**, *238*, 110048. [[CrossRef](#)]
182. Zhang, Y.; Li, F.; Yu, Q.; Ni, C.; Gu, X.; Li, Y.; You, J. Fabrication of PLLA with high ductility and transparency by blending with tiny amount of PVDF and compatibilizers. *Macromol. Mater. Eng.* **2019**, *304*, 1900316. [[CrossRef](#)]
183. Kar, E.; Bose, N.; Dutta, B.; Mukherjee, N.; Mukherjee, S. Ultraviolet-and microwave-protecting, self-cleaning e-skin for efficient energy harvesting and tactile mechanosensing. *ACS Appl. Mater. Interfaces* **2019**, *11*, 17501–17512. [[CrossRef](#)] [[PubMed](#)]
184. Chang, Y.; Zhu, Y.; Xu, F.; Zhang, M.; Liu, Y.; Wang, H. A  $\beta$ -phase crystal poly (vinylidene fluoride) incorporated epoxy-based composite coating with excellent oxygen barrier and anti-corrosion. *Compos. Commun.* **2023**, *37*, 101458. [[CrossRef](#)]
185. Peng, C.; Xing, S.; Yuan, Z.; Xiao, J.; Wang, C.; Zeng, J. Preparation and anti-icing of superhydrophobic PVDF coating on a wind turbine blade. *Appl. Surf. Sci.* **2012**, *259*, 764–768. [[CrossRef](#)]

186. Zhao, Y.; Zhang, P.; Gu, X.; Zhang, X.; Huo, M. Preparation of PVDF-PDMS-SiO<sub>2</sub> multi-stage rough superhydrophobic coating with excellent anti-corrosion and drag reduction performance via one-step cold spraying. *Surf. Coat. Technol.* **2023**, *471*, 129882. [[CrossRef](#)]
187. Huang, S.; Fang, Z.; Chen, D.; Yu, Z.; Sun, Z.; Zhang, Y. Fabrication of mechanochemically robust superhydrophobic coating based on MPVDF/epoxy resins composites. *Prog. Org. Coat.* **2022**, *163*, 106651. [[CrossRef](#)]
188. Ashrafizadeh, H.; Mertiny, P.; McDonald, A. Evaluation of the effect of temperature on mechanical properties and wear resistance of polyurethane elastomers. *Wear* **2016**, *368*, 26–38. [[CrossRef](#)]
189. Wu, Z.; Wang, H.; Tian, X.; Xue, M.; Ding, X.; Ye, X.; Cui, Z. Surface and mechanical properties of hydrophobic silica contained hybrid films of waterborne polyurethane and fluorinated polymethacrylate. *Polymer* **2014**, *55*, 187–194. [[CrossRef](#)]
190. Zhang, J.; Huang, W.; Han, Y. A composite polymer film with both superhydrophobicity and superoleophilicity. *Macromol. Rapid Commun.* **2006**, *27*, 804–808. [[CrossRef](#)]
191. Chauhan, N.P.S.; Jabgid, N.; Punjabi, P.B. Polyurethanes: Silicone-polyurethane copolymers and. *Polyurethane* **2015**, *13*, 6712–6723.
192. Roshan, S.; Jafari, R.; Momen, G. Multifunctional Polyurethane-based Coating with Corrosion Resistance and Anti-icing Performance for AA2024-T3 Alloy Protection. *Colloids Surf. A Physicochem. Eng. Asp.* **2024**, *698*, 134581. [[CrossRef](#)]
193. Wong, W.S.; Stachurski, Z.H.; Nisbet, D.R.; Tricoli, A. Ultra-durable and transparent self-cleaning surfaces by large-scale self-assembly of hierarchical interpenetrated polymer networks. *ACS Appl. Mater. Interfaces* **2016**, *8*, 13615–13623. [[CrossRef](#)] [[PubMed](#)]
194. Zheng, B.; Wang, H.; Wu, X.; Yang, K.; Yu, Y.; Cui, H.; Gao, F.; Qian, K.; Yao, H.; Li, J. Flexible nanocomposite electrothermal films based on carbon nanotubes and waterborne polyurethane with high reliability, stretchability and low-temperature performance for wind turbine blade deicing. *Compos. Part A Appl. Sci. Manuf.* **2022**, *158*, 106979. [[CrossRef](#)]
195. Pathak, S.M.; Kumar, V.P.; Bonu, V.; Mishnaevsky, L., Jr.; Lakshmi, R.; Bera, P.; Barshilia, H.C. Development of Cellulose-Reinforced Polyurethane Coatings: A Novel Eco-Friendly Approach for Wind Turbine Blade Protection. *Energies* **2023**, *16*, 1730. [[CrossRef](#)]
196. Lv, L.; Liu, H.; Zhang, W.; Chen, J.; Liu, Z. Facile UV-curable fabrication of robust, anti-icing superhydrophobic coatings based on polyurethane. *Mater. Lett.* **2020**, *258*, 126653. [[CrossRef](#)]
197. Qiao, X.; Chen, R.; Zhang, H.; Liu, J.; Liu, Q.; Yu, J.; Liu, P.; Wang, J. Outstanding cavitation erosion resistance of hydrophobic polydimethylsiloxane-based polyurethane coatings. *J. Appl. Polym. Sci.* **2019**, *136*, 47668. [[CrossRef](#)]
198. Liu, H.; Li, X.; Lv, L.; Liu, Z.; Chen, J. Fast fabrication of silicone-modified polyurethane/SiO<sub>2</sub> composite superhydrophobic coating with excellent anti-icing and self-cleaning behaviour. *Mater. Res. Express* **2020**, *7*, 116403. [[CrossRef](#)]
199. Zhao, X.; Li, Y.; Li, B.; Hu, T.; Yang, Y.; Li, L.; Zhang, J. Environmentally benign and durable superhydrophobic coatings based on SiO<sub>2</sub> nanoparticles and silanes. *J. Colloid Interface Sci.* **2019**, *542*, 8–14. [[CrossRef](#)] [[PubMed](#)]
200. Ibrahim, S.H.; El-Tayeb, N. Effect of nano-silica/alumina hybrid coating on erosion resistance of glass fibre-reinforced polymer for the application of wind turbine blades. *Proc. Inst. Mech. Eng. Part J J. Eng. Tribol.* **2022**, *236*, 2013–2031. [[CrossRef](#)]
201. Carreño, F.; Gude, M.; Calvo, S.; de la Fuente, O.R.; Carmona, N. Design and development of icephobic coatings based on sol-gel/modified polyurethane paints. *Mater. Today Commun.* **2020**, *25*, 101616. [[CrossRef](#)]
202. Golovin, K.; Boban, M.; Mabry, J.M.; Tuteja, A. Designing self-healing superhydrophobic surfaces with exceptional mechanical durability. *ACS Appl. Mater. Interfaces* **2017**, *9*, 11212–11223. [[CrossRef](#)]
203. Pathak, S.M.; Kumar, V.P.; Bonu, V.; Latha, S.; Mishnaevsky, L., Jr.; Lakshmi, R.; Bera, P.; Barshilia, H.C. Solid particle erosion studies of ceramic oxides reinforced water-based PU nanocomposite coatings for wind turbine blade protection. *Ceram. Int.* **2022**, *48*, 35788–35798. [[CrossRef](#)]
204. May, C. *Epoxy Resins: Chemistry and Technology*; Routledge: London, UK, 2018.
205. Lv, J.; Zhu, C.; Qiu, H.; Zhang, J.; Gu, C.; Feng, J. Robust icephobic epoxy coating using maleic anhydride as a crosslinking agent. *Prog. Org. Coat.* **2020**, *142*, 105561. [[CrossRef](#)]
206. Zheng, S.; Bellido-Aguilar, D.A.; Wu, X.; Zhan, X.; Huang, Y.; Zeng, X.; Zhang, Q.; Chen, Z. Durable waterborne hydrophobic bio-epoxy coating with improved anti-icing and self-cleaning performance. *ACS Sustain. Chem. Eng.* **2018**, *7*, 641–649. [[CrossRef](#)]
207. Yancheshme, A.A.; Allahdini, A.; Maghsoudi, K.; Jafari, R.; Momen, G. Potential anti-icing applications of encapsulated phase change material-embedded coatings; a review. *J. Energy Storage* **2020**, *31*, 101638. [[CrossRef](#)]
208. Koochaki, M.S.; Momen, G.; Lavoie, S.; Jafari, R. Enhancing Icephobic Coatings: Exploring the Potential of Dopamine-Modified Epoxy Resin Inspired by Mussel Catechol Groups. *Biomimetics* **2024**, *9*, 349. [[CrossRef](#)] [[PubMed](#)]
209. Zhou, H.; Chen, R.; Liu, Q.; Liu, J.; Yu, J.; Wang, C.; Zhang, M.; Liu, P.; Wang, J. Fabrication of ZnO/epoxy resin superhydrophobic coating on AZ31 magnesium alloy. *Chem. Eng. J.* **2019**, *368*, 261–272. [[CrossRef](#)]
210. Pan, L.; Xue, P.; Wang, M.; Wang, F.; Guo, H.; Yuan, X.; Zhong, L.; Yu, J. Novel superhydrophobic carbon fiber/epoxy composites with anti-icing properties. *J. Mater. Res.* **2021**, *36*, 1695–1704. [[CrossRef](#)]
211. Fan, J.; Long, Z.; Wu, J.; Gao, P.; Wu, Y.; Si, P.; Zhang, D. Electrothermal superhydrophobic epoxy nanocomposite coating for anti-icing/deicing. *J. Coat. Technol. Res.* **2023**, *20*, 1557–1568. [[CrossRef](#)]
212. Cattin, R. Icing of wind turbines: Vindforsk projects, a survey of the development and research needs. *Elforsk Rep.* **2013**, *12*, 13.

213. Zhang, X.; Si, Y.; Mo, J.; Guo, Z. Robust micro-nanoscale flowerlike ZnO/epoxy resin superhydrophobic coating with rapid healing ability. *Chem. Eng. J.* **2017**, *313*, 1152–1159. [[CrossRef](#)]
214. Zhao, Z.; Chen, H.; Zhu, Y.; Liu, X.; Wang, Z.; Chen, J. A robust superhydrophobic anti-icing/de-icing composite coating with electrothermal and auxiliary photothermal performances. *Compos. Sci. Technol.* **2022**, *227*, 109578. [[CrossRef](#)]
215. Nistal, A.; Ruiz-González, A.; Choy, K.-L. Robust icephobic nanocomposite coatings with superior abrasion resistance. *Appl. Mater. Today* **2022**, *27*, 101480. [[CrossRef](#)]
216. Atta, A.M.; Ezzat, A.O.; El-Saeed, A.M.; Wahby, M.H.; Abdallah, M.M. Superhydrophobic organic and inorganic clay nanocomposites for epoxy steel coatings. *Prog. Org. Coat.* **2020**, *140*, 105502. [[CrossRef](#)]
217. Qin, C.C.; Mulrone, A.T.; Gupta, M.C. Anti-icing epoxy resin surface modified by spray coating of PTFE Teflon particles for wind turbine blades. *Mater. Today Commun.* **2020**, *22*, 100770. [[CrossRef](#)]
218. Kozera, R.; Ziętkowska, K.; Przybyszewski, B.; Boczkowska, A.; Sztorch, B.; Pakuła, D.; Przekop, R.E.; Trzciński, J.; Borrás, A. Spherosilicate-modified epoxy coatings with enhanced icephobic properties for wind turbines applications. *Colloids Surf. A Physicochem. Eng. Asp.* **2023**, *679*, 132475. [[CrossRef](#)]
219. He, Z.; Jamil, M.I.; Li, T.; Zhang, Q. Enhanced surface icephobicity on an elastic substrate. *Langmuir* **2021**, *38*, 18–35. [[CrossRef](#)] [[PubMed](#)]
220. Gao, L.; Liu, Y.; Hu, H. An experimental investigation of dynamic ice accretion process on a wind turbine airfoil model considering various icing conditions. *Int. J. Heat Mass Transf.* **2019**, *133*, 930–939. [[CrossRef](#)]
221. He, Z.; Xie, H.; Jamil, M.I.; Li, T.; Zhang, Q. Electro-/Photo-Thermal Promoted Anti-Icing Materials: A New Strategy Combined with Passive Anti-Icing and Active De-Icing. *Adv. Mater. Interfaces* **2022**, *9*, 2200275. [[CrossRef](#)]
222. Su, X.; Li, H.; Lai, X.; Yang, Z.; Chen, Z.; Wu, W.; Zeng, X. Vacuum-assisted layer-by-layer superhydrophobic carbon nanotube films with electrothermal and photothermal effects for deicing and controllable manipulation. *J. Mater. Chem. A* **2018**, *6*, 16910–16919. [[CrossRef](#)]
223. Rodert, L.A. *A Preliminary Study of the Prevention of Ice on Aircraft by the Use of Engine-Exhaust Heat*; NTRS—NASA Technical Reports Server: Washington, DC, USA, 1939.
224. Alemour, B.; Badran, O.; Hassan, M.R. A review of using conductive composite materials in solving lightning strike and ice accumulation problems in aviation. *J. Aerosp. Technol. Manag.* **2019**, *11*, e1919. [[CrossRef](#)]
225. Tönbul, B.; Can, H.A.; Öztürk, T.; Akyıldız, H. Solution processed aluminum-doped ZnO thin films for transparent heater applications. *Mater. Sci. Semicond. Process.* **2021**, *127*, 105735. [[CrossRef](#)]
226. Vertuccio, L.; De Santis, F.; Pantani, R.; Lafdi, K.; Guadagno, L. Effective de-icing skin using graphene-based flexible heater. *Compos. Part B Eng.* **2019**, *162*, 600–610. [[CrossRef](#)]
227. Sun, Y.; Wang, Y.; Sui, X.; Liang, W.; He, L.; Wang, F.; Yang, B. Biomimetic multiwalled carbon nanotube/polydimethylsiloxane nanocomposites with temperature-controlled, hydrophobic, and icephobic properties. *ACS Appl. Nano Mater.* **2021**, *4*, 10852–10863. [[CrossRef](#)]
228. Abbas, S.; Park, C.W. Frosting and defrosting assessment of carbon fiber reinforced polymer composite with surface wettability and resistive heating characteristics. *Int. J. Heat Mass Transf.* **2021**, *169*, 120883. [[CrossRef](#)]
229. Idris, M.K.; Qiu, J.; Melenka, G.W.; Grau, G. Printing electronics directly onto carbon fiber composites: Unmanned aerial vehicle (UAV) wings with integrated heater for de-icing. *Eng. Res. Express* **2020**, *2*, 025022. [[CrossRef](#)]
230. Raji, A.-R.O.; Varadhachary, T.; Nan, K.; Wang, T.; Lin, J.; Ji, Y.; Genorio, B.; Zhu, Y.; Kittrell, C.; Tour, J.M. Composites of graphene nanoribbon stacks and epoxy for joule heating and deicing of surfaces. *ACS Appl. Mater. Interfaces* **2016**, *8*, 3551–3556. [[CrossRef](#)] [[PubMed](#)]
231. Ibrahim, Y.; Kempers, R.; Amirfazli, A. 3D printed electro-thermal anti-or de-icing system for composite panels. *Cold Reg. Sci. Technol.* **2019**, *166*, 102844. [[CrossRef](#)]
232. Yao, X.; Hawkins, S.C.; Falzon, B.G. An advanced anti-icing/de-icing system utilizing highly aligned carbon nanotube webs. *Carbon* **2018**, *136*, 130–138. [[CrossRef](#)]
233. Chavan, D.S.; Yadav, R.; Sankpal, J.; Mishra, S.K.; Singh, A. Ice extraction from wind turbine using flow of hot air through blade. In Proceedings of the 2017 International Conference on Energy, Communication, Data Analytics and Soft Computing (ICECDS), Chennai, India, 1–2 August 2017; pp. 2707–2711.
234. Wang, L.; Luo, J.; Chen, Y.; Lin, L.; Huang, X.; Xue, H.; Gao, J. Fluorine-free superhydrophobic and conductive rubber composite with outstanding deicing performance for highly sensitive and stretchable strain sensors. *ACS Appl. Mater. Interfaces* **2019**, *11*, 17774–17783. [[CrossRef](#)] [[PubMed](#)]
235. Bustillos, J.; Zhang, C.; Boesl, B.; Agarwal, A. Three-dimensional graphene foam-polymer composite with superior deicing efficiency and strength. *ACS Appl. Mater. Interfaces* **2018**, *10*, 5022–5029. [[CrossRef](#)]
236. Jiang, H.; Wang, H.; Liu, G.; Su, Z.; Wu, J.; Liu, J.; Zhang, X.; Chen, Y.; Zhou, W. Light-weight, flexible, low-voltage electro-thermal film using graphite nanoplatelets for wearable/smart electronics and deicing devices. *J. Alloys Compd.* **2017**, *699*, 1049–1056. [[CrossRef](#)]

237. Lordan, D.; Burke, M.; Manning, M.; Martin, A.; Amann, A.; O'Connell, D.; Murphy, R.; Lyons, C.; Quinn, A.J. Asymmetric pentagonal metal meshes for flexible transparent electrodes and heaters. *ACS Appl. Mater. Interfaces* **2017**, *9*, 4932–4940. [[CrossRef](#)]
238. Rahimi, A.; Hojjati, M.; Dolatabadi, A.; Moreau, C. Thermal spray coating on polymeric composite for de-icing and anti-icing applications. *J. Manuf. Sci. Eng.* **2021**, *143*, 101008. [[CrossRef](#)]
239. Kiruthika, S.; Gupta, R.; Kulkarni, G.U. Large area defrosting windows based on electrothermal heating of highly conducting and transmitting Ag wire mesh. *Rsc Adv.* **2014**, *4*, 49745–49751. [[CrossRef](#)]
240. Antonini, C.; Innocenti, M.; Horn, T.; Marengo, M.; Amirfazli, A. Understanding the effect of superhydrophobic coatings on energy reduction in anti-icing systems. *Cold Reg. Sci. Technol.* **2011**, *67*, 58–67. [[CrossRef](#)]
241. Kraj, A.G.; Bibeau, E.L. Measurement method and results of ice adhesion force on the curved surface of a wind turbine blade. *Renew. Energy* **2010**, *35*, 741–746. [[CrossRef](#)]
242. Fortin, G.; Adomou, M.; Perron, J. *Experimental Study of Hybrid Anti-Icing Systems Combining Thermoelectric and Hydrophobic Coatings*; 0148-7191; SAE Technical Paper; SAE International: Warrendale, PA, USA, 2011.
243. Wang, T.; Zheng, Y.; Raji, A.R.O.; Li, Y.; Sikkema, W.K.; Tour, J.M. Passive Anti-Icing and Active Deicing Films. *ACS Appl. Mater. Interfaces* **2016**, *8*, 14169–14173. [[CrossRef](#)] [[PubMed](#)]
244. Karim, N.; Zhang, M.; Afroj, S.; Koncherry, V.; Potluri, P.; Novoselov, K.S. Graphene-based surface heater for de-icing applications. *RSC Adv.* **2018**, *8*, 16815–16823. [[CrossRef](#)] [[PubMed](#)]
245. Mangini, D.; Antonini, C.; Marengo, M.; Amirfazli, A. Runback ice formation mechanism on hydrophilic and superhydrophobic surfaces. *Cold Reg. Sci. Technol.* **2015**, *109*, 53–60. [[CrossRef](#)]
246. Golovin, K.; Dhyani, A.; Thouless, M.; Tuteja, A. Low-interfacial toughness materials for effective large-scale deicing. *Science* **2019**, *364*, 371–375. [[CrossRef](#)]
247. Mohseni, M.; Recla, L.; Mora, J.; Gallego, P.G.; Aguero, A.; Golovin, K. Quasicrystalline coatings exhibit durable low interfacial toughness with ice. *ACS Appl. Mater. Interfaces* **2021**, *13*, 36517–36526. [[CrossRef](#)] [[PubMed](#)]
248. Azimi Dijvejin, Z.; Jain, M.C.; Kozak, R.; Zarifi, M.H.; Golovin, K. Smart low interfacial toughness coatings for on-demand de-icing without melting. *Nat. Commun.* **2022**, *13*, 5119. [[CrossRef](#)] [[PubMed](#)]
249. Farzaneh, M.; Volat, C.; Leblond, A. Anti-icing and de-icing techniques for overhead lines. In *Atmospheric Icing of Power Networks*; Springer: Berlin/Heidelberg, Germany, 2008; pp. 229–268.
250. Jiang, G.; Chen, L.; Zhang, S.; Huang, H. Superhydrophobic SiC/CNTs coatings with photothermal deicing and passive anti-icing properties. *ACS Appl. Mater. Interfaces* **2018**, *10*, 36505–36511. [[CrossRef](#)] [[PubMed](#)]
251. Ma, L.; Wang, J.; Zhao, F.; Wu, D.; Huang, Y.; Zhang, D.; Zhang, Z.; Fu, W.; Li, X.; Fan, Y. Plasmon-mediated photothermal and superhydrophobic TiN-PTFE film for anti-icing/deicing applications. *Compos. Sci. Technol.* **2019**, *181*, 107696. [[CrossRef](#)]
252. Dash, S.; de Ruyter, J.; Varanasi, K.K. Photothermal trap utilizing solar illumination for ice mitigation. *Sci. Adv.* **2018**, *4*, eaat0127. [[CrossRef](#)] [[PubMed](#)]
253. Wu, S.; Du, Y.; Alsaid, Y.; Wu, D.; Hua, M.; Yan, Y.; Yao, B.; Ma, Y.; Zhu, X.; He, X. Superhydrophobic photothermal icephobic surfaces based on candle soot. *Proc. Natl. Acad. Sci. USA* **2020**, *117*, 11240–11246. [[CrossRef](#)]
254. Wu, B.; Cui, X.; Jiang, H.; Wu, N.; Peng, C.; Hu, Z.; Liang, X.; Yan, Y.; Huang, J.; Li, D. A superhydrophobic coating harvesting mechanical robustness, passive anti-icing and active de-icing performances. *J. Colloid Interface Sci.* **2021**, *590*, 301–310. [[CrossRef](#)]
255. Guo, H.; Liu, M.; Xie, C.; Zhu, Y.; Sui, X.; Wen, C.; Li, Q.; Zhao, W.; Yang, J.; Zhang, L. A sunlight-responsive and robust anti-icing/deicing coating based on the amphiphilic materials. *Chem. Eng. J.* **2020**, *402*, 126161. [[CrossRef](#)]
256. Zhang, G.; Zhang, Q.; Cheng, T.; Zhan, X.; Chen, F. Polyols-infused slippery surfaces based on magnetic Fe<sub>3</sub>O<sub>4</sub>-functionalized polymer hybrids for enhanced multifunctional anti-icing and deicing properties. *Langmuir* **2018**, *34*, 4052–4058. [[CrossRef](#)] [[PubMed](#)]
257. Yin, X.; Zhang, Y.; Wang, D.; Liu, Z.; Liu, Y.; Pei, X.; Yu, B.; Zhou, F. Integration of self-lubrication and near-infrared photothermogenesis for excellent anti-icing/deicing performance. *Adv. Funct. Mater.* **2015**, *25*, 4237–4245. [[CrossRef](#)]
258. Weng, D.; Xu, F.; Li, X.; Li, Y.; Sun, J. Bioinspired photothermal conversion coatings with self-healing superhydrophobicity for efficient solar steam generation. *J. Mater. Chem. A* **2018**, *6*, 24441–24451. [[CrossRef](#)]
259. Jamil, M.I.; Wang, Q.; Ali, A.; Hussain, M.; Aziz, T.; Zhan, X.; Zhang, Q. Slippery Photothermal Trap for Outstanding Deicing Surfaces. *J. Bionic Eng.* **2021**, *18*, 548–558. [[CrossRef](#)]
260. Wang, J.; Li, P.; Yu, P.; Leydecker, T.; Bayer, I.S.; Losic, D.; Neogi, A.; Wang, Z. Efficient photothermal deicing employing superhydrophobic plasmonic MXene composites. *Adv. Compos. Hybrid Mater.* **2022**, *5*, 3035–3044. [[CrossRef](#)]
261. Guo, Y.; Zhao, H.; Zhang, C.; Zhao, G. Super photothermal/electrothermal response and anti-icing/deicing capability of superhydrophobic multi-walled carbon nanotubes/epoxy coating. *Chem. Eng. J.* **2024**, *497*, 154383. [[CrossRef](#)]
262. Wang, H.; Zhang, Z.; Wang, Z.; Liang, Y.; Cui, Z.; Zhao, J.; Li, X.; Ren, L. Multistimuli-responsive microstructured superamphiphobic surfaces with large-range, reversible switchable wettability for oil. *ACS Appl. Mater. Interfaces* **2019**, *11*, 28478–28486. [[CrossRef](#)] [[PubMed](#)]

263. Zhou, Y.; Huang, S.; Tian, X. Magneto-responsive surfaces for manipulation of nonmagnetic liquids: Design and applications. *Adv. Funct. Mater.* **2020**, *30*, 1906507. [[CrossRef](#)]
264. Jeyadevan, B. Present status and prospects of magnetite nanoparticles-based hyperthermia. *J. Ceram. Soc. Jpn.* **2010**, *118*, 391–401. [[CrossRef](#)]
265. Fan, X.; Xiao, J.; Wang, W.; Zhang, Y.; Zhang, S.; Tang, B. Novel magnetic-to-thermal conversion and thermal energy management composite phase change material. *Polymers* **2018**, *10*, 585. [[CrossRef](#)]
266. Gossuin, Y.; Gillis, P.; Hocq, A.; Vuong, Q.L.; Roch, A. Magnetic resonance relaxation properties of superparamagnetic particles. *Wiley Interdiscip. Rev. Nanomed. Nanobiotechnol.* **2009**, *1*, 299–310. [[CrossRef](#)] [[PubMed](#)]
267. Grigoryev, A.; Tokarev, I.; Kornev, K.G.; Luzinov, I.; Minko, S. Superomniphobic magnetic microtextures with remote wetting control. *J. Am. Chem. Soc.* **2012**, *134*, 12916–12919. [[CrossRef](#)]
268. Irajizad, P.; Hasnain, M.; Farokhnia, N.; Sajadi, S.M.; Ghasemi, H. Magnetic slippery extreme icephobic surfaces. *Nat. Commun.* **2016**, *7*, 13395. [[CrossRef](#)] [[PubMed](#)]
269. Cheng, T.; He, R.; Zhang, Q.; Zhan, X.; Chen, F. Magnetic particle-based super-hydrophobic coatings with excellent anti-icing and thermoresponsive deicing performance. *J. Mater. Chem. A* **2015**, *3*, 21637–21646. [[CrossRef](#)]
270. DiPlacido, N.; Soltis, J.; Palacios, J. Enhancement of ultrasonic de-icing via tone burst excitation. *J. Aircr.* **2016**, *53*, 1821–1829. [[CrossRef](#)]
271. Palacios, J.; Smith, E.; Rose, J.; Royer, R. Instantaneous de-icing of freezer ice via ultrasonic actuation. *AIAA J.* **2011**, *49*, 1158–1167. [[CrossRef](#)]
272. Zeng, J.; Song, B. Research on experiment and numerical simulation of ultrasonic de-icing for wind turbine blades. *Renew. Energy* **2017**, *113*, 706–712. [[CrossRef](#)]
273. Villeneuve, É.; Harvey, D.; Zimcik, D.; Aubert, R.; Perron, J. Piezoelectric deicing system for rotorcraft. *J. Am. Helicopter Soc.* **2015**, *60*, 1–12. [[CrossRef](#)]
274. Gastaldo, G.; Palanque, V.; Budinger, M.; Pommier-Budinger, V. Stress and Energy Release Rate Influence on Ice Shedding with Resonant Electro-Mechanical De-icing Systems. In Proceedings of the ICAS 2022-33rd Congress of the International Council of the Aeronautical Sciences, Stockholm, Sweden, 4–9 September 2022.
275. Marbœuf, A.; Bennani, L.; Budinger, M.; Pommier-Budinger, V. Electromechanical resonant ice protection systems: Numerical investigation through a phase-field mixed adhesive/brittle fracture model. *Eng. Fract. Mech.* **2020**, *230*, 106926. [[CrossRef](#)]
276. Venna, S.V.; Lin, Y.-J.; Botura, G. Piezoelectric transducer actuated leading edge de-icing with simultaneous shear and impulse forces. *J. Aircr.* **2007**, *44*, 509–515. [[CrossRef](#)]
277. Tepylo, N.R. *A Coupled Icephobic Coating and Piezoelectric Actuator System for Aircraft De-Icing Applications*; Carleton University: Ottawa, ON, Canada, 2017.
278. Wang, Z.; Xu, Y.; Gu, Y. A light lithium niobate transducer design and ultrasonic de-icing research for aircraft wing. *Energy* **2015**, *87*, 173–181. [[CrossRef](#)]

**Disclaimer/Publisher’s Note:** The statements, opinions and data contained in all publications are solely those of the individual author(s) and contributor(s) and not of MDPI and/or the editor(s). MDPI and/or the editor(s) disclaim responsibility for any injury to people or property resulting from any ideas, methods, instructions or products referred to in the content.